

BACHELOR THESIS

Investigation into the Production of ^{66}Ga from Natural Zinc for the Calibration of a NaI(Tl) Scintillation Detector

Author:

Adrian P.J. Sidhu
S3340058

First Supervisor:

Dr. Emiel van der Graaf

Second Supervisor:

Dr. Peter Dendooven



Medical Physics Group of KVI-CART
Faculty of Science and Engineering
University of Groningen
Groningen, the Netherlands
July 2020



Investigation into the Production of ^{66}Ga from Natural Zinc for the Calibration of a NaI(Tl) Scintillation Detector

Adrian Parveet James Sidhu

Abstract

The research carried out in this paper is part of a larger ongoing experiment, the ^{12}N production experiment, being conducted by the Medical Physics Group at KVI-CART. The ^{12}N production experiment requires a NaI(Tl) scintillation detector which is to be calibrated. The aim of this research was to investigate the production of ^{66}Ga via proton irradiation on natural zinc, with a water degraded proton beam, for use in calibrating this NaI(Tl) scintillation detector. Cross section data for the $^{\text{nat}}\text{Zn}(\text{p}, x)\text{Y}$ reactions was compiled from external sources (Y represents ^{66}Ga and relevant contaminants). Data of the proton fluence in the natural zinc target plate, at specific water depths, was combined with the cross section data to obtain the reaction rate per starting proton for each isotope Y . Using the reaction rates, a Python function was written to determine the activity and corresponding γ -spectra of each isotope, for a given beam current, water depth, irradiation time, and activity measurement time. It was found that, for a 90 MeV proton beam and a beam degrading water tank placed 50 cm from the beam exit, the natural zinc plate should be placed at a water depth of 60 mm for optimal ^{66}Ga production. Furthermore, for a water depth of 60 mm, a beam current of 30 nA, an irradiation time of 2 hours, and an activity measurement time of 10 hours, it was found that the 1039.231 keV γ -decay line of ^{66}Ga is the best line to use for the detector calibration. This is due to its high intensity (37%) and activity, its energy being within the detectable range, and the line being clear from any major γ -decay interference. It should be noted that the research conducted in this paper is yet to be experimentally verified, but if verified, offers a method of optimisation for experiments of a similar nature.

Investigation into the Production of ^{66}Ga from Natural Zinc for the Calibration of a NaI(Tl) Scintillation Detector

Adrian Parveet James Sidhu

Acknowledgements

I would like to firstly thank my first supervisor, Emiel van der Graaf, whose help, guidance, and support was essential in the making of this thesis. Even in the midst of a pandemic, he has helped me to stay motivated and determined to do the best I can, and has fostered a passion for medical physics in me I hope to carry into the future.

I would also like to thank my family, and especially my parents, who have supported me unconditionally throughout these turbulent times. They helped bring me home and have provided me with comfort and security in the months of writing this thesis.

Contents

1	Introduction	4
2	Theoretical Overview	6
2.1	Interaction of Radiation with Matter	6
2.1.1	Proton Interaction with Matter	6
2.1.2	Production of ^{66}Ga	9
2.1.3	γ -ray Interaction with Matter	13
2.2	Principles of Radiation Detection	15
2.2.1	NaI(Tl) Scintillation Detector	19
2.2.2	High-Purity Germanium (HPGe) Detector	22
3	Methods	24
3.1	Excitation Function of $^{\text{nat}}\text{Zn}(\text{p}, x)\text{Y}$	25
3.2	Determination of Zinc Depth	27
3.3	Gamma Spectra	29
4	Results	30
4.1	Average Excitation Functions	30
4.2	^{66}Ga Production Rates and Water Depth	42
4.3	Contaminant Production	46
4.4	Activities and γ -Spectra	49
5	Discussion	52
6	Conclusion	57
	Appendix	64
I	Theory Appendices	64
II	Method Appendices	65

Chapter 1

Introduction

Despite the seemingly novel technology, proton therapy has been in use for over half a century. The idea of using protons in cancer therapy was first conceived by Robert R. Wilson in 1946[1]. In the following decade, the Lawrence Berkeley National Laboratory and Uppsala University were the first institutes (respectively) to perform proton therapy on human patients[2][3]. After this, the field of proton therapy (along with other ionic beam therapies) burgeoned, with an increasing number of institutes investing their efforts into proton therapy research[4][5].

One of the most advantageous features of proton beam therapy, as compared to other radiation therapies, is the nature of its dose (energy) deposition. Ion (including protons) beams, when penetrating a medium, are characterized by a slow dose deposition followed by the Bragg peak, a highly concentrated area of dose deposition occurring promptly before the particle comes to rest[6]. When applied to cancer treatment, this concentrated dose enables effective targeting of the tumour while minimising dose deposition in the surrounding healthy tissue. However, the position of the Bragg peak in a specific tissue is quite sensitive to tissue characteristics and experimental conditions, such as the tissue density and the proton beam energy. Furthermore, there are also other treatment planning and dosimetric challenges that need to be accounted for (for more information, please refer to Lee et al. (2018)[7] and Yajnik (2012)[8]).

These dependencies and challenges give rise to uncertainties in the prediction of the position of the Bragg peak. To help alleviate these uncertainties, conservative treatment planning is necessary, such as having to use significant safety margins around the tumour and having to avoid beam directions pointing at vital organs[9]. These cautious measures can result in inefficient treatment plans, and can still cause unwanted tissue damage. Furthermore, unlike photon therapy, protons do not exit the patient, meaning there is little way to verify dose delivery. Thus, a real time in vivo dose delivery verification (RTIVDDV) method can ensure safety and efficiency

while reducing the time, effort, and costs involved in drafting prediction measures. In addition, there has been increasing evidence that hypofractionation¹ is more effective than the current conventions in radiation therapy[11–13]. This growing utilisation of hypofractionation emphasizes the need to develop a RTIVDDV method to ensure productive yet safe radiation therapy.

Many products of the proton-nuclei reactions in the tissue of the patient undergo β^+ -decay, γ -decay, or both. The positrons emitted from β^+ -decay annihilate almost immediately after their production, resulting in characteristic 511 keV γ -rays. Therefore, positron emission tomography (PET) provides a very promising method for RTIVDDV. There have been numerous studies in using PET imaging as a RTIVDDV method during proton therapy. In the past five years, research has shown that the short lived ($t_{1/2} = 11.000$ ms[14]) ^{12}N isotope is a prime candidate in beam-on PET imaging[15–17]. According to Dendooven et al.[16], ^{12}N was produced in copious amounts in proton beam interactions with carbon, and was the dominant source of PET decay for irradiation times of up to 70 seconds in adipose tissue.² Thus, research into ^{12}N as a beam-on PET imaging source in proton therapy is currently being conducted at KVI-CART and partner institutions. This thesis is part of a larger ongoing experiment at KVI-CART to measure the production of ^{12}N (via proton beam interaction on ^{12}C) versus water equivalent thickness (WET) by measurement of the characteristic 4.44 MeV γ -ray decay of ^{12}N . The experiment utilises a sodium iodide (NaI) scintillation detector.

Initially, the aim of this thesis was to perform an efficiency calibration on the NaI(Tl) detector using an irradiated ^{66}Ga source for use in the ^{12}N production experiment. However, in light of the COVID-19 pandemic, it was decided best for the experiment to be replaced by an investigation into the production of ^{66}Ga from natural zinc. Two major areas related to the initial experiment are covered. First is the production of ^{66}Ga and other contaminants via proton beam irradiation on natural zinc $^{\text{nat}}\text{Zn}$, and second is the determination of the best γ -decay line to use in the efficiency calibration. It is hoped that the results discovered here can be used by the Medical Physics Group of KVI-CART in the production of ^{66}Ga and subsequent calibration of the NaI(Tl) detector.

¹I.e. delivering higher doses per fraction while reducing the total number of fractions[10].

²Adipose tissue is carbon rich[15, 16].

Chapter 2

Theoretical Overview

This chapter serves as a brief overview of the relevant theory involved in ^{66}Ga production and radiation detection. It has been written with the aid of Knoll (2000)[18], Kamal (2014)[19], D’Auria (2019)[20] and De Sanctis et al. (2016)[21], along with some online sources[22–24].

2.1 Interaction of Radiation with Matter

2.1.1 Proton Interaction with Matter

This section borrows heavily from the content found in Chapter 2 of Knoll (2000)[18]. Therefore, for further reading or clarification, the author recommends to refer to Knoll. As mentioned prior, the NaI(Tl) scintillation detector to be used in the ^{12}N experiment requires an efficiency calibration prior to its use. ^{66}Ga is to be used as a reference source, whereby the measurement of its activity will be used in the determination of the detector efficiency. To produce the ^{66}Ga sample, natural zinc $^{\text{nat}}\text{Zn}$ will be bombarded with protons. Thus this section covers the relevant theory of proton interaction with matter. Please note that proton interaction with biological matter, as the case with proton therapy, will not be covered here.

There are several interactions that affect the path of a proton in a medium. The interaction which is primarily responsible for its energy loss in the medium is the Coulomb interaction between the proton and the electrons of the atoms within the medium. There are also other interactions, such as Rutherford scattering and in the case of interest here, proton induced reactions on atomic nuclei. However, to fully understand the latter, one must first be accustomed with the basic facts of proton interactions with matter.

Due to its positive charge, a proton is susceptible to the Coulomb force. When a proton enters a medium, the atomic electrons of the medium within the vicinity¹ of the proton immediately experience an attractive force exerted by the proton. The impulse created by the passing proton can either excite the electron to a higher atomic orbital or eject the electron from the atom, resulting in an ion. The extent to which the electron is affected is dependent on the proximity of the proton. Conservation of energy then stipulates that the proton must lose some of its own energy. According to Knoll[25] the maximum energy that can be transferred to an electron of mass m_e by a proton with energy E and mass m_p is $4Em_e/m_p$ or around $E/500$. Thus the proton must go through a lot of these collisions before losing all of its energy (multiple scattering). The linear stopping power is given by the (mean) differential energy loss over the associated differential path length of the proton in the medium

$$S = -\left\langle \frac{dE}{dx} \right\rangle. \quad (2.1)$$

In medical physics, this is related to the *dose* ($\text{J}\cdot\text{kg}^{-1}$). In the case of ^{66}Ga production, the bombarding protons are non-relativistic (as will be seen, ideal energies are in the range of 10 to 20 MeV). Thus the expression for the non-relativistic linear stopping power is given by the classical Bethe formula[26]

$$-\left\langle \frac{dE}{dx} \right\rangle = \left(\frac{e^4}{4\pi\epsilon_0^2} \right) \frac{z^2}{m_e v^2} Z N \ln \left(\frac{2m_e v^2}{I} \right) \quad (2.2)$$

where z and v are the charge and velocity of the incident particle (i.e. a proton) respectively and I is the mean excitation potential. Plotting (2.2) against the distance traversed by the particle yields the Bragg curve. For heavy charged particles, such as protons, the Bragg curve exhibits a peak, named the Bragg peak, which occurs directly before the particle stops. As mentioned before, it is this peak that allows a highly concentrated dose deposition in proton therapy. Fig. 2.1 shows the relative dose of protons as compared to X-rays in an example patient, with clear indication of the Bragg peak.

Related to the Bragg peak is the range. Consider a proton beam incident on an absorbing medium with variable thickness which has been placed in front of a detector. If the medium thickness is small, the protons lose energy (via interactions with electrons), but the total number N' of protons reaching the detector is equal to the number N of protons which would reach the detector without the medium present, so $N'/N = 1$. When the thickness is increased, the number of protons incident on the detector begins to attenuate when the thickness starts to match the shortest proton track in the medium. Further increasing the thickness causes N' to quickly drop to 0. The mean range R_m is defined as the thickness of the medium which causes the number of protons incident on the detector to drop to half of its initial

¹The magnitude of the force felt is given by Coulomb's law.

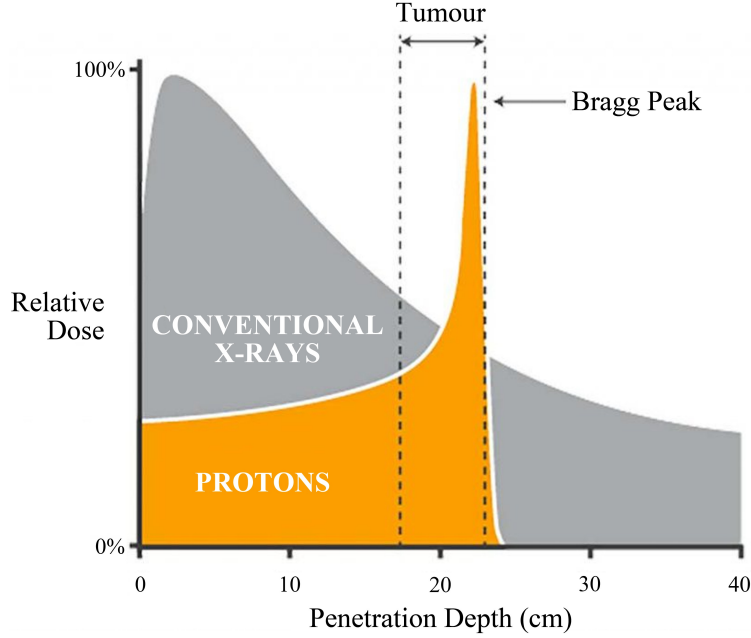


Figure 2.1: Proton dose (with Bragg peak) as compared to X-rays in example patient[27]

value, or in other words the thickness at the point $N'/N = 0.5$. The extrapolated range R_e is obtained by extrapolating the linear part of the attenuation curve to zero. In applications, to be able to measure the full energy of a particle, detectors must have an active region with a greater thickness than the range of the particle in the detector material.

When a monoenergetic proton beam enters a medium, the interactions of the individual protons of the beam with the particles in the medium are quite random. Therefore the energy loss of the beam is a stochastic process. After the beam has penetrated a certain depth into the medium, the energy of the beam (at that specific depth) is then no longer monoenergetic, but instead a distribution of energies. The width of this distribution is a measure of the energy straggling of the beam. The energy straggling (and thus the distribution of energies) varies along the penetration path of the beam. This is of special importance to this thesis; as will be seen, the ideal energies for ^{66}Ga production from natural zinc is in the range of 10-20 MeV. However, the ^{66}Ga will be produced during the ^{12}N production experiment, which requires a 90 MeV proton beam. Therefore, the beam must first be degraded by placing the target in water. The energy straggling of the beam in water must therefore be analysed to maximise the production yield of ^{66}Ga .

The range is dependent on the energy of the particle and the absorbing material. Thus, if a beam is subject to energy straggling, this consequentially results in range straggling. Range straggling is defined as fluctuations in the path length of individual particles with the same initial energy[18]. For protons, range straggling is typically on the order of a few percent of the mean range.

One of the most important parameters in determining the ideal beam conditions for a required reaction is the cross section. The cross section σ of a reaction is a measure used to quantify the probability of said reaction happening. It has dimensions of area, and a typical unit used is the barn ($1 \text{ b} = 10^{-28} \text{ m}^2$). As it has the dimensions of area, it is commonly interpreted as the ‘effective’ area of interaction of an atom or molecule in the absorbing medium. If a penetrating particle enters the vicinity of the cross section (whose face is perpendicular to the particle trajectory) of an atom/molecule, it will interact with the atom/molecule. However it is important to note that this area is fictitious, and the cross section is actually related to the forces in play between particles. It is dependent on several factors, including the medium composition, medium density, and the energy of the incoming particle.

2.1.2 Production of ^{66}Ga

Due to the presence of the Coulomb force, the cross sections of proton-induced reactions as a function of proton energy are hard to determine analytically, and are instead determined through empirical or computational means. This thesis will cover data from both, and from that determine the best proton beam energy for the production of ^{66}Ga . While cross sections are energy dependent, the excitation functions (plots of cross section as a function of proton energy) begin at the threshold energy, the minimum kinetic energy required of the proton to initiate a reaction. Thus, the threshold energy is a fixed and readily comparable value for specific reactions. The required reaction is $^{\text{nat}}\text{Zn}(p, x)^{66}\text{Ga}$, where x represents additional products. The stable isotopes present in natural zinc and their abundances are ^{64}Zn ($49.17 \pm 0.75\%$), ^{66}Zn ($27.73 \pm 0.98\%$), ^{67}Zn ($4.04 \pm 0.16\%$), ^{68}Zn ($18.45 \pm 0.63\%$), and ^{70}Zn ($0.61 \pm 0.10\%$)[28]. The threshold energies for ^{66}Ga production from the relevant zinc isotopes (i.e. the three isotopes present in natural zinc capable of producing ^{66}Ga via proton bombardment) are given in Table 2.1.

Table 2.1: Natural abundances of relevant zinc isotopes and corresponding threshold energies for ^{66}Ga production via proton bombardment on natural zinc[29]

Reaction	Natural Abundance of Zinc Isotope (%)	Threshold Energy (MeV)
$^{66}\text{Zn}(p, n)^{66}\text{Ga}$	27.73 ± 0.98	6.04847
$^{67}\text{Zn}(p, 2n)^{66}\text{Ga}$	4.04 ± 0.16	13.20554
$^{68}\text{Zn}(p, 3n)^{66}\text{Ga}$	18.45 ± 0.63	23.55225

While ^{66}Ga is to be used as the calibration source, it is also important to identify other γ -ray sources that will be produced in the proton bombardment of natural zinc, as these contaminants might interfere with the calibration. Around fifty contaminants[29] are produced in this reaction, but only those with a half-life $t_{1/2}$ that might interfere with the γ -spectra of ^{66}Ga ($t_{1/2} = 9.49$ h) were considered. Thus, only the contaminants with a half-life of more than one hour were analysed. Table 2.2 shows the relevant contaminants X and their half-lives.

 Table 2.2: Relevant contaminants X and their half-lives[29][30]

Contaminant Isotope	Half-Life $t_{1/2}$
^{61}Cu	3.33 h
^{64}Cu	12.7 h
^{67}Cu	61.9 h
^{67}Ga	3.26 d
^{68}Ga	67.6 min
^{62}Zn	9.13 h
^{65}Zn	244.26 d

Proton beam fluence ϕ distribution data for imaginary 0.1 mm slices in a 1 mm natural zinc plate in a water tank (at a specific water depth) was acquired from external simulations[31]. Cross section data for the $^{\text{nat}}\text{Zn}(\text{p}, x)^{66}\text{Ga}$ and $^{\text{nat}}\text{Zn}(\text{p}, x)X$ reactions was collected from past research and a regression technique applied to each data set to produce an averaged excitation function for each reaction. Using both the fluence and the averaged excitation functions, the number R of a specific isotope Y^2 produced per starting proton (sp^{-1}) can also be determined. R is given by

$$R = \phi \sigma a \rho_a \frac{N_A}{A} \quad (2.3)$$

where

- ϕ is the proton beam fluence - $[\phi] = \text{cm}^{-2}\text{sp}^{-1}$;
- σ is the energy dependent cross section in the $^{\text{nat}}\text{Zn}(\text{p}, x)Y$ reaction - $[\sigma] = \text{cm}^2$;
- $a = 6.25\text{cm}^2$ is the frontal area of the zinc plate;
- $\rho_a = \rho \cdot l = 0.0714 \text{ g}\cdot\text{cm}^{-2}$ is the areal density of the zinc plate. Here $l = 0.1$ mm is the width of one imaginary zinc slice and $\rho = 7.14 \text{ g}\cdot\text{cm}^{-3}$ is the density of natural zinc[28];
- $N_A = 6.022 \times 10^{23} \text{ mol}^{-1}$ is the Avogadro constant;
- $A = 65.38 \text{ g}\cdot\text{mol}^{-1}$ [32] is the atomic mass of natural zinc.

² Y represents both ^{66}Ga and the contaminants X .

It is clear to see that $[R] = \text{sp}^{-1}$. In practice, it is customary to use per nanoampere hour ($\text{nA}^{-1} \cdot \text{h}^{-1}$) rather than per starting proton. This conversion is relatively straightforward. Noting that the charge of one proton is $1.602 \times 10^{-19} \text{C}$ [33], 1 C of charge is then given by

$$1 \text{ C} = 1 \text{ A} \cdot \text{s} = \frac{1}{1.602 \times 10^{-19}} \text{ sp}$$

and thus

$$1 \text{ sp}^{-1} = \frac{10^{-9}}{1.602 \times 10^{-19}} \text{ nA}^{-1} \cdot \text{s}^{-1} \times 3600 \text{ s} \cdot \text{h}^{-1} = 2.247 \times 10^{13} \text{ nA}^{-1} \cdot \text{h}^{-1}. \quad (2.4)$$

Therefore R can be converted from per starting proton to per nanoampere hour by multiplication of $2.247 \times 10^{13} \text{ nA}^{-1} \cdot \text{h}^{-1}$. In determining the best γ -decay line to be used for calibration, it is necessary to first determine the activity of each source for a given proton beam irradiation time t_R , proton beam current i_p , and activity measurement time t_A (i.e. the time at which the activity is recorded, as measured from the start of irradiation). During irradiation, the change per unit time in the number N of a specific isotope Y is given by

$$\frac{dN}{dt} = P - \lambda N \quad (2.5)$$

where P is the production term and λ is the decay constant of the isotope. The production term P is the number of Y being produced per second as a consequence of proton beam irradiation. Although R and P are similar, it is important to note that R is the number of Y being produced per nanoampere hour (or per starting proton), while P is the number of Y being produced per second for a given beam current. For a given R ($[R] = \text{nA}^{-1} \cdot \text{h}^{-1}$) and proton beam current i_p , the production term is given by

$$P = R \cdot i_p \cdot \frac{1}{3600} \text{ h} \cdot \text{s}^{-1}. \quad (2.6)$$

There were initially some concerns that P would decrease over time as an increasing number of zinc atoms would be lost during irradiation. However it was found that even after an irradiation of 10 hours the loss in zinc was negligible. Furthermore, as the irradiation time in practice will be around 2 hours, P can be taken as constant without any loss in accuracy. Solving (2.5) for N gives

$$N(t) = \frac{P(1 - e^{-\lambda t})}{\lambda} \quad (2.7)$$

and noting that activity is given by $A(t) = \lambda N(t)$, the activity of Y during irradiation is given by

$$A(t) = P(1 - e^{-\lambda t}). \quad (2.8)$$

After irradiation, the change per unit time in the number N of Y is given by

$$\frac{dN}{dt} = -\lambda N \quad (2.9)$$

and solving for N gives

$$N(t) = N_0 e^{-\lambda t} \quad (2.10)$$

which is the well known exponential decay equation. Here N_0 is the initial number of Y present. N_0 is given by

$$N_0 = \frac{P(1 - e^{-\lambda t_R})}{\lambda} \quad (2.11)$$

or the number of Y present at the end of the irradiation time t_R . The activity of Y after irradiation is then

$$A(t) = \lambda N_0 e^{-\lambda t}. \quad (2.12)$$

If the activity measurement is taken during or at the end of irradiation, $t_A \leq t_R$, then the activity is given by (2.8). However, if the activity measurement is taken after irradiation, $t_A > t_R$, the activity is given by (2.12). To summarise

$$t_A \leq t_R : A(t_A) = P(1 - e^{-\lambda t_A}) \quad (2.13)$$

$$t_A > t_R : A(T) = \lambda N_0 e^{-\lambda T} \quad (2.14)$$

where $T = t_A - t_R$. It is necessary to use T as t_A is measured from the beginning of irradiation, and N_0 as given by (2.11) accounts for both the production and decay of isotope Y during irradiation. After irradiation, the change in the amount of Y is governed solely by decay, and thus only the time T after irradiation should be accounted for. Once the activity is determined, it is a simple matter of finding the intensity I ($[I] = \%$) of a certain γ -decay line and multiplying this intensity by the activity. Doing this yields the number of γ -rays of a specific energy produced by Y per second i.e. the γ -decay activity.

2.1.3 γ -ray Interaction with Matter

This section borrows heavily from the content found in Chapter 2 of Knoll (2000)[18]. Therefore, for further reading or clarification, the author recommends to refer to Knoll. Here, γ -ray interactions with matter relevant to the operation of the γ -ray scintillation detectors are covered. There are three relevant³ interaction types. In order of ascending energy ranges, they are the photoelectric effect, Compton scattering, and pair production.

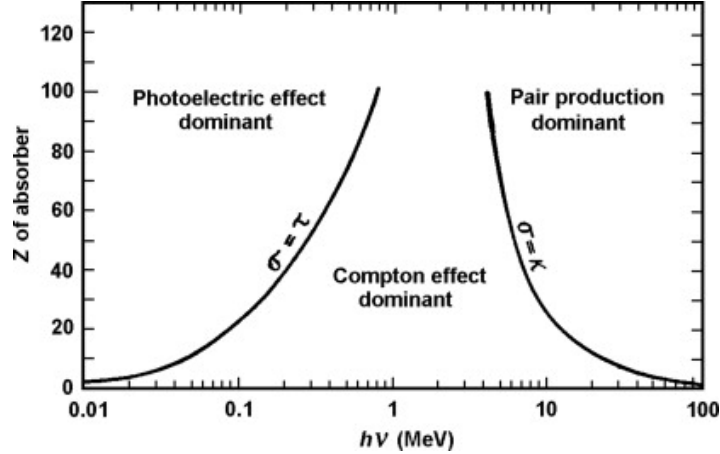


Figure 2.2: The relative importance of each interaction regime with respect to the atomic number Z of the absorber and the energy of the γ -ray[34]

Fig. 2.2 shows the importance of each interaction with respect to the atomic number of the absorbing medium against increasing γ -ray energy. The curves on the figure represent the values of Z and $h\nu$ for which the neighbouring interaction regimes have equal cross sections (i.e. equal probabilities of occurrence).

Photoelectric Effect

The photoelectric effect is a phenomenon whereby a photon is fully absorbed by an atom resulting in the ejection of an orbital electron. The energy of the photon is used to free the electron from its atomic binding, meaning the photon must have an energy equal to or higher than the binding energy of the electron. If the photon has energy higher than the binding energy of the electron, the excess energy is transferred to the electron as kinetic energy. This is neatly summarised in the expression

$$E_k = h\nu - W \quad (2.15)$$

where E_k is the kinetic energy of the ejected electron, $h\nu$ is the energy of the incident

³Coherent scattering has been omitted as it is not very relevant in γ -ray detection.

photon, and W is the binding energy of the electron. As detailed by Fig. 2.2, the photoelectric effect is dominant for low energy photons paired with high Z materials. It is useful in scintillation detectors, whereby photomultiplier tubes (PMTs) in the detector utilise the effect to convert scintillation photons into electrical signals.

In the case of (low energy) γ -rays, tightly bounded (K or L shell) electrons are typically ejected from the atom. This ionizes the atom, and the empty shell is filled by either a higher energy electron or by capture of a free electron from the medium. The former can result in the emission of characteristic X-rays, and while these are typically reabsorbed close by (again via the photoelectric effect), a small fraction escape. It is important to account for these escaped X-rays in detector measurements, otherwise they may interfere with the results. Auger electrons may also be emitted instead of a characteristic X-ray.

Compton Scattering

Compton scattering is the scattering of photons off of charged particles, primarily electrons. Of interest here is the scattering of γ -rays with free electrons in the absorbing medium. In the collision the electron is assumed to be stationary. The incident γ -ray is deflected through an angle θ with respect to its original trajectory while transferring some of its energy to the electron. The recoiling electron is appropriately termed a recoil electron.

All scattering angles are possible, meaning the amount of energy transferred to the electron can be small ($\theta \sim 0$) or very large ($\theta \sim \pi$, backwards scattering). It is obvious that the photon always retains some of its energy after a Compton scattering event. The energy $E' = h\nu'$ of a scattered photon as a function of the corresponding incident photon $E = h\nu$ and scattering angle θ is given by

$$E' = \frac{E}{1 + \frac{E}{m_e c^2}(1 - \cos\theta)}. \quad (2.16)$$

The angular distribution of the scattered γ -rays is given by the Klein-Nishina formula for the differential scattering cross section, though it has not been expressed here.

Pair Production

Pair production is the creation of a particle-antiparticle pair from a neutral boson. In the case of interest, a sufficiently energetic γ -ray photon creates an electron-positron pair in the presence of an external Coulomb field (e.g. an atomic nucleus). The latter condition is to ensure momentum and energy conservation is satisfied. By conservation of energy pair production only becomes energetically possible for γ -rays above $2m_e c^2 = 1.022$ MeV. However the probability of pair production occurring is normally only significant if the γ -ray has an energy of a few MeV (refer to Fig. 2.2).

Similar to the photoelectric effect, if the γ -ray has energy in excess of the required energy for pair production (1.022 MeV), this excess energy is transferred to the electron and positron as kinetic energy (this sharing of energy is not necessarily equal). After the interaction, the positron quickly annihilates producing two more γ -ray photons.

2.2 Principles of Radiation Detection

This section follows the general structure and content of Chapter 4 of Knoll (2000) [18]. Therefore, please refer there for more information. Interaction of radiation with a detector, in most detectors, results in the appearance of a small electric charge Q . When interpreting this charge, it is assumed that the charge appears at the time $t = 0$, when the quantum of radiation interacted with the detector. In the case of scintillation detectors, this is not strictly true, as the electric charge appears in the PMTs (as a result of the scintillation light) instead of the scintillation material itself. This electric charge needs to then be collected, which is normally done by application of an external electric field. The collection time t_c of detectors vary, though generally the current $I(t)$ measured over this time is related to the charge Q by

$$\int_0^{t_c} I(t) dt = Q. \quad (2.17)$$

There are three modes of detector operation- pulse mode, current mode, and mean square voltage (MSV) mode. Pulse mode is of relevance to the ^{12}N production experiment and to this thesis. In pulse mode, each photon interacting with the detector is measured as an individual pulse. Thus pulse mode maintains information on the energy of the incident photon and the timing between interaction events.

After collection, information pertaining to the pulse amplitude is most commonly displayed through the differential pulse height distribution. The distribution relates the quotient dN/dH of the infinitesimal number of pulses dN with an amplitude H within an infinitesimal range of amplitudes dH in the y -direction, with an increasing linear scale from zero to an amplitude larger than one observed in the pulse spectra (to be able to determine the zero of dN/dH) in the x -direction. The number $N_{1 \rightarrow 2}$ of pulses with amplitudes between H_1 and H_2 can then be determined by

$$N_{1 \rightarrow 2} = \int_{H_1}^{H_2} \frac{dN}{dH} dH. \quad (2.18)$$

Note that $[H]=\text{V}$ and $[dN/dH]=\text{V}^{-1}$. The total number N_0 of pulses can similarly be determined by integrating over the entire spectra

$$N_0 = \int_0^{\infty} \frac{dN}{dH} dH. \quad (2.19)$$

Instead of the differential pulse height distribution, one can also use the integral pulse height distribution. The information displayed by these distributions are the same, just differing in form, and can be easily derived from each other. The x -axis is equivalent to the differential pulse height distribution, but here the y -axis represents the number N of pulses which have an amplitude larger than a given amplitude H of the x -axis.

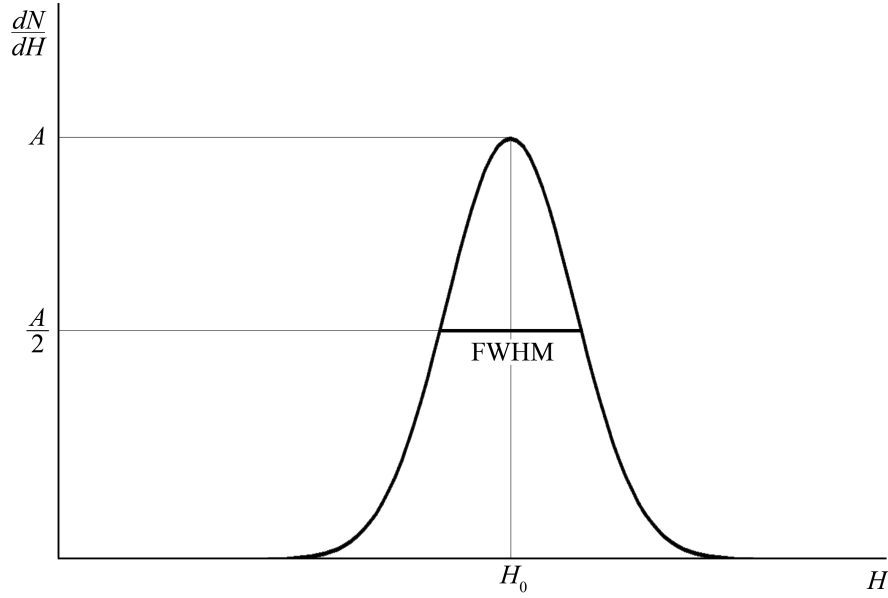


Figure 2.3: Response Function of a Hypothetical Detector for a Monoenergetic Radiation Source

In radiation detection, energy resolution is of great importance. Fig. 2.3 shows the differential pulse height distribution for a hypothetical detector in response to a monoenergetic source. In the context of a single energy, the differential pulse height distribution is termed the response function of the detector for that specific energy. A broader distribution indicates a worse resolution, while a narrow distribution indicates a good resolution. This is due to the fact that the width of the distribution is directly affected by the amount of fluctuation in pulse measurements. Wide distributions result from a large amount of fluctuations between pulse measurements, despite the energy being constant throughout, while narrow distributions represent little fluctuation between measurements. While resolution can be compared qualitatively between response functions, it is defined quantitatively by

$$R = \frac{FWHM}{H_0}. \quad (2.20)$$

Here FWHM is the full width at half maximum. It is defined as the width of the distribution at the level where dN/dH is half that of the maximum peak. In Fig. 2.3, the FWHM is indicated by the bold line inside the distribution corresponding to the y -value of $A/2$. H_0 is the value of H (on the x -axis) corresponding to the maximum peak, and intersects the FWHM at its halfway point. R is dimensionless, and is often denoted by a percentage. Since the larger the width of the distribution the worse the resolution, it is obvious that the smaller the value of R , the better the resolution. For more information regarding the sources and nature of fluctuations which affect the energy resolution of detectors please refer to Knoll.

Detection efficiency is the main concern of this thesis. As mentioned, an NaI(Tl) scintillation detector is to be calibrated. This calibration will be an efficiency calibration, a measure of how many particles are recorded by the detector as a fraction of either the number of particles emitted by the source or the number of particles incident on the detector. The former is called the absolute detector efficiency and is given by

$$\epsilon_{abs} = \frac{\text{Number of Particles (Pulses) Recorded by the Detector}}{\text{Number of Particles Emitted by the Source}}. \quad (2.21)$$

The latter is called the intrinsic detector efficiency and is given by

$$\epsilon_{ins} = \frac{\text{Number of Particles (Pulses) Recorded by the Detector}}{\text{Number of Particles Incident on the Detector}}. \quad (2.22)$$

Detectors which detect charged particles such as α particles, protons, and β particles can typically be calibrated in such a way to yield a nearly 100% detector efficiency. This is due to the fact that charged particles interact (typically via ionization or excitation) nearly immediately upon entering the active region of the detector. During its path, the particle will cause a significant amount of ionization, ensuring that the generated pulse will be large enough to be recorded even before the particle reaches its range. Unfortunately, this is not the case with neutral particles such as photons and neutrons.

In particular, γ -rays interact solely via the electromagnetic interaction. They are not subject to the Coulomb force and therefore when they enter the active region of a detector they must undergo a significant reaction (refer to §2.1.2) for a large enough pulse to be generated and subsequently recorded. Furthermore, the range of γ -rays is typically much larger than that of massive charged particles. Thus, there is a chance that incident γ -rays go through the active region without interaction and hence are not recorded. This is why it is necessary to determine the efficiency of the detector. The detector efficiency allows one to derive the activity of a source, and the amount of radiation incident on the detector, by analysing the number of pulses recorded by the detector.

The absolute efficiency is heavily dependent on the source-detector distance and the counting geometry, along with the detector characteristics. The intrinsic efficiency

is much less affected by the counting geometry and is primarily dependent on the detector and the incident radiation. In particular, the detector material, the energy of the incident radiation, and the thickness of the active region along the path of the incident radiation are some of the main factors affecting the intrinsic efficiency. The intrinsic efficiency is still dependent on the source-detector distance however, as this distance will affect the range of incident radiation in the active region. The two efficiencies are related by

$$\epsilon_{int} = \epsilon_{abs} \frac{4\pi}{\Omega}. \quad (2.23)$$

Here Ω is the solid angle subtended by the (active region of the) detector at the source position. Along with the absolute and intrinsic efficiencies, counting efficiencies can also be defined by the nature of the interactions recorded. In particular, one has the total efficiency and the peak efficiency. The (theoretical) total efficiency assumes that all interactions, regardless of their energies, are recorded. In reality however, detectors have energy thresholds. This means that the energy released by interactions taking place in the active region of the detector must surpass this threshold to be recorded by the detector. The total efficiency can be approached by setting this energy threshold to the minimum possible value. Fortunately, the peak efficiency can be acquired in practice, as it assumes only events which deposit the full energy of the incident radiation are counted. These events are evidenced by a peak on the highest end of the respective differential pulse height distributions. The area under this peak is the number of interactions in which the full energy of the incident radiation has been deposited. It is also important to note that peak efficiencies are not affected by variable effects (e.g. noise). Detector efficiencies should be specified according to both intrinsic or absolute and total or peak. In γ -ray spectroscopy, the intrinsic peak efficiency is most often used.

If the efficiency of a detector is known it can be used to determine the activity of a source. In regards to this thesis, the detector of known efficiency to be used is the High-Purity Germanium (HPGe) detector, which will in turn be used to calibrate the NaI(Tl) detector. If it is assumed that a source emits radiation isotropically and that no attenuation occurs between the source and the detector, the intrinsic peak efficiency ϵ_{ip} is related to the activity of the source by

$$S = N \frac{4\pi}{\epsilon_{ip}\Omega}. \quad (2.24)$$

Here S is the number of particles (of the specific radiation being detected) emitted by the source during the measurement period⁴ and N is the number of events in the full energy peak. The solid angle Ω is defined as it was for (2.23) and is wholly dependent on the source-detector geometry. For more information on Ω , please refer to Knoll.

⁴Dividing S by the measurement period in seconds yields the activity in Bq.

2.2.1 NaI(Tl) Scintillation Detector

This section borrows heavily from the content found in Chapter 8 of Knoll (2000)[18]. Therefore, for further reading or clarification, the author recommends to refer to Knoll. Scintillation is the physical phenomenon whereby visible or UV electromagnetic radiation is produced inside a scintillation material due to interactions resulting from the passage of a particle through said material. Particles incident on a scintillation detector interact with the inorganic scintillation material (NaI activated with thallium) and produce light. This light is registered by a PMT which utilises the photoelectric effect to convert the scintillation photons into electrical pulses. These pulses are subsequently amplified and analysed. A schematic of this process can be seen in Fig. 2.4. According to Knoll, there are six properties the ideal scintillation material should possess- these properties can be found in the Appendix. In practice though, no material simultaneously meets all six, and therefore choosing a material always compromises one or more of these qualities in favour of another. The material of interest here is thallium activated sodium iodide crystal, which is the scintillation material found in the detector to be used in the ^{12}N production experiment (i.e. the detector which is to be calibrated with the ^{66}Ga gamma spectrum).

Pure scintillation crystals are inefficient in the scintillation process and typically produce photons which are of too high an energy for PMTs to detect. This is usually due to the large band gaps present in their lattice structure. Therefore, impurities must be introduced into the crystal. This process is called activation and the impurities are called activators. In semiconductor production, this process is known as doping. The introduction of impurities creates special sites in the crystal lattice. At these sites, previously forbidden energy levels are formed within the band gap (forbidden gap). When a γ -ray traverses the material, many electron-hole pairs are produced. Holes travel through the material, and upon encountering an activation site, ionize it. This allows electrons to drop into the site. If the electron drops into an excited configuration, and subsequently drops to the activator ground state, it will release a photon. If the activation material is chosen appropriately, these scintillation photons will be in the visible or UV range. Thallium is the activating agent for the sodium iodide crystal in the detector which will be used in the ^{12}N production experiment. Fig. 2.5 shows the energy band structure in an activation site.

There are other processes which compete with the activator ionization process described above, but they will not be detailed here. For a range of materials, NaI(Tl) included, the photon energy required to produce one electron-hole pair is around three times that of the band gap. For NaI(Tl), this is about 20 eV. According to Knoll, the absolute efficiency of thallium activated sodium iodide is around 12%. Thus, for example, if a 1 MeV γ -ray is fully absorbed, around 120 keV of scintillation light energy will be produced. This is actually one of the most prominent features of NaI(Tl) as a scintillation material, it has a superb light yield as compared to other

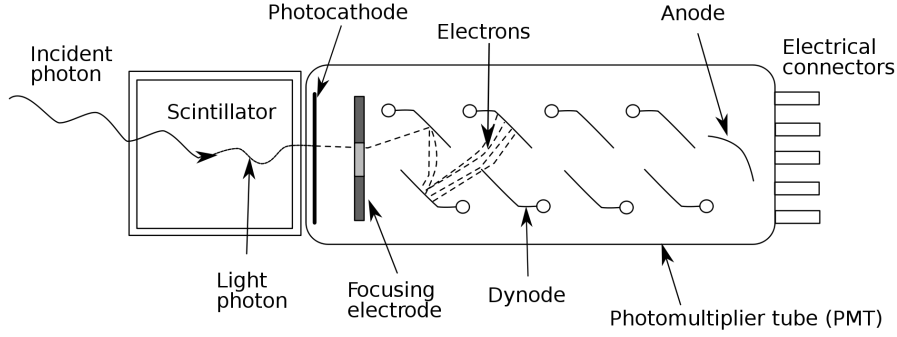


Figure 2.4: Diagram of a Scintillation Detector[35]

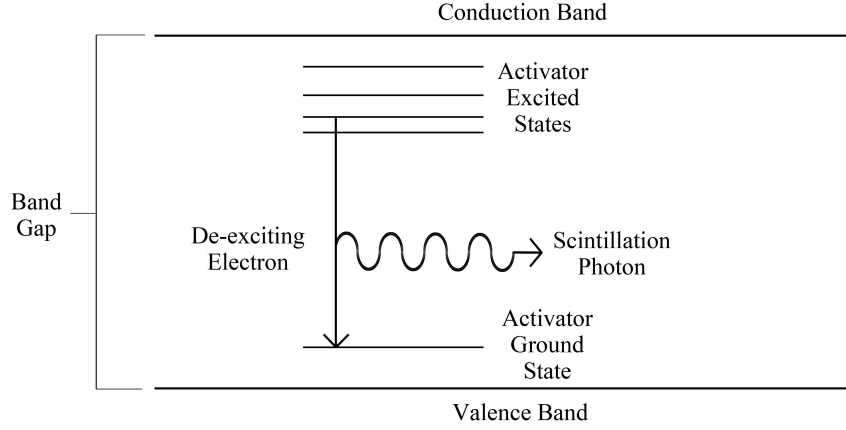


Figure 2.5: Energy Band Structure in an Activated Scintillation Material

inorganic materials. Despite this high absolute efficiency, the efficiency in practice is dependent on the sample shape, the detector geometry, and on the γ -ray energy. Thus, it is wise to expect a lower efficiency, meaning that the γ -ray calibration source should be quite powerful.

The NaI(Tl) detector to be used has dimensions of $91 \text{ mm} \times 91 \text{ mm} \times 150 \text{ mm}$ and is enclosed in a 1 mm thick, 98 mm wide aluminium housing. A schematic of the detector can be seen in Fig. 2.6. Furthermore, the detector is also enclosed in a Eurogam Clover detector housing. There is a tungsten collimator at the top of the housing. Monte Carlo simulations ran by van der Graaf[36] for a source modelled as a point source 17.3 cm above the tungsten collimator found the geometrical efficiency to be 3.29×10^{-3} . The simulated efficiencies for a 0.9 MeV, 1 MeV, and 1.25 MeV γ -ray were found to be 2.31×10^{-3} , 2.22×10^{-3} , and 2.03×10^{-3} respectively. As will be seen, the ideal ^{66}Ga γ -decay line lies at around 1 MeV, so these energies and

CHAPTER 2. THEORETICAL OVERVIEW

their corresponding efficiencies are the most relevant. Note that while efficiencies have been acquired from simulation, the detector must still be calibrated with an actual source (i.e. ^{66}Ga).

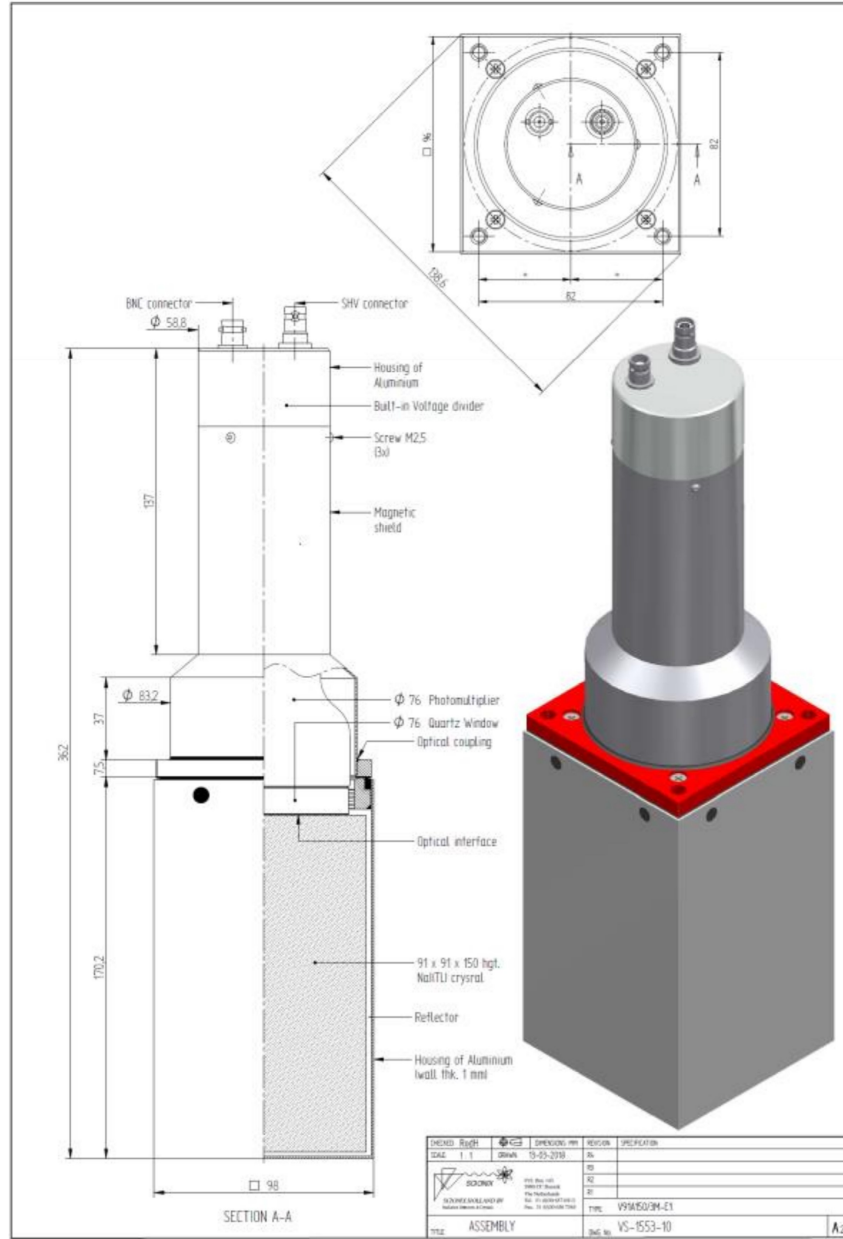


Figure 2.6: Scionix Scintillation Detector Type V91A150/3M-E1 to be used in the ^{12}N production experiment[36]

2.2.2 High-Purity Germanium (HPGe) Detector

This section borrows heavily from the content found in Chapter 12 of Knoll (2000) [18] and several online resources[22–24]. Thus, for further reading please refer to these sources. Typical semiconductor detectors are useful in detecting massive, short-ranged, and charged particles, but are not suited for detecting more penetrating radiation, such as γ -rays. This is due to their limited depletion depths, or active regions. The depletion depth d of a semiconductor is given by

$$d = \left(\frac{2\epsilon V}{eN} \right)^{1/2} \quad (2.25)$$

where V is the reverse bias voltage, N is the net impurity concentration in the semiconductor material, ϵ is the relative permittivity, and e is the elementary charge. Germanium of normal semiconductor purity has a depletion depth of 2 or 3 mm, but as γ -rays are highly penetrating, this is not large enough. By severely reducing impurity concentration in the semiconductor material, it is possible to achieve higher depletion depths which are capable of detecting γ -rays. For example, given an impurity concentration of 10^{10} atoms per cm^3 and a reverse bias voltage of less than 1000 V, a depletion depth of 10 mm can be achieved. However, it is important to note that this is an extremely low impurity concentration. Such levels of purity can be achieved in germanium, and detectors utilising high-purity germanium are appropriately termed high-purity germanium (HPGe) detectors.

Germanium has a relatively low band gap, so HPGe detectors must be operated at low temperatures to prevent the thermal generation of charge carriers and the noise induced by the consequential leakage current. When a γ -ray traverses the semiconductor material (i.e. high-purity germanium), it ionizes some of the semiconductor atoms, resulting in the creation of electron-hole pairs. Electrons from the valence band jump to the conduction band, forming holes in the valence band. Since, as mentioned, high-purity germanium has a large depletion depth, this allows the electrons in its atoms to absorb high-energy γ -rays. Furthermore, the number of electron-hole pairs is typically proportional to the energy of the γ -ray. In the detector, the germanium is subject to an electric field. Upon the creation of the electron-hole pairs, these charge carriers travel to the respective electrode. The potential difference between the electrodes results in an electric pulse, which can then be analysed to yield information about the energy of the incident γ -ray. This method, while seemingly similar, is distinct from the scintillation method. In scintillation materials, electrons de-exciting in ionized activator sites result in the emission of scintillation photons. These photons are registered in PMTs, creating electrical signals which are amplified and analysed. In HPGe detectors, the recorded electric pulse is a direct result of the incident γ -ray.

With regards to the HPGe detector to be used in the experiment, a few drops of radioactive solution⁵ were placed on a paper filter. This paper was subsequently placed directly on the surface of the HPGe detector and yielded efficiencies of 0.049 for a 898 keV γ -ray and 0.038 for a 1173 keV γ -ray[31]. Note that these efficiencies are in general one order of magnitude larger than the efficiencies from the NaI(Tl) detector simulation.

⁵A liquid in which a known amount of radioactive substance has been dissolved in.

Chapter 3

Methods

As mentioned prior, the aim of this research was to calibrate a NaI(Tl) scintillation detector to be used for a larger ongoing project. Due to the COVID-19 pandemic, access to experimental equipment was not permitted and therefore the research was adapted. There were several stages in this research, culminating in the determination of the optimal ^{66}Ga γ -decay line to be used for the activity measurement.

The source to be used for the activity measurement is ^{66}Ga . This source must be produced at KVI-CART via proton bombardment on a 1 mm thick natural zinc plate. The fundamental components of the set up are the beam (more specifically, the position of the beam exit), a water tank which will degrade the beam¹ (water also acts as a tissue substitute in the ^{12}N experiment), and the zinc plate. To make a good calibration source, a large amount of ^{66}Ga must be produced. Therefore, based on the given apparatus, the position of the zinc plate in the water which produces the largest amount of ^{66}Ga for a given fluence needed to be determined. To do this, a fluence profile needed to be examined along with a reliable excitation function for $^{\text{nat}}\text{Zn}(p, x)^{66}\text{Ga}$. The activities and gamma spectra of ^{66}Ga and various other contaminants were also determined. The γ -decay line of ^{66}Ga which was both the most prominent and as clear from interference as possible was ascertained.

¹As mentioned prior, the ^{66}Ga will be produced during the ^{12}N production experiment, which requires a 90 MeV beam. Thus, the beam must be degraded to produce ^{66}Ga .

3.1 Excitation Function of $^{\text{nat}}\text{Zn}(\text{p}, x)Y$

The physics of nuclear transmutation, especially for Coulomb interacting particles (such as the proton), is very complicated. Therefore, excitation functions are not determined analytically, but rather experimentally or computationally. Unfortunately, the author was unable to acquire the appropriate software to compute the $^{\text{nat}}\text{Zn}(\text{p}, x)Y$ excitation functions. For the interested reader, two simulation codes which can be used are ALICE2017 and EMPIRE-II[37][38]. Since experimental and computational methods were not feasible, cross section data was collected from a range of sources.

The cross section data for each $^{\text{nat}}\text{Zn}(\text{p}, x)Y$ reaction was compiled in MS Excel. The data was then loaded into Python for regression.² Prior to this, several functions were tested against the compiled data using Logger Pro from Vernier,³ and it was determined that a high degree polynomial fit was appropriate for the interpolation. This could be achieved either through polynomial regression or spline interpolation. Thus three SciPy (Python module) interpolation techniques were used, Polyfit (and Polyval), UnivariateSpline, and InterpolatedUnivariateSpline. After a visual and statistical comparison of all three, it was clear that the polynomial regression (Polyfit) provided both the most accurate and precise fit. The spline interpolations required high levels of smoothing (due to their sensitivity resulting from the large distribution in data) to eliminate noise, but this was at the expense of precision in several areas of the plot. As this average excitation function was needed for further analysis, it was imperative that the plot represented the experimental data as accurately and precisely as possible.

One MS Excel document was used for each individual $^{\text{nat}}\text{Zn}(\text{p}, x)Y$ reaction. In a document, each sheet contained data from one cross section data source, along with a final sheet containing the combined data. The combined data was used for the polynomial regression. The data consisted of proton energies (in MeV) versus the corresponding cross sections (in mb). The proton energies were sorted to be strictly increasing, as Polyfit regression only works for strictly increasing x -values. Using the Pandas module the data was imported from Excel into the Python workbook. According to Table 2.1, the lowest threshold energy for ^{66}Ga production from natural zinc comes from the reaction $^{66}\text{Zn}(\text{p}, \text{n})^{66}\text{Ga}$. The threshold energy of this reaction (minimum proton kinetic energy required) is just below 6.05 MeV. Thus the cross section should be 0 mb below this value. However, this seemed not to be the case according to the data from several sources. While these values contradict theoretical expectations, they fitted the trend quite well and could be explained by experimental and random error. Initially the author considered omitting these values, but resolved

²Python 3.7 - Spyder 3.3.6 Environment.

³Logger Pro was used for the test functions as it has a large list of pre-made functions with automatic fitting. Python was used for the final plotting however due to its versatility.

to include them to account for the uncertainty present in the original experiments. Inclusion of these values resulted then in a threshold energy of around 5 MeV, not too far off the theoretical expectation. This phenomenon (nonzero cross sections below the threshold energy) was also seen in several other reactions, and for similar reasons, all the data was included.

For some of the regressions, a rank warning was given by Python. This occurs when the degree of the polynomial is too high to the extent that the fit may be poorly conditioned to the data. Fortunately, this was not the case within the required energy intervals (typically around 1 MeV to 90 MeV). While there was of course uncertainty in each polynomial regression, the fit was always optimized in the required range. However, the rank warning becomes relevant beyond this range. Therefore, the fit could not be used to predict cross sections outside of this interval. This proved not to be a problem however, as cross section predictions outside of the respective energy ranges were not needed.

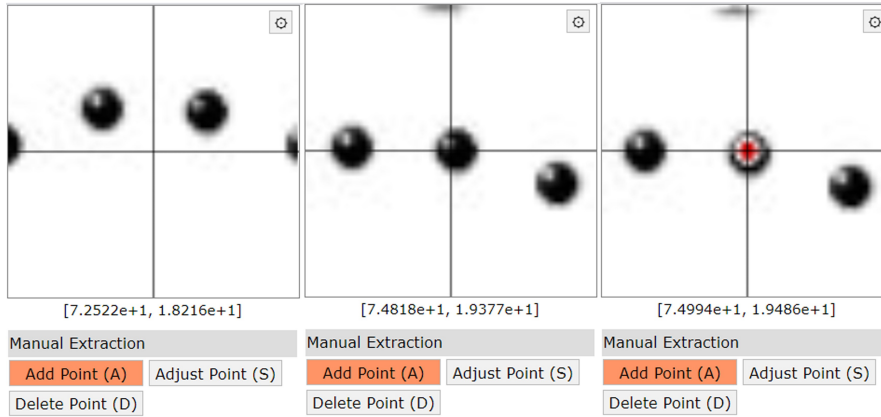


Figure 3.1: Process of selecting data point using Web Plot Digitizer

Another problem found was that in some papers, the cross section data was only provided in graphs, and not in tables. Thus, the data needed to be extracted directly from the graph. To do this, a screenshot of the graph was taken and enlarged (and if necessary, straightened) in Adobe Photoshop. This enlarged image was uploaded onto the online application Web Plot Digitizer[39]. Here the axes of the plot were scaled appropriately, and the data points acquired by clicking on them. This obviously led to some random error in all the data sets which were acquired via this method, but this error was minimized by enlarging the graphs. As the resolution of each graph was very high, the cursor was always placed within a data point. Thus the random error was concluded to be negligible. Furthermore, to increase precision, the sensitivity of the cursor was also reduced to its minimum during this process. This enabled careful placement of the cursor. Fig. 3.1 shows the

process of selecting a data point on Web Plot Digitizer. The first image (left) shows the cursor (intersection between horizontal and vertical lines), the second image (middle) shows the cursor hovering over a data point from the graph (in black), and the final image (right) shows the addition of a data point from the application (in red).

There were also reactions for which there was very limited data. In the few cases where cross section data on $^{\text{nat}}\text{Zn}(p, x)Y$ reactions could not be found, reactions with specific zinc isotopes were used instead. Each cross section was multiplied by the isotopic abundance of said zinc isotope in the sample used in the experiment (typically around 95-99%) and then subsequently multiplied by the abundance of that specific isotope in natural zinc. This method was used by Hermanne et al.[40]. The data sets which were extracted via Web Plot Digitizer and the cross sections which were determined by isotopic abundance multiplication are outlined in Table 4.1 in the results section.

3.2 Determination of Zinc Depth

A 1 mm thick zinc plate will be placed in a water tank, as seen in Fig. 3.2. The water tank is used to degrade the beam. To optimise ^{66}Ga production, it is necessary to determine the best position to place the zinc plate in the water. The proton fluence ϕ in the zinc at different water depths was obtained via external simulations[31]. Within these simulations, the zinc plate was separated into ten imaginary 0.1 mm slices to allow for the fluence data at each slice to be individually analysed. These simulations were done using the Monte Carlo N-Particle Transport (MCNP) code. Simulations were carried out for water depths between 10 mm and 60 mm in steps of 10 mm, with an additional simulation at 55 mm. The proton beam energy was set to 90 MeV, as this energy will be used for the actual experiment. At each water depth, there were ten fluence profiles, one for every 0.1 mm slice in the zinc plate. Initially, the position of the water tank in the simulation was 329.6 cm from the beam exit. Due to scattering in the air and the Beam Ionization Monitor, the total proton fluence at all water depths was very low. Thus the position of the water tank was moved to 50 cm from the beam exit, which resulted in a much larger fluence.

For each profile (i.e. for a specific water depth and zinc slice), the fluence was given for every 0.1 MeV step between 1.05 MeV and 99.95 MeV. Thus, to determine the region of highest ^{66}Ga production, R needed to be calculated using (2.3). Note that the fluence was in $\text{sp}^{-1}\cdot\text{cm}^{-2}$, and as detailed in (2.3), needed to be multiplied by a , the frontal area of the zinc plate. In the simulation, a was set to 6.25 cm^2 , as this is the proposed zinc area for the experiment. A set of points from the averaged ^{66}Ga excitation function was extracted from Python. The data set had energy values from 1.05 MeV to 90.05 MeV, in steps of 0.1 MeV, and the corresponding average

cross section for each energy value. This data was then compiled with the fluence data in MS Excel. Data for each water depth was contained on a separate sheet. R was then calculated for each zinc slice at a certain water depth. The data was then imported into Python, and a plot was made for each water depth. Each plot displayed ten curves, one for every zinc depth, and a plot was made with all the curves combined. From these plots, it was determined that the best position to place the zinc plate in the water would be at 60 mm.

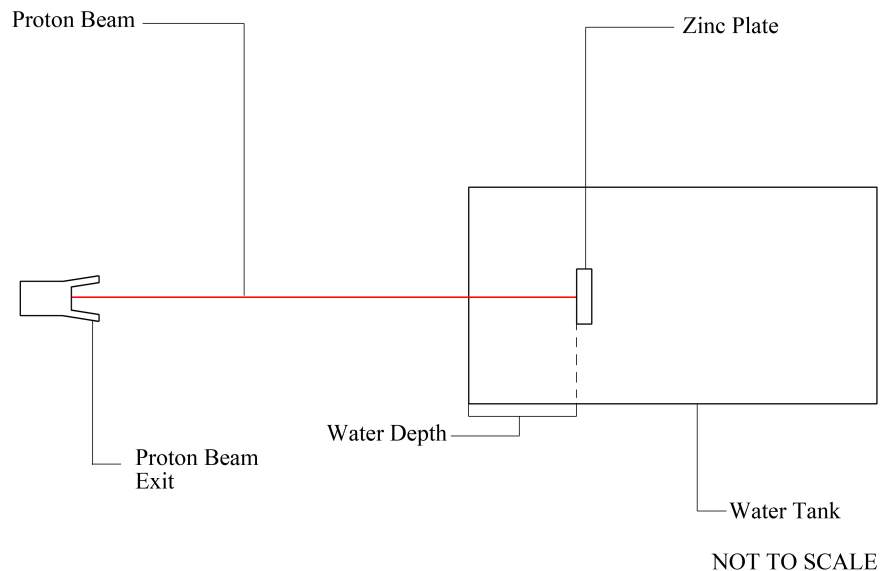


Figure 3.2: Bird's-eye view of proposed experimental setup

To make the data more visually accessible, the R values for each zinc slice were summed over the energies and a plot of R versus zinc depth for each water depth was made. Then, the ten R values for each water depth were summed and a plot of R versus water depth was made. These plots both reaffirmed that 60 mm was the best position to place the zinc plate. Once this was concluded, a similar process was carried out for all the contaminant reactions. However, instead of calculating R for all water depths, only data for the 50 mm, 55 mm, and 60 mm water depths was processed. Plots of R versus zinc depth and R versus water depth were also made for each reaction.

3.3 Gamma Spectra

Before a gamma spectrum could be made, the gamma intensities for each isotope needed to be recorded. These intensities, also known as branching ratios, represent the fraction of particles (of the respective isotope) which decay by a particular mode. A mode in this context pertains to γ -decay of a specific energy. For example, the 1039.231 keV γ -decay line of ^{66}Ga has an intensity of 37%. Thus, if 100 ^{66}Ga particles were to decay in a second (i.e. an activity of 100 Bq), then roughly 37 of those decays would result in 1039.231 keV γ -rays. All the γ -decay intensities were acquired from the Lund/LBNL Nuclear Data Search[41].

Once R was known for each reaction, water depth, and zinc depth, and the gamma intensities for each isotope compiled, a Python function was made to calculate the activities of all the isotopes, and to produce a gamma spectrum. The function takes four arguments; water depth (50 mm, 55 mm, or 60 mm), beam current, irradiation time, and activity measurement time. Using the theoretical treatment as described by (2.3) - (2.14), the function can calculate the activity of each isotope and produce a complete gamma spectrum of all the isotopes. To determine the ideal γ -decay line to be used in the calibration, the function was then run using the proposed values for the actual experiment; a depth of 60 mm, a 30 nA beam current, an irradiation time of 2 hours, and an activity measurement time of both 10 and 12 hours. The Python scripts for this activity function and the ^{66}Ga average excitation function can be found in the Appendix.

Chapter 4

Results

4.1 Average Excitation Functions

Cross section data and the corresponding averaged excitation functions can be found in this section. While not exactly convention, the author found it most practical to list the sources used with their corresponding citations. As the graphs were constructed in Python, there was no way to automatically link a source to the correct citation number. Thus Table 4.1 contains the sources used, in chronological publication order, and their citation numbers in this paper, along with additional notes where relevant.

Table 4.2 and 4.3 contain the relevant reactions, the degrees of the polynomials used in the regressions, and the coefficients of determination R^2 (not to be confused with the number of isotopes produced per starting proton R) and root mean square errors (RMSE) of the respective polynomial fits. Furthermore, in Table 4.3, the RMSE has also been calculated as a percentage of the maximum cross section (respective to each reaction) to standardise the error for comparison. Since the minimum cross section of all the reactions is 0 mb, the maximum cross section is equal to the range of the data. The coefficient of determination and RMSE were calculated using the sklearn module in Python.

The excitation functions can be found after the tables, in Figs. 4.1 - 4.8. It can be seen that in the majority of the graphs there is a peak in the range of 10 MeV to 30 MeV. In Fig. 4.1, there are two peaks in the excitation function for ^{66}Ga . The first at around 12 MeV, and the second at around 35 MeV. Other excitation functions which have similar peaks are Fig. 4.2 ($^{\text{nat}}\text{Zn}(\text{p}, x)^{61}\text{Cu}$) with a peak at around 14 MeV, Fig. 4.5 ($^{\text{nat}}\text{Zn}(\text{p}, x)^{67}\text{Ga}$) with a peak at around 22 MeV, Fig. 4.6 ($^{\text{nat}}\text{Zn}(\text{p}, x)^{68}\text{Ga}$) with a peak at around 12 MeV, and Fig. 4.8 ($^{\text{nat}}\text{Zn}(\text{p}, x)^{65}\text{Zn}$) with a peak at around 25 MeV. It will be seen later that the products of these reactions are the

most prominent contaminants at a water depth of 60 mm.

It is also important to note that in Fig. 4.4 there seems to be a large deviation in the data of Levkovskii (1991)(2) and Kastleiner et al. (1999) from the average fit. The reason for this is that the majority of the $^{\text{nat}}\text{Zn}(p, x)^{67}\text{Cu}$ data was actually taken from $^{68}\text{Zn}(p, x)^{67}\text{Cu}$ and $^{70}\text{Zn}(p, x)^{67}\text{Cu}$ cross section data, and multiplied with both the experimental and natural abundances of ^{68}Zn and ^{70}Zn respectively. In fact, only Bonardi et al. (2005) had cross section data for the $^{\text{nat}}\text{Zn}(p, x)^{67}\text{Cu}$ reaction, while the rest were derived from the aforementioned zinc reactions (see Table 4.1 for further clarification). Fortunately, the peak of the $^{\text{nat}}\text{Zn}(p, x)^{67}\text{Cu}$ excitation function is little over 2 mb. Therefore, while its average fit has the largest error (RMSE is 11.09% as percentage of range), and the data might not be very precise nor accurate, its cross section is sufficiently low throughout such that these errors are negligible.

Table 4.1: References used for cross sections, their inline citations, and additional notes

Cross Section References	Notes
McGee et al. (1970)[42]	Data for reaction $^{68}\text{Zn}(p, x)^{67}\text{Cu}$ Data obtained from Stoll (2002) Data obtained via Web Plot Digitiser
Bonardi & Birattari (1983)[43]	Data obtained from Szelecsenyi (1998) Data obtained via Web Plot Digitiser
Little & Lagunas-Solar (1983)[44]	Data obtained from Kopecky (1990) Data obtained via Web Plot Digitiser
Kopecky (1990)[45]	Data obtained via Web Plot Digitiser
Levkovskii (1991)(1)[46]	Data for reaction $^{68}\text{Zn}(p, x)^{67}\text{Cu}$ Data obtained from Stoll (2002) Data obtained via Web Plot Digitiser
Levkovskii (1991)(2)[46]	Data for reaction $^{70}\text{Zn}(p, x)^{67}\text{Cu}$ Data obtained from Kastleiner (1999) Data obtained via Web Plot Digitiser
Nortier et al. (1991)[47] Hermanne (1994)[48] Szelecsenyi et al. (1998)[48] Hermanne et al. (1999)[40]	Data obtained from Szelecsenyi et al. (1998)
Kastleiner et al. (1999)[49]	Data for reaction $^{70}\text{Zn}(p, x)^{67}\text{Cu}$ Data obtained via Web Plot Digitiser
Stoll et al. (2002)[50] Szelecsenyi et al. (2003)[51] Bonardi et al. (2005)[52] Szelecsenyi et al. (2005)(1)[53] Szelecsenyi et al. (2005)(2)[54] Szelecsenyi et al. (2005)(3)[55] Tarkanyi et al. (2005)[56] Al-Saleh et al. (2007)[57] Uddin et al. (2007)[58] Asad et al. (2014)[59]	Data for reaction $^{68}\text{Zn}(p, x)^{67}\text{Cu}$ Data obtained via Web Plot Digitiser

Table 4.2: Polynomial degrees used in regression and corresponding coefficients of determination

Reaction	Degree of Polynomial Used in Regression	Coefficient of Determination R^2
${}^{\text{nat}}\text{Zn}(\text{p}, x)^{61}\text{Cu}$	17	0.980
${}^{\text{nat}}\text{Zn}(\text{p}, x)^{64}\text{Cu}$	4	0.849
${}^{\text{nat}}\text{Zn}(\text{p}, x)^{67}\text{Cu}$	8	0.882
${}^{\text{nat}}\text{Zn}(\text{p}, x)^{66}\text{Ga}$	19	0.918
${}^{\text{nat}}\text{Zn}(\text{p}, x)^{67}\text{Ga}$	22	0.975
${}^{\text{nat}}\text{Zn}(\text{p}, x)^{68}\text{Ga}$	25	0.996
${}^{\text{nat}}\text{Zn}(\text{p}, x)^{62}\text{Zn}$	11	0.975
${}^{\text{nat}}\text{Zn}(\text{p}, x)^{65}\text{Zn}$	8	0.962

Table 4.3: RMSEs for each polynomial fit

Reaction	RMSE (mb)	Maximum Cross Section (mb)	RMSE as a Percentage of Max. Cross Section (%)
${}^{\text{nat}}\text{Zn}(\text{p}, x)^{61}\text{Cu}$	3.03	77.78	3.90
${}^{\text{nat}}\text{Zn}(\text{p}, x)^{64}\text{Cu}$	2.39	24.88	9.61
${}^{\text{nat}}\text{Zn}(\text{p}, x)^{67}\text{Cu}$	0.24	2.20	11.09
${}^{\text{nat}}\text{Zn}(\text{p}, x)^{66}\text{Ga}$	12.14	172.30	7.05
${}^{\text{nat}}\text{Zn}(\text{p}, x)^{67}\text{Ga}$	7.68	153.00	5.02
${}^{\text{nat}}\text{Zn}(\text{p}, x)^{68}\text{Ga}$	3.28	155.90	2.10
${}^{\text{nat}}\text{Zn}(\text{p}, x)^{62}\text{Zn}$	2.46	50.30	4.89
${}^{\text{nat}}\text{Zn}(\text{p}, x)^{65}\text{Zn}$	13.25	228.24	5.80

$^{\text{nat}}\text{Zn}(p, x)^{66}\text{Ga}$ Excitation Function

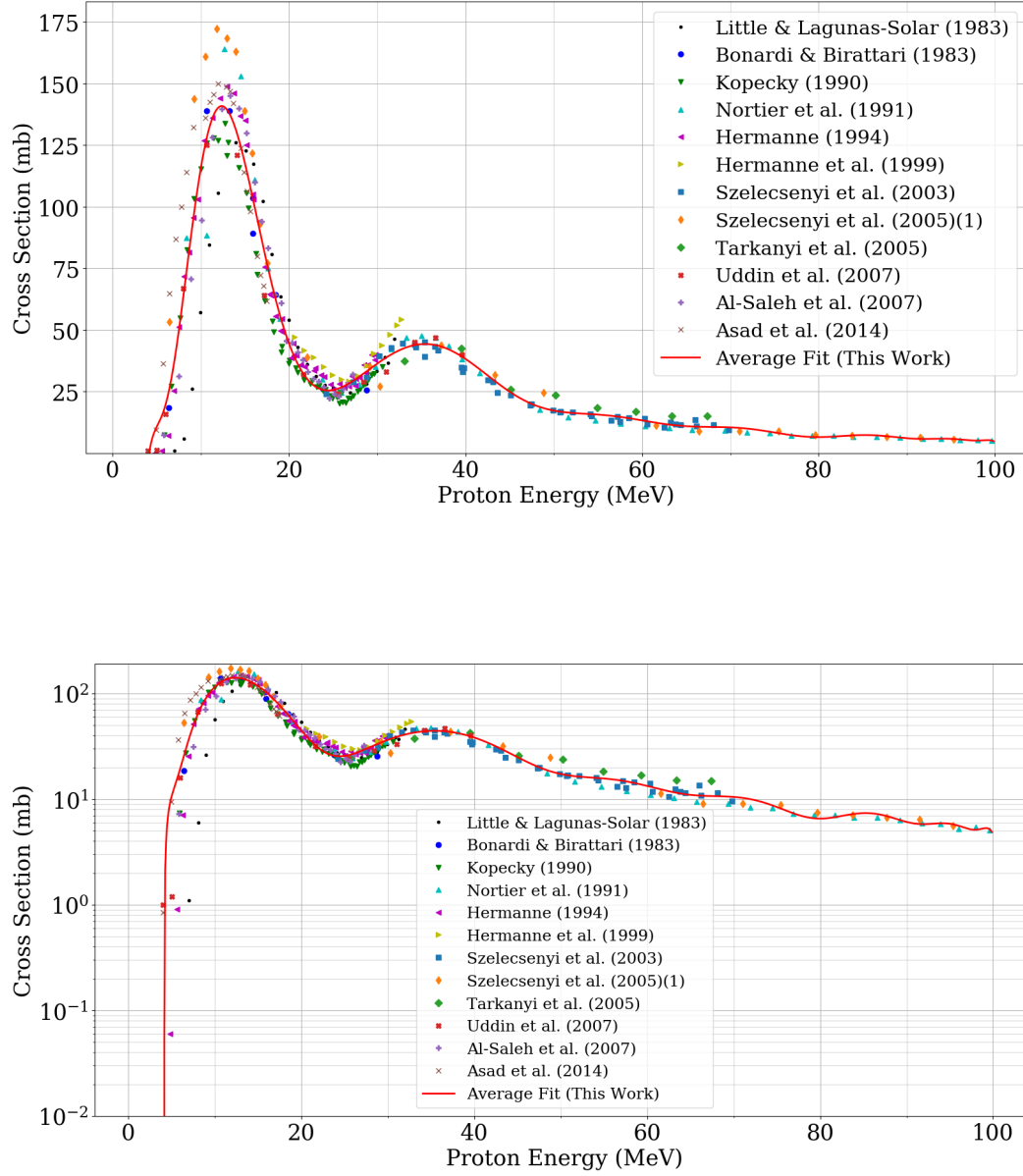


Figure 4.1: Excitation function for the $^{\text{nat}}\text{Zn}(p, x)^{66}\text{Ga}$ reaction: linear vertical scale (upper graph) and logarithmic vertical scale (lower graph)

$^{\text{nat}}\text{Zn}(p, x)^{61}\text{Cu}$ Excitation Function

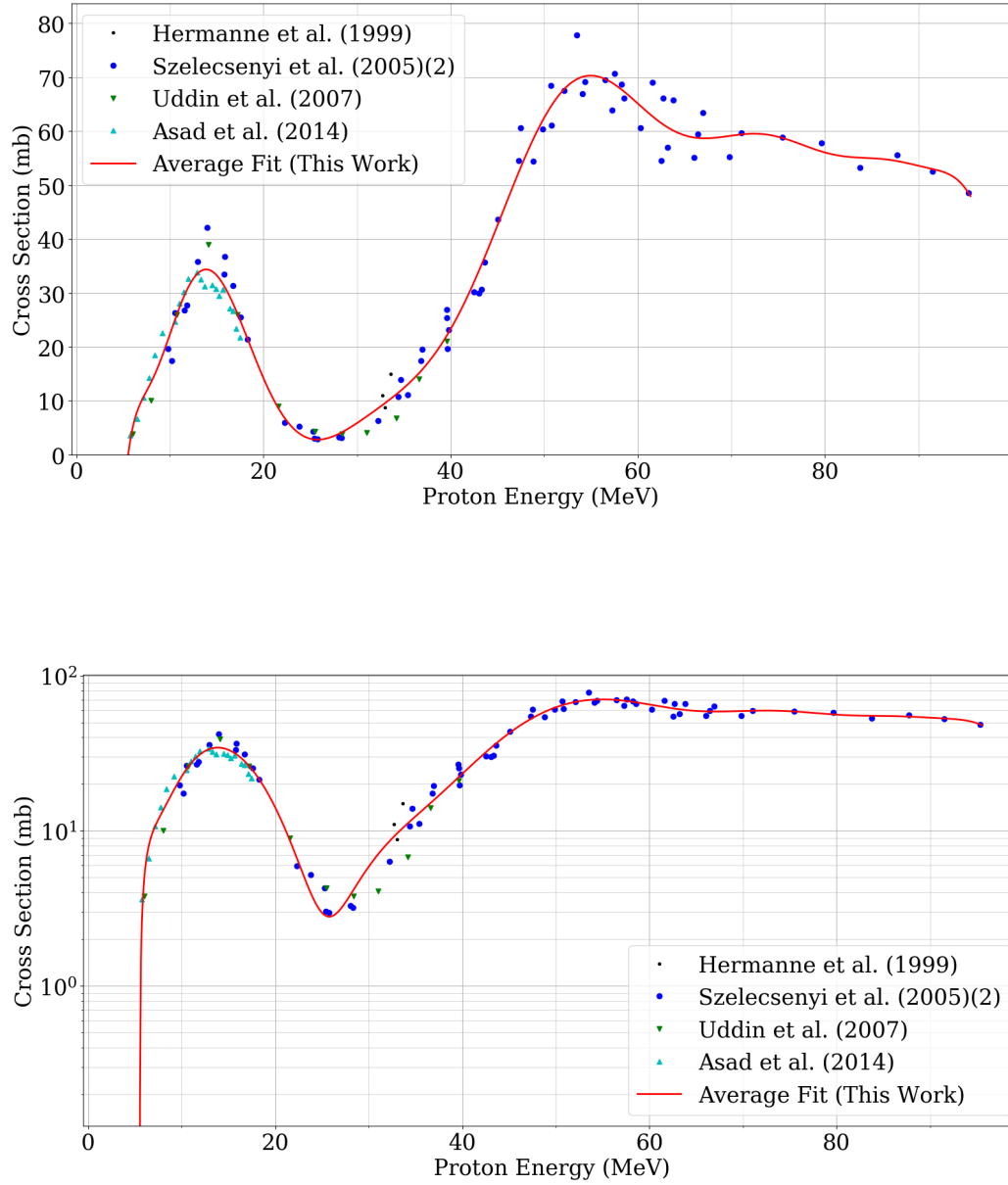


Figure 4.2: Excitation function for the $^{\text{nat}}\text{Zn}(p, x)^{61}\text{Cu}$ reaction: linear vertical scale (upper graph) and logarithmic vertical scale (lower graph)

$^{\text{nat}}\text{Zn}(p, x)^{64}\text{Cu}$ Excitation Function

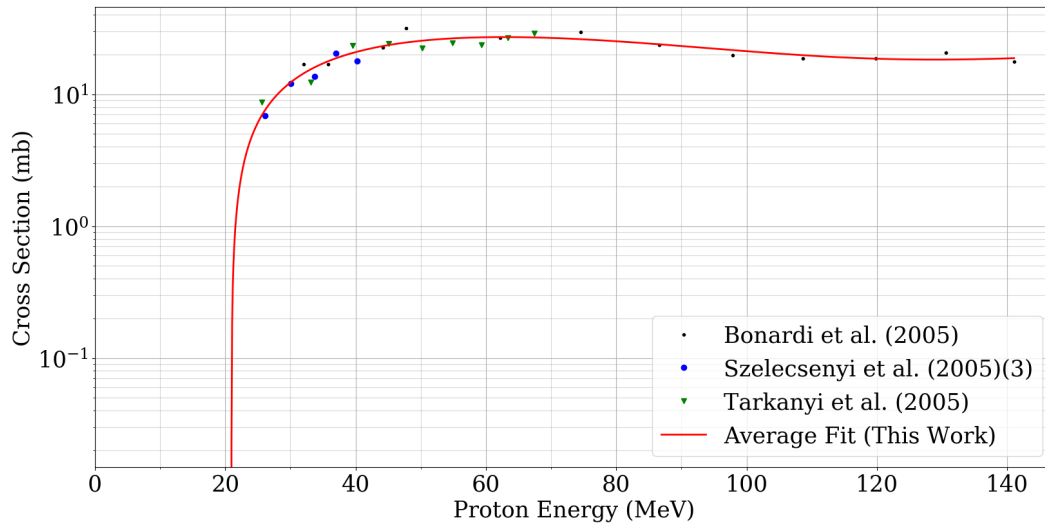
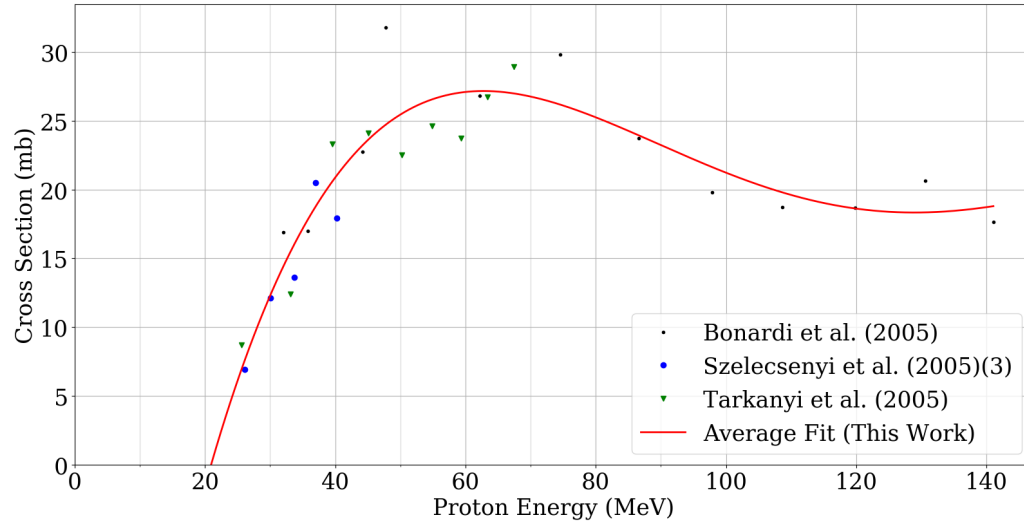


Figure 4.3: Excitation function for the $^{\text{nat}}\text{Zn}(p, x)^{64}\text{Cu}$ reaction: linear vertical scale (upper graph) and logarithmic vertical scale (lower graph)

$^{\text{nat}}\text{Zn}(p, x)^{67}\text{Cu}$ Excitation Function

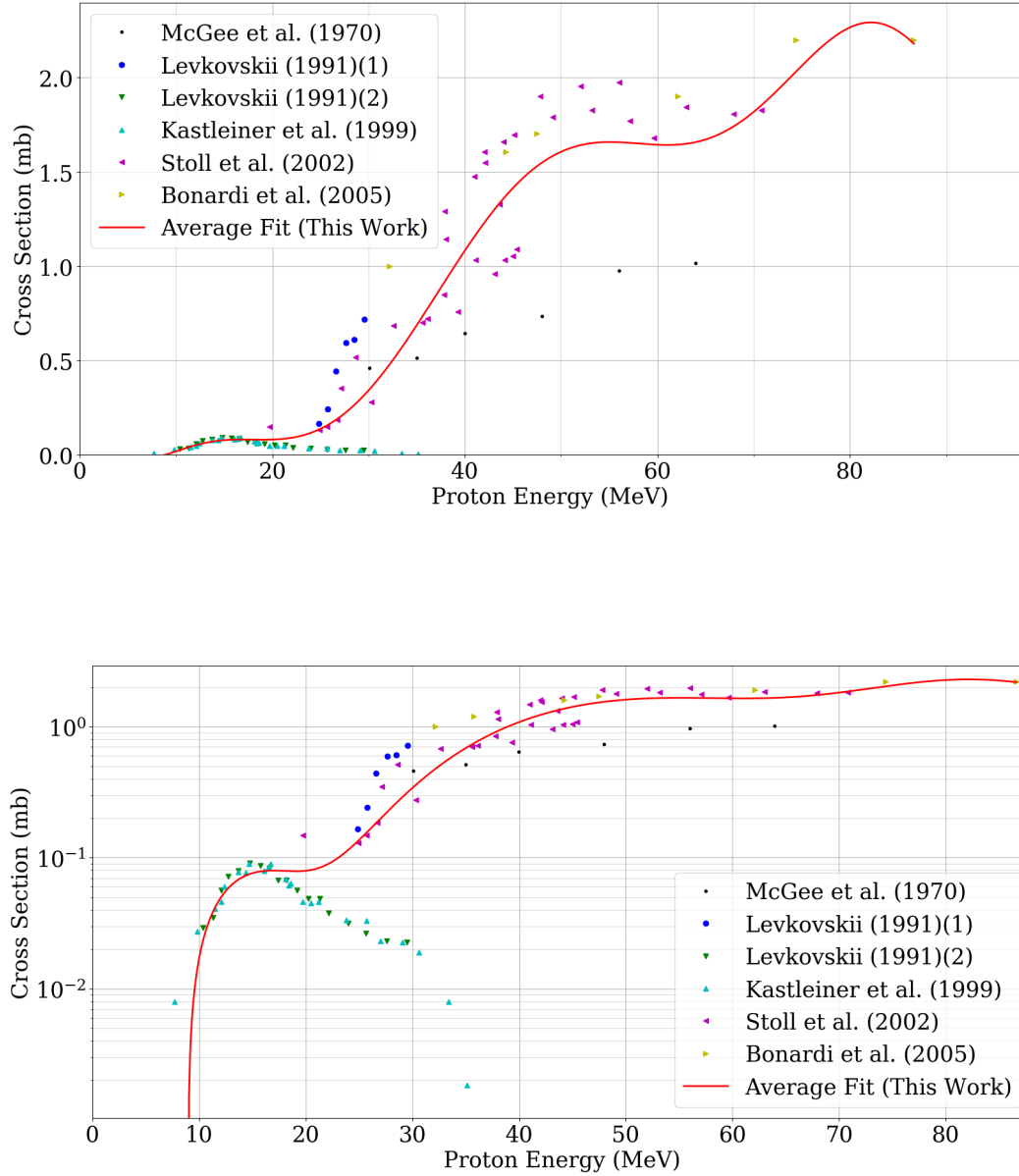


Figure 4.4: Excitation function for the $^{\text{nat}}\text{Zn}(p, x)^{67}\text{Cu}$ reaction: linear vertical scale (upper graph) and logarithmic vertical scale (lower graph)

$^{\text{nat}}\text{Zn}(p, x)^{67}\text{Ga}$ Excitation Function

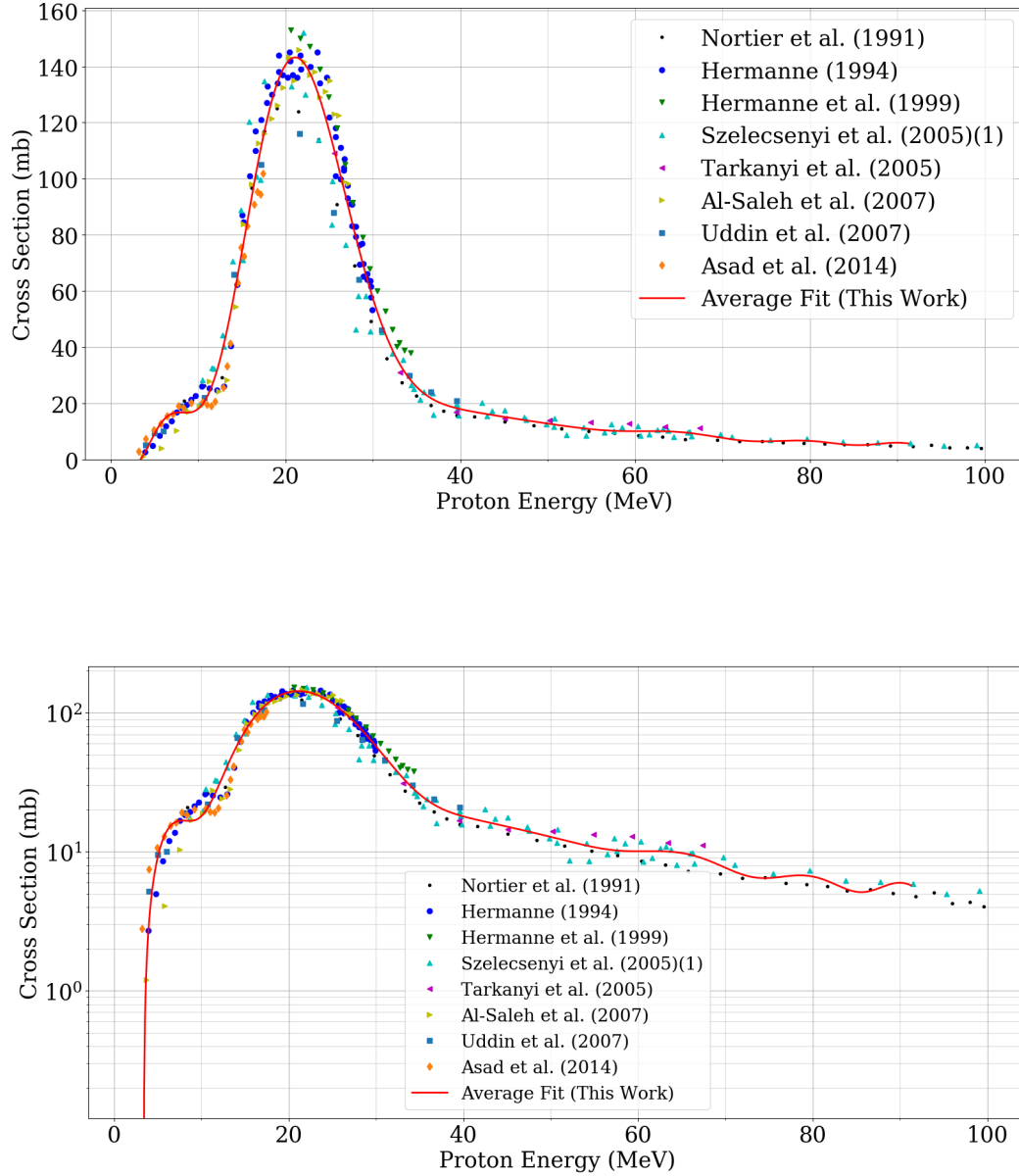


Figure 4.5: Excitation function for the $^{\text{nat}}\text{Zn}(p, x)^{67}\text{Ga}$ reaction: linear vertical scale (upper graph) and logarithmic vertical scale (lower graph)

$^{\text{nat}}\text{Zn}(p, x)^{68}\text{Ga}$ Excitation Function

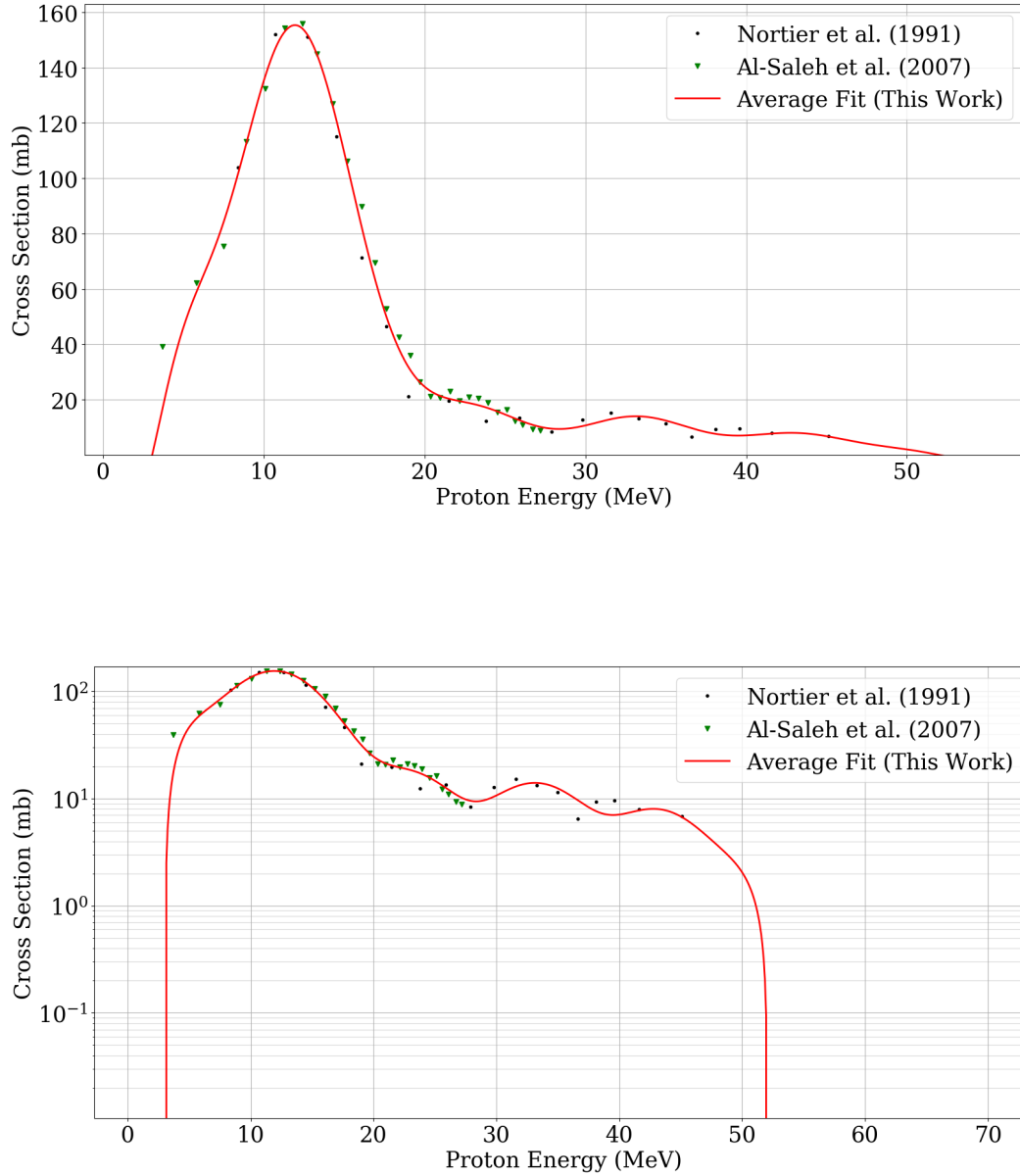


Figure 4.6: Excitation function for the $^{\text{nat}}\text{Zn}(p, x)^{68}\text{Ga}$ reaction: linear vertical scale (upper graph) and logarithmic vertical scale (lower graph)

$^{\text{nat}}\text{Zn}(p, x)^{62}\text{Zn}$ Excitation Function

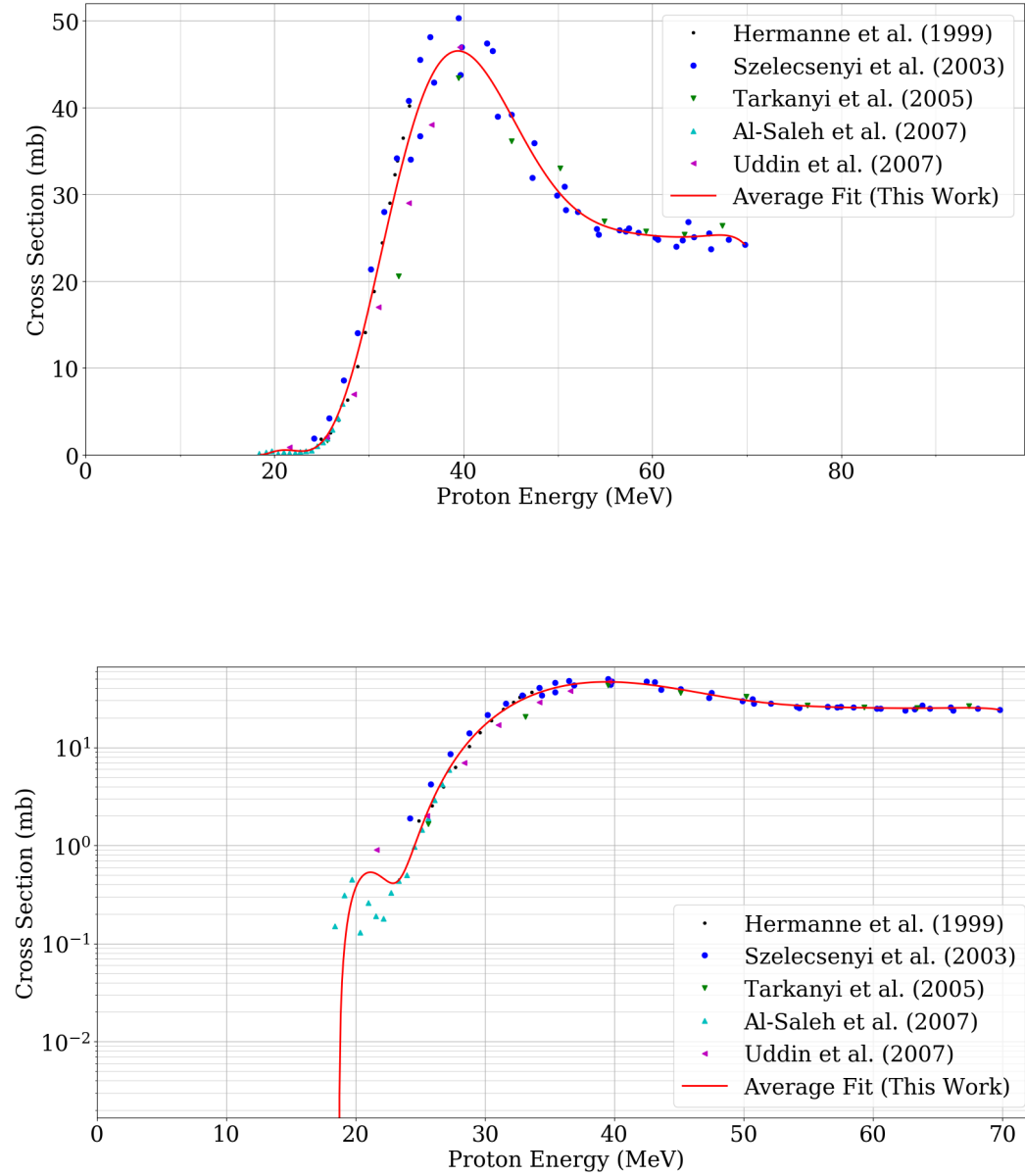


Figure 4.7: Excitation function for the $^{\text{nat}}\text{Zn}(p, x)^{62}\text{Zn}$ reaction: linear vertical scale (upper graph) and logarithmic vertical scale (lower graph)

$^{\text{nat}}\text{Zn}(p, x)^{65}\text{Zn}$ Excitation Function

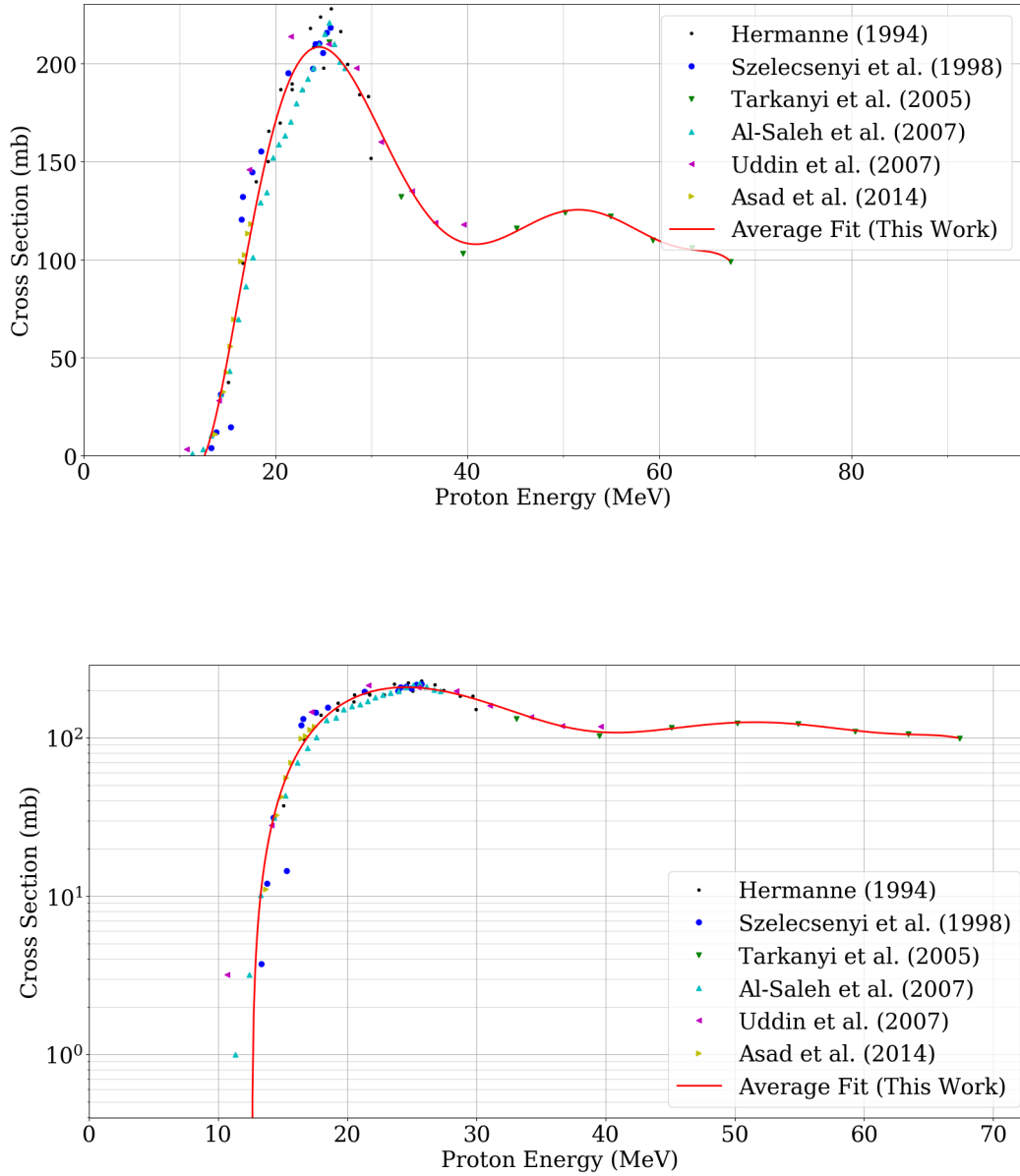


Figure 4.8: Excitation function for the $^{\text{nat}}\text{Zn}(p, x)^{65}\text{Zn}$ reaction: linear vertical scale (upper graph) and logarithmic vertical scale (lower graph)

4.2 ^{66}Ga Production Rates and Water Depth

As mentioned prior, a data set of 1.05 MeV to 90.05 MeV in steps of 0.1 MeV, and the corresponding cross section at each step, was obtained from the average fit as seen in Fig. 4.1. Fluence profiles of the zinc plate at different water depths were acquired via simulations[31]. Simulations were ran for seven water depths, with each water depth having fluence profiles for (imaginary) 0.1 mm slices in the 1 mm zinc plate. The proton beam energy was set to 90 MeV, and the water tank was placed 50 cm from the proton beam exit. R was calculated using (2.3). From the following results, it is clear to see that a water depth of 60 mm is the best position for the zinc plate to obtain the highest ^{66}Ga production.

Fig. 4.9 shows R (for ^{66}Ga) as a function of proton energy, for ten zinc depths, at a water depth of 60 mm. Fig. 4.10 shows the curves of all the water depths with each water depth labelled. Figs. 4.11 - 4.16 show R (for ^{66}Ga) versus proton energy distributions for the remaining water depths. It is interesting to note that in Fig. 4.10, as the water depth increases, the energy distributions widen. This is an example of energy straggling.

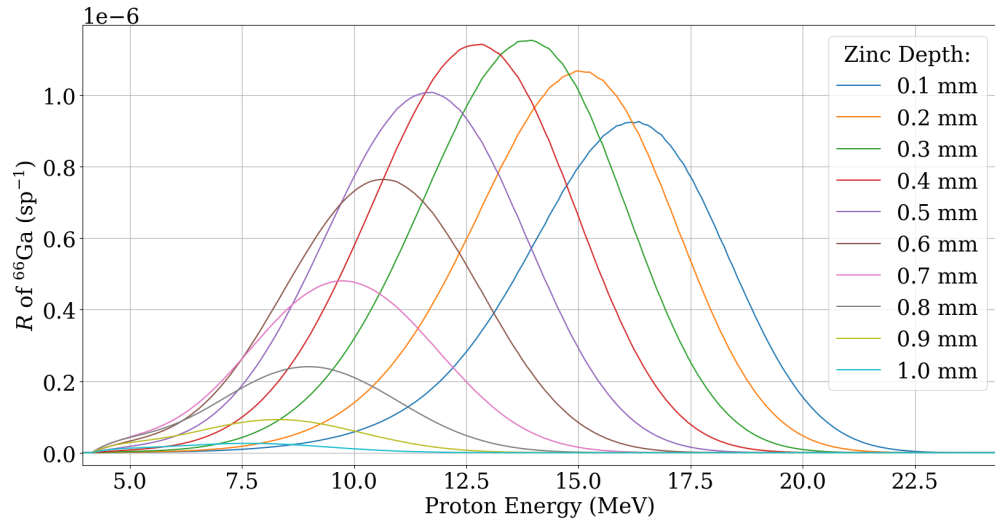


Figure 4.9: R versus proton energy at a water depth of 60 mm for ^{66}Ga

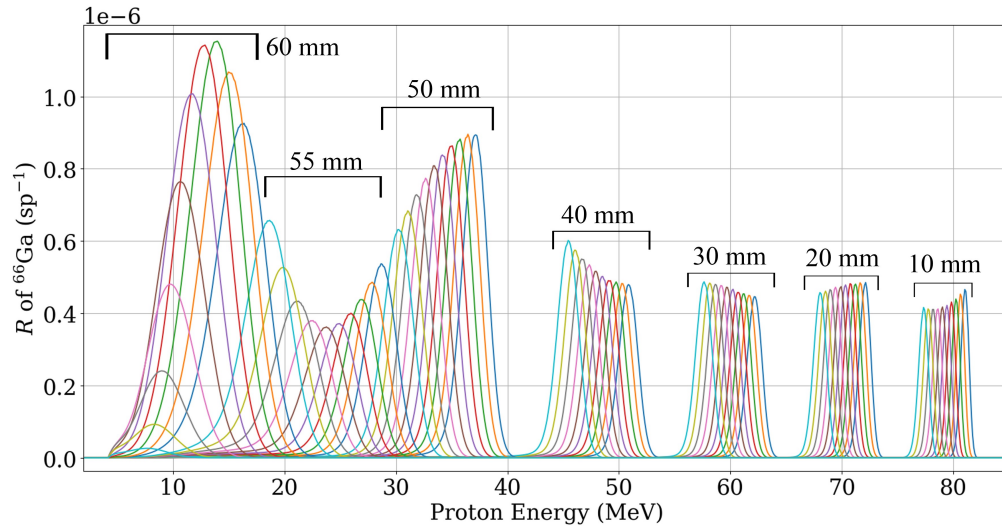


Figure 4.10: R versus proton energy for all water depths for ^{66}Ga

R versus Proton Energy Distributions for ^{66}Ga

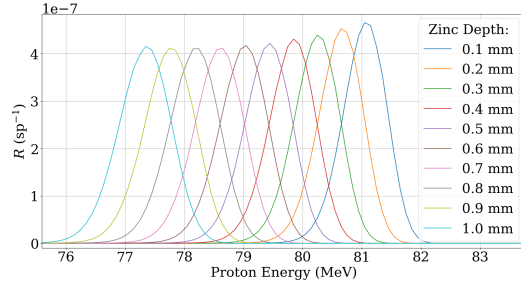


Figure 4.11: Water Depth of 10 mm

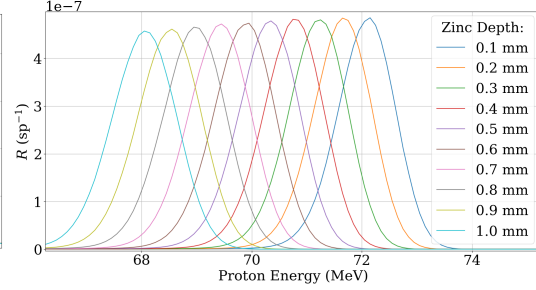


Figure 4.12: Water Depth of 20 mm

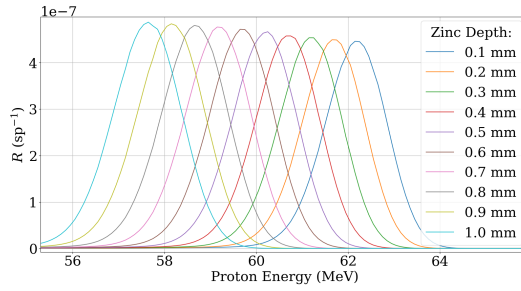


Figure 4.13: Water Depth of 30 mm

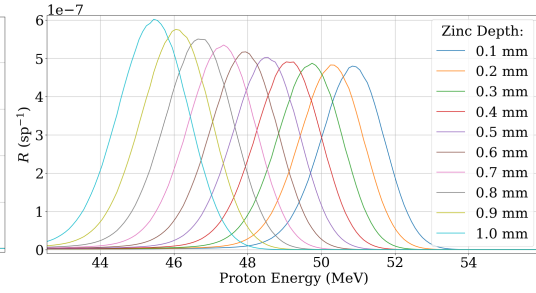


Figure 4.14: Water Depth of 40 mm

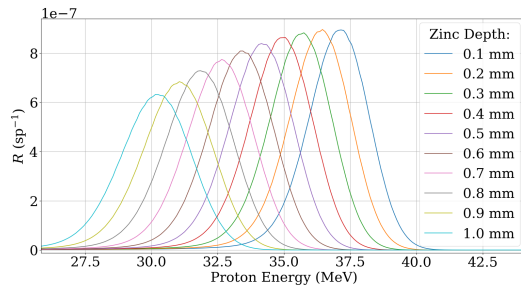


Figure 4.15: Water Depth of 50 mm

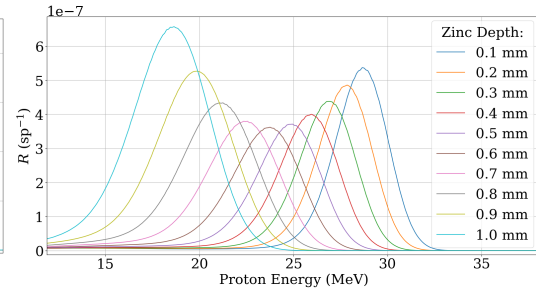


Figure 4.16: Water Depth of 55 mm

CHAPTER 4. RESULTS

To make the data more visually accessible, the R values for each zinc depth (i.e. the normal distribution curves) were summed and each water depth was plotted. This can be seen in Fig. 4.17. The R values for each water depth were then summed and plotted as a function of water depth. This can be seen in Fig. 4.18. Note that the R values have been converted from sp^{-1} to $\text{nA}^{-1} \cdot \text{h}^{-1}$. From this point onward, per nanoampere hour will be used in place of per starting proton. Again, it is easy to see that 60 mm is the optimum position.

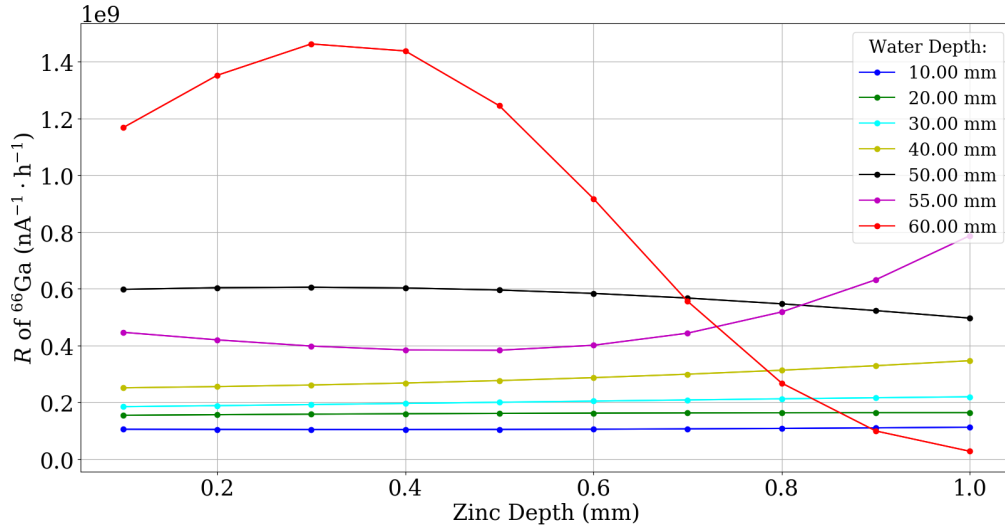


Figure 4.17: R versus zinc depth for each water depth for ^{66}Ga

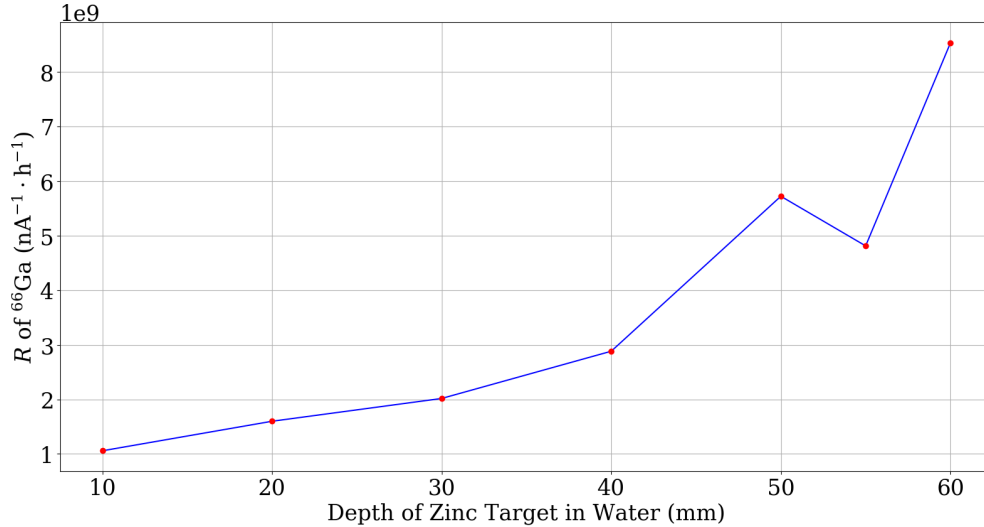


Figure 4.18: R versus water depth for ^{66}Ga

4.3 Contaminant Production

Once it had been determined that 60 mm is the optimum water depth, a similar process was carried out for the contaminants. However, as 50 mm, 55 mm, and 60 mm were the most productive depths, only these were considered. From each averaged excitation function (red line in Figs. 4.2 - 4.8) a set of cross sections were taken. The majority of the data sets had proton energies ranging from 1.05 MeV to 90.05 MeV, in steps of 0.1 MeV. However, for the $^{\text{nat}}\text{Zn}(p, x)^{62}\text{Zn}$ and $^{\text{nat}}\text{Zn}(p, x)^{65}\text{Zn}$ reactions, the excitation functions ended before 90.05 MeV and there was not enough data to predict their behaviour. Fortunately, this was not a problem as the fluence between 50 mm and 60 mm was always zero above 55 MeV, and there were no excitation function cutoffs below 60 MeV. Thus even if the cross section data were available, R would simply be zero.

Figs. 4.19 - 4.21 show R as a function of zinc depth for all the products, for the water depths of 50 mm, 55 mm, and 60 mm respectively. Fig. 4.22 shows R for all the products at each water depth, with a linear vertical scale (upper graph) and a logarithmic vertical scale (lower graph). From the graphs it is clear to see that ^{67}Ga , ^{68}Ga , ^{61}Cu , and ^{65}Zn are the most prominent contaminants.

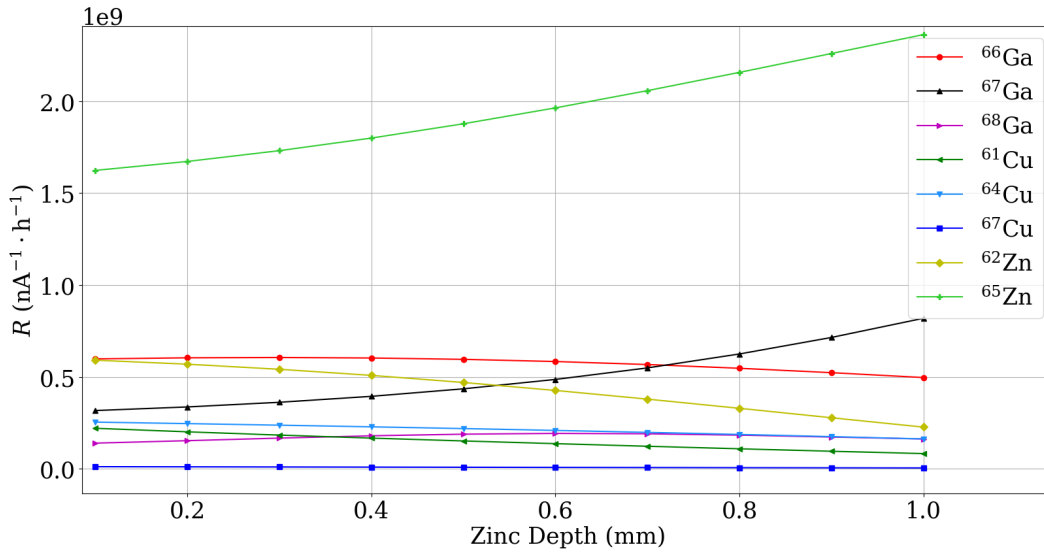


Figure 4.19: R versus zinc depth for all products at a water depth of 50 mm

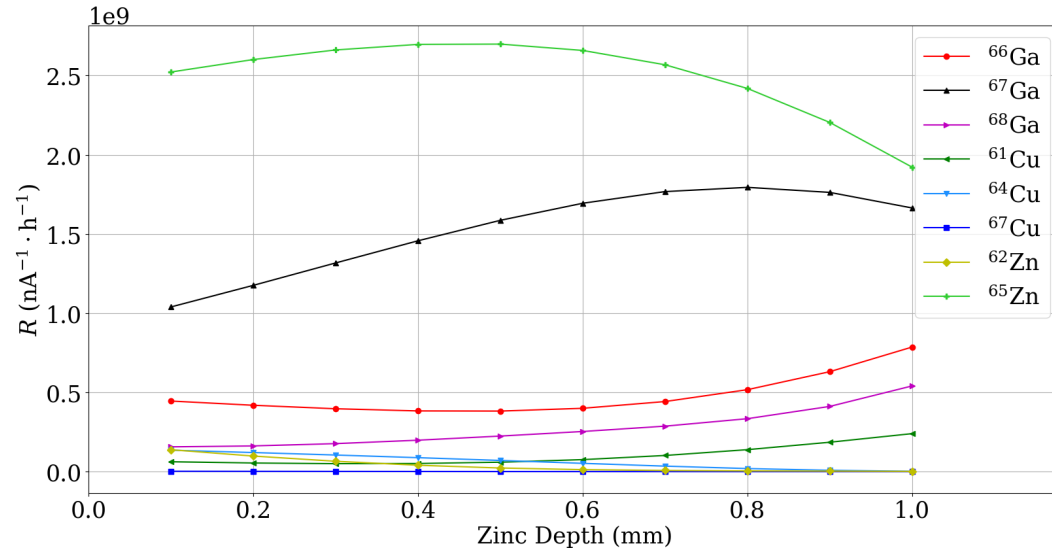


Figure 4.20: R versus zinc depth for all products at a water depth of 55 mm

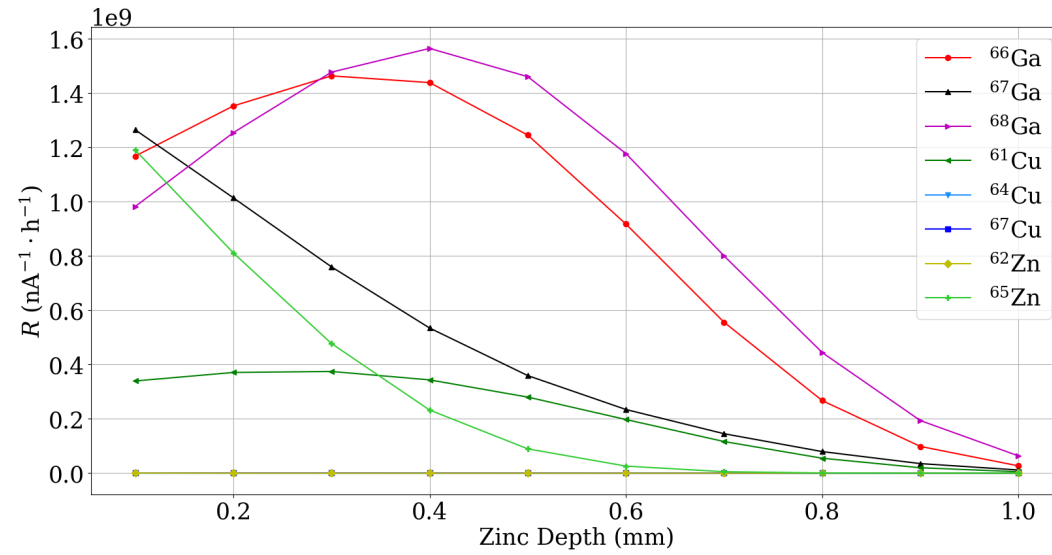


Figure 4.21: R versus zinc depth for all products at a water depth of 60 mm

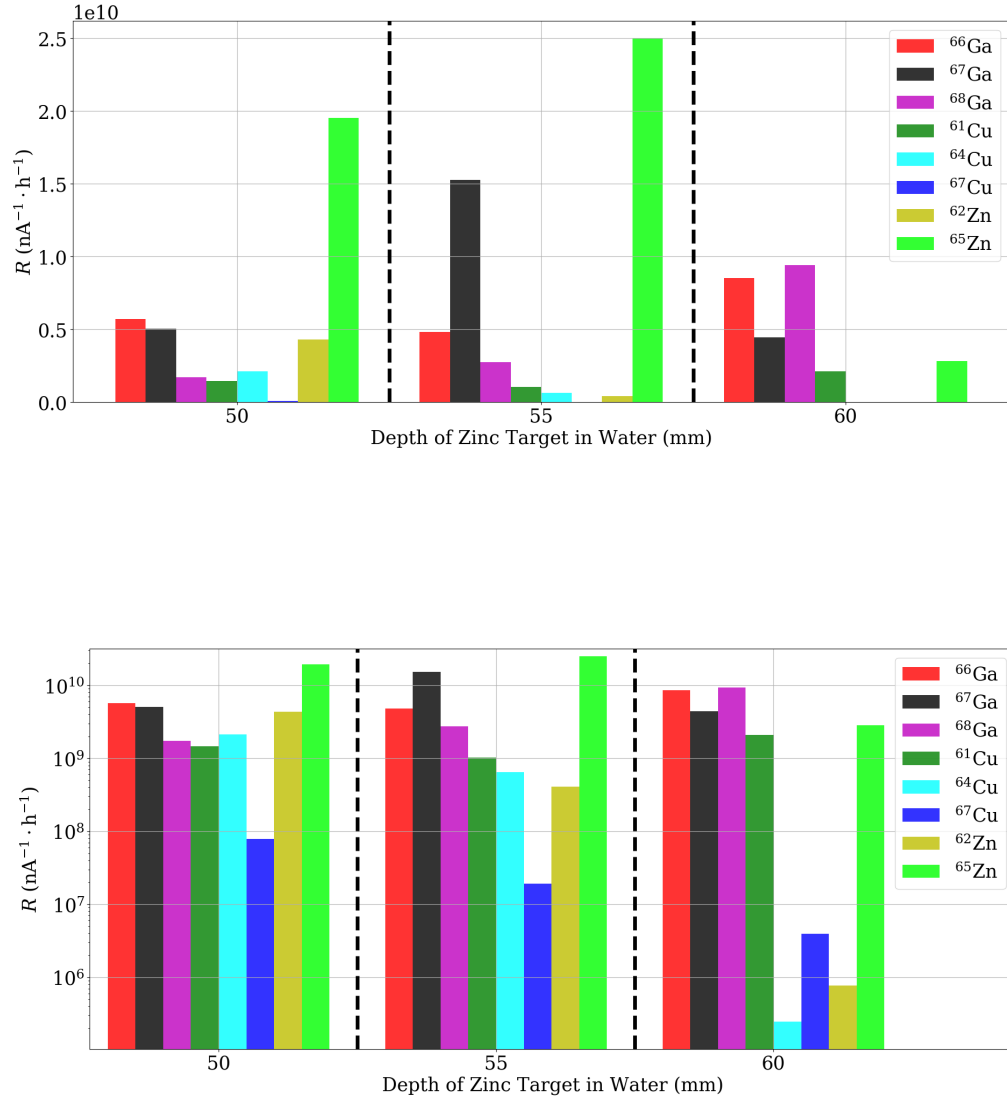


Figure 4.22: R versus water depth for all products: linear vertical scale (upper graph) and logarithmic vertical scale (lower graph)

4.4 Activities and γ -Spectra

As mentioned prior, once R was determined for all the products, a function was written to determine the activity of each isotope and produce a γ -spectrum. The function has four arguments; water depth (50 mm, 55 mm, or 60 mm), beam current, irradiation time, and the activity measurement time. For the final results, the water depth was set to 60 mm, the beam current to 30 nA, the irradiation time to 2 hours, and the activity measurement time to both 10 and 12 hours. Note that the activity measurement time is measured from the start of the irradiation. For example, an activity measurement time of 10 hours means it was taken 8 hours after the end of a 2 hour irradiation session. From Figs. 4.23 and 4.24 it is clear to see that the 1039.231 keV γ -decay line is the most prominent and also relatively free of interference. Thus, it is concluded that this is the line which should be used for the calibration.

Table 4.4: Activities for a water depth of 60 mm, beam current of 30 nA, and irradiation time of 2 hours

Activity Measurement Time (h)	Isotope	Activity (Bq)
10	Ga-66	5.39×10^6
	Ga-67	6.05×10^5
	Ga-68	4.08×10^5
	Cu-61	1.13×10^6
	Cu-64	1.37×10^2
	Cu-67	6.61×10^2
	Zn-62	4.88×10^2
	Zn-65	5.58×10^3
12	Ga-66	4.65×10^6
	Ga-67	5.94×10^5
	Ga-68	1.19×10^5
	Cu-61	7.47×10^5
	Cu-64	1.23×10^2
	Cu-67	6.46×10^2
	Zn-62	4.20×10^2
	Zn-65	5.58×10^3

Water Depth: 60 mm — Beam Current: 30 nA — Irradiation Time: 2 h

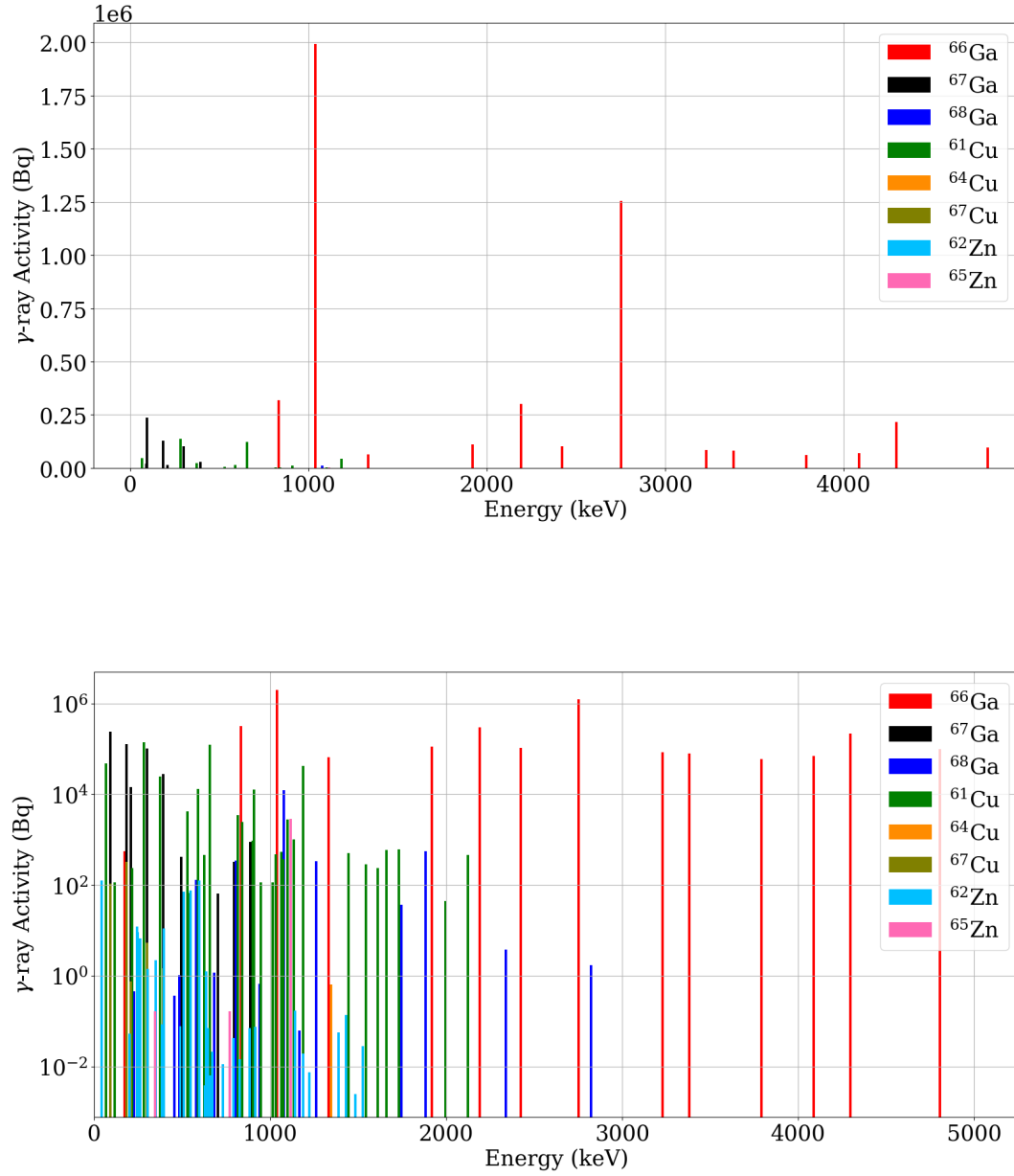


Figure 4.23: γ -ray activity at activity measurement time of 10 hours: linear vertical scale (upper graph) and logarithmic vertical scale (lower graph)

Water Depth: 60 mm — Beam Current: 30 nA — Irradiation Time: 2 h

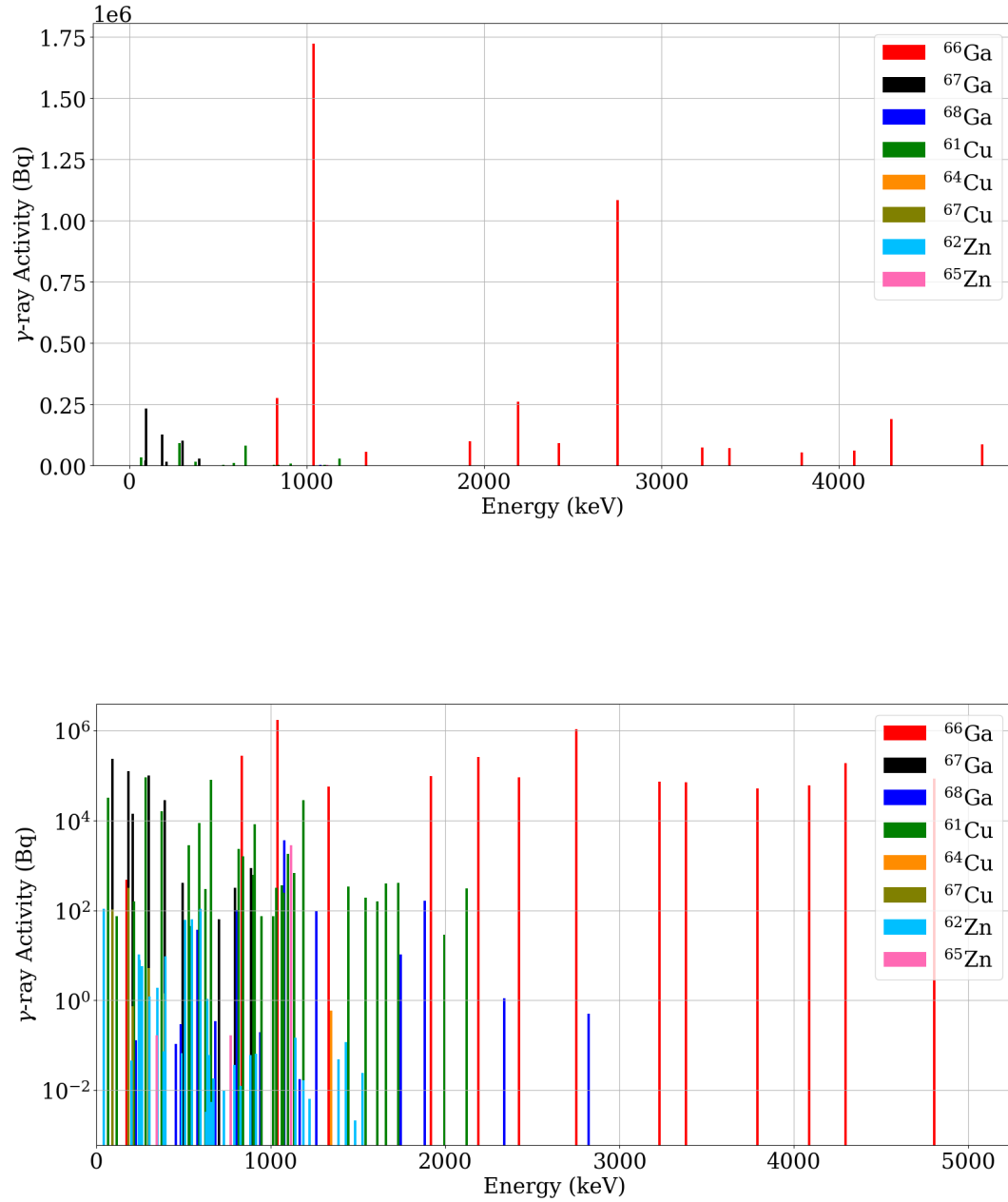


Figure 4.24: γ -ray activity at activity measurement time of 12 hours: linear vertical scale (upper graph) and logarithmic vertical scale (lower graph)

Chapter 5

Discussion

It is clear to see from the results that during the proposed ^{66}Ga production experiment, a water depth of 60 mm should be chosen for the position of the zinc plate. This is due to 60 mm being the water depth with the highest ^{66}Ga production. Furthermore, it is also clear to see that the 1039.231 keV gamma line of ^{66}Ga should be used for the activity determination. Reinforcing this is the fact that the HPGe detector which will be used to determine the activity of the source has an efficiency which drastically decreases above 2 MeV. Thus, the 1039.231 keV line is the most appropriate for the activity determination, due to its high intensity (37%) and activity, its energy being within the suitable range of both detectors, and the line being clear from any major γ -decay interference. However, there were a few problems present in the research conducted in this paper which need to be addressed before any finalising conclusions can be made.

First and foremost is the fact that the majority of the research conducted in this paper was either theoretical or computational. Experimental results were solely used during the excitation function analysis, and even then, the results were taken from other research and further processed in this paper (i.e. averaging of the excitation function using polynomial regression techniques). This is not to say that the methods used in this paper are invalid, but before anything can be concretely said about them, this research should be considered with slight skepticism. Thankfully, plans are underway to verify the research done in this paper. In the likely event that this research is indeed valid, there are exciting inferences which can be made. Validating this research would imply that the excitation function analyses, paired with the MCNP simulation data and γ -ray intensity data, can be used in the future in preparation for similar experiments. It seems to be a relatively common occurrence in which a particle beam must be degraded (not necessarily with water) before it hits its intended target. Thus, to prevent waste of both beam time and the target material itself, it would be a good idea to utilise the methods from this research to

optimise the amount of degrading material required, and if necessary, analyse the resulting spectra, before actually carrying out the experiment. Again however, this is on the assumption that the research is valid.

If the research presented in this paper is not valid (by means of experimental refutation), then it will be revised and the relevant problems hopefully determined. Nevertheless, beyond the lack of experimental proof, there were still a few considerable problems present. A rather obvious one is the lack of any real error analysis. The most extensive error analysis done in this paper was the ascertainment of the coefficients of determination (R^2 values) and root mean square errors (RMSEs) in the excitation function fitting. The R^2 values for the majority of the reactions were above 0.9, with the exception of $^{\text{nat}}\text{Zn}(p, x)^{64}\text{Cu}$ and $^{\text{nat}}\text{Zn}(p, x)^{67}\text{Cu}$ which had R^2 values of 0.849 and 0.882 respectively (still relatively good values). From this it can be said that all the fits were quite precise, and seemed to reflect the data well. Unfortunately, while the R^2 values were used to manipulate and hone the fits with statistical precision, they were not used in any other analysis.

There are also many caveats in using R^2 analysis, and a few of them were clear in the regression techniques used in this paper. For some of the reactions, the polynomial fit had a very high degree. This resulted in a very high (i.e. supposedly very good) R^2 value, but beyond the given range of data, the polynomial behaved erratically (a consequence of over fitting). For example, after crossing through the final data point, some functions would rapidly increase, or fluctuate wildly about the x -axis. Therefore, while the fits were very well adjusted within a range of data, they could not be used in predicting the behaviour of the excitation function outside of this range. In the context of the theory, this is fine, as cross sections for proton-nuclei reactions are based on highly complicated and probability-oriented physics. That is why they must be determined experimentally or computationally. Regardless, the point still holds that the polynomial fits were poorly conditioned outside the required data range. The only way to properly remedy this is by collecting more data or running simulations for the required proton-nuclei reaction. As mentioned prior, the ALICE2017 and EMPIRE-II codes can be used for this.

Another caveat present in the use of R^2 analysis is that it does not indicate whether the correct regression was used. As mentioned prior, a polynomial regression was used after testing the $^{\text{nat}}\text{Zn}(p, x)^{66}\text{Ga}$ cross section data with several different functions and interpolation techniques. The regression technique seemed to also work for the other reactions, so was used for all the fits. While polynomial fitting seemed the most appropriate at the time, and the R^2 values seem to reflect that, other techniques that were not tested or were abandoned early might have actually resulted in better fits. Spline interpolation, while tested, was abandoned after a few cases of severe over fitting. However, if more time was given to refine the interpolation technique, and considering that spline interpolation is done through combining polynomials of different degrees, the author believes that for some curves it would have

been a better choice. Despite the caveats, the polynomial fits were still a relatively good choice and represented the data quite well.

The RMSEs, and more importantly their values relative to the respective maximum cross sections, indicate that the final results are probably of the right order of magnitude, but do not reflect the actual numerical values. For example, the activity of ^{66}Ga in Table 4.4 at an activity measurement time of 10 hours is given by 5.39×10^6 Bq. However, the RMSE of the fit as a percentage of the maximum cross section was 7.05%. This means that the spread of data (as easily seen in Fig. 4.1) was quite large. Thus, if a hypothetical detector with 100% efficiency was able to detect all the radiation (i.e. a 4π steradian detection area) coming from a recently irradiated natural zinc source with the same specifications as detailed in Table 4.4, it would still not detect 5.39×10^6 Bq. It will definitely detect an activity on the order of 10^6 , but the numerical values cannot be accurately discerned, in part due to the presence of a nonzero RMSE. However, even if the RMSE was 0 and the R^2 value 1, the final results must still be interpreted as order of magnitude estimates due to the fact that radioactive decay is a stochastic process and thus can never be determined with full accuracy in a theoretical context. Be that as it may, an order of magnitude estimate is still extremely useful, especially in the context of the proposed ^{66}Ga production experiment. Order of magnitude estimates still enable fully reliable comparisons of production rates and γ -spectra. If experiment verifies the validity of this research (i.e. 60 mm is the most productive water depth and the 1039.231 keV line is the best calibration line), then this method can be used for the optimization of similar experiments and give predictions on the order of magnitude expected for production rates and activities.

There are a few improvements which could be made on the excitation function fitting. First, as mentioned, is further analysing different regression and interpolation techniques to find if there are any with better capabilities than polynomial regression. Another improvement which could have been made would be the propagation of error obtained from the cross section data (i.e. the errors measured by the authors in Table 4.1) for both the cross sections and the proton energies. This could have helped in honing the fits to the data. Preliminary calculations were done to propagate the RMSEs and errors for the proton fluence data when calculating R (using (2.3)). However, as mentioned above, since it is clear that the data obtained from this research should be used to estimate orders of magnitude, and since the error in R was too small to cause any changes in the order of magnitude for any reaction, it was decided best to disregard the errors in R and subsequent errors in the activities. With regards to the error analysis, the conclusion would be that errors could have been used to improve the fitting of the excitation functions, but would not be too productive for the rest of the research as the errors did not affect the orders of magnitude of the final results. The only other computational method used were the simulations for the proton fluence data using MCNP. However, the

author was not involved in the making of these simulations and therefore cannot comment on their functioning.

Despite the problems outlined above, the author hopes that the research presented in this paper will prove fruitful in the future experiments the Medical Physics Group at KVI-CART intends to pursue. In terms of calibrating the NaI(Tl) scintillation detector, the ^{66}Ga source will first be made via proton irradiation on natural zinc. Directly after the irradiation period, a series of measurements will be taken with the NaI(Tl) scintillation detector. The geometry and configuration of the detector with respect to the source will be the same as that of the ^{12}N production experiment. To a good approximation the produced ^{66}Ga source will act as a point source 25 cm away from the NaI(Tl) scintillation detector, similar to the detector geometry used in the simulations mentioned in §2.2.1. The detector will record the number of counts N during a measurement period T . N is then related to the activity A of the source by

$$A = \frac{N}{T \cdot \epsilon \cdot I_\gamma} \quad (5.1)$$

where ϵ is the efficiency of the detector,¹ and I_γ is the intensity or branching ratio of the measured γ -decay line. Once N has been measured with the NaI(Tl) scintillation detector, the count rate (of the 1039.231 keV line) will then be measured with the HPGe detector. The HPGe detector measurement will take place around 10 hours after the end of the irradiation. Since the efficiency of the HPGe detector is known, (5.1) can be used to determine the activity of the ^{66}Ga source. The activity measurement time for the HPGe detector will be recorded, and along with (2.13) and (2.14), the activity at the time of the NaI(Tl) scintillation detector measurement can be determined. Once this activity is known, it is simply a matter of rearranging (5.1) and using the values of N and T as measured by the NaI(Tl) scintillation detector to determine its efficiency. It is important to note that the γ -spectra as presented in Figs. 4.23 - 4.24 are not what is to be expected by the detector count measurements. These graphs display the absolute activities of the source and do not take into account detector efficiency or geometry. Thus, while it is true that the methods (once experimentally verified) used in this research can be used for optimisation and prediction for experiments of a similar nature, the detector efficiencies and geometry must also be taken into account.

An example of the above process is as follows. If measurements from the HPGe detector determine the ^{66}Ga source to have an activity of 5 MBq, and the NaI(Tl) scintillation detector records 60000 counts within 5 minutes (300 seconds) for the 4295.224 keV line², then the efficiency of the NaI(Tl) scintillation detector at this

¹For a specific detector geometry.

²Note that the NaI(Tl) scintillation detector will be used to measure the 4.44 MeV line of ^{12}N , thus the efficiency of the detector around this region must be determined.

energy is around

$$\epsilon = \frac{60000 \text{ counts}}{300 \text{ s} \cdot 5 \text{ MBq} \cdot 0.0404} \approx 1 \times 10^{-3}$$

where the 0.0404 term in the denominator is the branching ratio of the 4295.224 keV line (i.e. $I_\gamma=4.04\%$ [41]).

Chapter 6

Conclusion

In conclusion, if the energy of the proton beam used for the ^{66}Ga production experiment is 90 MeV, the beam degrading water tank should be placed 50 cm from the beam exit and the zinc plate should be placed at a water depth of 60 mm for maximum ^{66}Ga production. The major contaminants which will result from proton irradiation on the natural zinc plate at this position are ^{67}Ga , ^{68}Ga , ^{61}Cu , and ^{65}Zn . Thankfully, these contaminants either have sufficiently short half-lives (e.g. the half-life of ^{68}Ga is 67.6 minutes, thus after 10 hours the majority of the isotope has decayed), sufficiently long half-lives (e.g. ^{65}Zn has a half-life of 244.26 days, resulting in consistently low activity), sufficiently low γ -decay intensities (e.g. the highest γ -ray intensity of ^{61}Cu is 12.2%), or a combination of the former two with the latter. Thus, as can be seen in Figs. 4.23 and 4.24, the ^{66}Ga γ -spectrum seems to dominate, with the best calibration line at 1039.231 keV. This has been concluded to be the best line to use for calibration due to its high intensity (37%) and activity, its energy being within the suitable range of both detectors, and the line being clear from any major γ -decay interference. Note that all results from this paper should be taken as order of magnitude estimates.

It is also worth noting that the research from this paper has yet to be verified experimentally. If it is verified, this implies that the methods used in this paper can be used for future experimental planning in similar proton beam/ isotope production experiments. It is necessary however to account for detector efficiency and geometry when using the γ -spectra presented by this method, as it only presents the absolute activities, and not the activities as measured by the detectors. Nonetheless, it is relatively easy to account for both detector efficiency and geometry.

To finalise, the methods presented in this paper intend to help optimise the experimental set up of the ^{66}Ga production experiment and NaI(Tl) scintillation detector calibration to be carried out by the Medical Physics Group of KVI-CART later in 2020.

Bibliography

- [1] R. R. Wilson, “Radiological Use of Fast Protons,” *Radiology*, vol. 47, no. 5, pp. 487–491, 1946.
- [2] C. Tobias, J. Lawrence, J. Born, R. McCombs, J. Roberts, H. Anger, B. Low-Beer, and C. Huggins, “Pituitary Irradiation With High-Energy Proton Beams: a Preliminary Report,” *Cancer research*, vol. 18, no. 2, pp. 121–134, 1958.
- [3] IBA Dosimetry. (2011) IBA Signs a Contract With Skandionkliniken for the Installation of Scandinavia First Dedicated Proton Therapy Center. [Online]. Available: <https://iba-worldwide.com/content/iba-signs-contract-skandionkliniken-installation-scandinavia-first-dedicated-proton-therapy>. Accessed: 24/04/2020.
- [4] J. Munzenrider, M. Austin-Seymour, P. Blitzner, R. Gentry, M. Goitein, E. Gragoudas, K. Johnson, A. Koehler, P. McNulty, and G. Moulton, “Proton Therapy at Harvard,” *Strahlentherapie*, vol. 161, no. 12, pp. 756–763, 1985.
- [5] Particle Therapy Co-Operative Group (PTCOG). (2020) Particle Therapy Facilities in Clinical Operation. [Online]. Available: <https://www.ptcog.ch/index.php/facilities-in-operation>. Accessed: 24/04/2020.
- [6] S. Yajnik, *Proton Beam Therapy: How Protons Are Revolutionizing Cancer Treatment*. Springer Science & Business Media, 2012, p. 2.
- [7] N. Y. Lee, J. E. Leeman, O. Cahlon, K. Sine, G. Jiang, J. J. Lu, and S. Both, *Target Volume Delineation and Treatment Planning for Particle Therapy*. Springer, 2018.
- [8] S. Yajnik, *Proton Beam Therapy: How Protons Are Revolutionizing Cancer Treatment*. Springer Science & Business Media, 2012, pp. 32-34, 52-56, 66-68, 76-78, 90-91, 98-99, 107-109.
- [9] P. Dendooven, I. Ozoemelum, S. Brandenburg, E. van der Graaf, and M.-J. van Goethem, “Beam Time Proposal Form,” *University of Groningen*, 2019.

BIBLIOGRAPHY

- [10] National Cancer Institute (USA). (2020) Hypofractionated Radiation Therapy. [Online]. Available: <https://www.ptcog.ch/index.php/facilities-in-operation>. Accessed: 24/04/2020.
- [11] D. A. Bush, G. Cheek, S. Zaheer, J. Wallen, H. Mirshahidi, A. Katerelos, R. Grove, and J. D. Slater, “High-Dose Hypofractionated Proton Beam Radiation Therapy Is Safe and Effective for Central and Peripheral Early-Stage Non-Small Cell Lung Cancer: Results of a 12-Year Experience at Loma Linda University Medical Center,” *International Journal of Radiation Oncology, Biology, Physics*, vol. 86, no. 5, pp. 964–968, 2013.
- [12] M.-C. Vozenin, J. H. Hendry, and C. Limoli, “Biological Benefits of Ultra-High Dose Rate FLASH Radiotherapy: Sleeping Beauty Awoken,” *Clinical Oncology*, vol. 31, no. 7, pp. 407–415, 2019.
- [13] V. P. Muriel, “Hypofractionation in Radiotherapy,” *Clinical and Translational Oncology*, vol. 9, no. 1, pp. 21–27, 2007.
- [14] G. Audi, F. Kondev, M. Wang, W. Huang, and S. Naimi, “The NUBASE2016 Evaluation of Nuclear Properties,” *Chinese Physics C*, vol. 41, no. 3, p. 030001, 2017.
- [15] P. Dendooven, H. Buitenhuis, F. Diblen, P. Heeres, A. Biegun, F. Fiedler, M. Van Goethem, E. Van der Graaf, and S. Brandenburg, “Short-Lived Positron Emitters in Beam-On Pet Imaging During Proton Therapy,” *Physics in Medicine & Biology*, vol. 60, no. 23, p. 8923, 2015.
- [16] P. Dendooven, H. Buitenhuis, F. Diblen, P. Heeres, A. Biegun, F. Fiedler, M. van Goethem, E. van der Graaf, and S. Brandenburg, “Corrigendum: Short-lived positron emitters in beam-on pet imaging during proton therapy (2015 phys. med. biol. 60 8923),” *Physics in Medicine & Biology*, vol. 64, no. 12, p. 129501, 2019.
- [17] H. Buitenhuis, F. Diblen, K. Brzezinski, S. Brandenburg, and P. Dendooven, “Beam-on imaging of short-lived positron emitters during proton therapy,” *Physics in Medicine & Biology*, vol. 62, no. 12, p. 4654, 2017.
- [18] G. F. Knoll, *Radiation Detection and Measurement*, 3rd ed. John Wiley & Sons, 2000.
- [19] A. Kamal, *Nuclear Physics*. Springer, 2014.
- [20] S. D’Auria, *Introduction to Nuclear and Particle Physics*. Springer, 2019.
- [21] E. De Sanctis, S. Monti, and M. Ripani, *Energy from Nuclear Fission*, 1st ed., ser. Undergraduate Lecture Notes in Physics. Springer, 2016.
- [22] Nuclear Power for Everybody. (2020) Principle of Operation of HPGe

BIBLIOGRAPHY

- Detectors. [Online]. Available: <https://www.nuclear-power.net/nuclear-engineering/radiation-detection/semiconductor-detectors/high-purity-germanium-detectors-hpge/principle-of-operation-of-hpge-detectors/>. Accessed: 23/06/2020
- [23] N. Connor. (2020) What is High Purity Germanium Detector – HPGe – Definition. [Online]. Available: <https://www.radiation-dosimetry.org/what-is-high-purity-germanium-detector-hpge-definition/>. Accessed: 23/06/2020
- [24] Mirion Technologies. (2020) High-Resolution Gamma-Ray Spectroscopy with HPGe Detectors. [Online]. Available: <https://www.mirion.com/learning-center/lab-experiments/high-resolution-gamma-ray-spectroscopy-with-hpge-detectors-lab-experiments>. Accessed: 23/06/2020
- [25] G. F. Knoll, *Radiation Detection and Measurement*, 3rd ed. John Wiley & Sons, 2000, p. 30.
- [26] S. D’Auria, *Introduction to Nuclear and Particle Physics*. Springer, 2019, p. 83.
- [27] Provision Healthcare. (2020) What is Proton Therapy? [Online]. Available: <https://provisionhealthcare.com/about-proton-therapy/advantages-of-proton/>. Accessed: 22/06/2020.
- [28] J. Brugger and W. M. White, *Encyclopedia of Geochemistry: A Comprehensive Reference Source on the Chemistry of the Earth*. Cham: Springer International Publishing, 2018, pp. 1521-1524.
- [29] M. Sabet, P. Rowshanfarzad, A. Jalilian, M. Ensaf, and A. Rajamand, “Production and Quality Control of ^{66}Ga Radionuclide,” *Nukleonika*, vol. 51, no. 3, pp. 147–154, 2006.
- [30] International Atomic Energy Agency (IAEA), “Isotope Browser,” 2016, Note: Latest Update Published in 2020.
- [31] “Personal Communication with Emiel van der Graaf,” 2020.
- [32] Commission on Isotopic Abundances and Atomic Weights (CIAAW). (2007) Atomic Weight of Zinc. [Online]. Available: <https://ciaaw.org/zinc.htm>. Accessed: 08/05/2020.
- [33] Committee on Data for Science and Technology. (2018) Elementary Charge. [Online]. Available: <https://physics.nist.gov/cgi-bin/cuu/Value?e>. Accessed: 15/05/2020.
- [34] G. Choppin, J. O. Liljenzin, and J. Rydberg, *Radiochemistry and Nuclear Chemistry*, 3rd ed. Butterworth-Heinemann, 2013, Fig. 2.20. p. 188.

BIBLIOGRAPHY

- [35] Scintillator Materials Group, Stanford University. (2009) Research Fundamentals: What Are Scintillator Materials? [Online]. Available: <https://web.stanford.edu/group/scintillators/scintillators.html>. Accessed: 23/06/2020
- [36] Emiel van der Graaf, “Detector Efficiency Simulations Efficiencies for a 91x91x150 mm NaI Detector in the Eurogam Clover Detector Housing,” *University of Groningen*, 2020.
- [37] Radiation Safety Information Computational Center (RSICC). (2017) RSICC CODE PACKAGE PSR-550. [Online]. Available: <https://rsicc.ornl.gov/codes/psr/psr5/psr-550.html>. Accessed: 17/05/2020.
- [38] —. (2012) RSICC CODE PACKAGE PSR-497. [Online]. Available: <https://rsicc.ornl.gov/codes/psr/psr4/psr-497.html>. Accessed: 17/05/2020.
- [39] Web Plot Digitizer 4.2. [Online]. Available: <https://apps.automeris.io/wpd/>. Accessed: 29/04/2020.
- [40] A. Hermanne, F. Szelecsényi, M. Sonck, S. Takács, F. Tárkányi, and P. Van den Winkel, “New Cross Section Data on $^{68}\text{Zn}(p, 2n)^{67}\text{Ga}$ and $^{\text{nat}}\text{Zn}(p, xn)^{67}\text{Ga}$ Nuclear Reactions for the Development of a Reference Data Base,” *Journal of Radioanalytical and Nuclear Chemistry*, vol. 240, no. 2, pp. 623–630, 1999.
- [41] S. Chu, L. Ekström, and R. Firestone. (1999) The Lund/LBNL Nuclear Data Search. [Online]. Available: <http://nucleardata.nuclear.lu.se/toi/index.asp>. Accessed: 25/05/2020.
- [42] T. McGee, C. Rao, G. Saha, and L. Yaffe, “Nuclear Interactions of ^{45}Sc and ^{68}Zn With Protons of Medium Energy,” *Nuclear Physics A*, vol. 150, no. 1, pp. 11–29, 1970.
- [43] M. Bonardi and C. Birattari, “Optimization of Irradiation Parameters for ^{67}Ga Production from $^{\text{nat}}\text{Zn}(p, xn)$ Nuclear Reactions,” *Journal of Radioanalytical and Nuclear Chemistry*, vol. 76, no. 2, pp. 311–318, 1983.
- [44] F. E. Little and M. C. Lagunas-Solar, “Cyclotron Production of ^{67}Ga . Cross Sections and Thick-Target Yields for the $^{67}\text{Zn}(p, n)$ and $^{68}\text{Zn}(p, 2n)$ Reactions,” *The International Journal of Applied Radiation and Isotopes*, vol. 34, no. 3, pp. 631–637, 1983.
- [45] P. Kopecký, “Cross Sections and Production Yields of ^{66}Ga and ^{67}Ga for Proton Reactions in Natural Zinc,” *International Journal of Radiation Applications and Instrumentation. Part A. Applied Radiation and Isotopes*, vol. 41, no. 6, pp. 606–608, 1990.
- [46] V. Levkovskii, “Activation Cross Sections for the Nuclides of Medium Mass

BIBLIOGRAPHY

- Region ($A=40\text{--}100$) With Medium Energy ($E=10\text{--}50$ MeV) Protons and Alpha Particles (Experiment and Systematics),” *Inter-Vesti, Moscow*, 1991.
- [47] F. Nortier, S. Mills, and G. Steyn, “Excitation Functions and Yields of Relevance to the Production of ^{67}Ga by Proton Bombardment of $^{\text{nat}}\text{Zn}$ and $^{\text{nat}}\text{Ge}$ up to 100 MeV,” *International Journal of Radiation Applications and Instrumentation. Part A. Applied Radiation and Isotopes*, vol. 42, no. 4, pp. 353–359, 1991.
- [48] F. Szelecsényi, T. E. Boothe, S. Takács, F. Tárkányi, and E. Tavano, “Evaluated Cross Section and Thick Target Yield Data Bases of $\text{Zn} + \text{p}$ Processes for Practical Applications,” *Applied radiation and isotopes*, vol. 49, no. 8, pp. 1005–1032, 1998.
- [49] S. Kastleiner, H. Coenen, and S. Qaim, “Possibility of Production of ^{67}Cu at a Small-Sized Cyclotron via the (p, α) -Reaction on Enriched ^{70}Zn ,” *Radiochimica Acta*, vol. 84, no. 2, pp. 107–110, 1999.
- [50] T. Stoll, S. Kastleiner, Y. N. Shubin, H. H. Coenen, and S. M. Qaim, “Excitation Functions of Proton Induced Reactions on ^{68}Zn from Threshold up to 71 MeV, With Specific Reference to the Production of ^{67}Cu ,” *Radiochimica Acta*, vol. 90, no. 6, pp. 309–313, 2002.
- [51] F. Szelecsényi, Z. Kovács, T. Van der Walt, G. Steyn, K. Suzuki, and K. Okada, “Investigation of the $^{\text{nat}}\text{Zn}(\text{p}, x)^{62}\text{Zn}$ Nuclear Process up to 70 MeV: a New $^{62}\text{Zn}/^{62}\text{Cu}$ Generator,” *Applied Radiation and Isotopes*, vol. 58, no. 3, pp. 377–384, 2003.
- [52] M. Bonardi, F. Groppi, H. Mainardi, V. Kokhanyuk, E. Lapshina, M. Mebel, and B. Zhuikov, “Cross Section Studies on ^{64}Cu With Zinc Target in the Proton Energy Range From 141 Down to 31 MeV,” *Journal of Radioanalytical and Nuclear Chemistry*, vol. 264, no. 1, pp. 101–105, 2005.
- [53] F. Szelecsenyi, G. Steyn, Z. Kovacs, T. Van der Walt, K. Suzuki, K. Okada, and K. Mukai, “New Cross-Section Data for the $^{66}\text{Zn}(\text{p}, \text{n})^{66}\text{Ga}$, $^{68}\text{Zn}(\text{p}, 3\text{n})^{66}\text{Ga}$, $^{\text{nat}}\text{Zn}(\text{p}, x)^{66}\text{Ga}$, $^{68}\text{Zn}(\text{p}, 2\text{n})^{67}\text{Ga}$ and $^{\text{nat}}\text{Zn}(\text{p}, x)^{67}\text{Ga}$ Nuclear Reactions up to 100 MeV,” *Nuclear Instruments and Methods in Physics Research Section B: Beam Interactions With Materials and Atoms*, vol. 234, no. 4, pp. 375–386, 2005.
- [54] F. Szelecsényi, Z. Kovács, K. Suzuki, K. Okada, T. Van der Walt, G. Steyn, and S. Mukherjee, “Production Possibility of ^{61}Cu Using Proton Induced Nuclear Reactions on Zinc for PET Studies,” *Journal of Radioanalytical and Nuclear Chemistry*, vol. 263, no. 2, pp. 539–546, 2005.
- [55] F. Szelecsényi, G. Steyn, Z. Kovács, C. Vermeulen, N. Van Der Meulen, S. Dole, T. Van Der Walt, K. Suzuki, and K. Mukai, “Investigation of the $^{66}\text{Zn}(\text{p},$

BIBLIOGRAPHY

- $2p_n$) ^{64}Cu and $^{68}\text{Zn}(p, x)^{64}\text{Cu}$ Nuclear Processes up to 100 MeV: Production of ^{64}Cu ,” *Nuclear Instruments and Methods in Physics Research Section B: Beam Interactions With Materials and Atoms*, vol. 240, no. 3, pp. 625–637, 2005.
- [56] F. Tárkányi, F. Ditrói, J. Csikai, S. Takács, M. Uddin, M. Hagiwara, M. Baba, Y. N. Shubin, and A. Dityuk, “Activation Cross-Sections of Long-Lived Products of Proton-Induced Nuclear Reactions on Zinc,” *Applied Radiation and Isotopes*, vol. 62, no. 1, pp. 73–81, 2005.
- [57] F. Al-Saleh, K. Al Mugren, and A. Azzam, “Excitation Function Measurements and Integral Yields Estimation for $^{\text{nat}}\text{Zn}(p, x)$ Reactions at Low Energies,” *Applied Radiation and Isotopes*, vol. 65, no. 10, pp. 1101–1107, 2007.
- [58] M. Uddin, M. Khandaker, K. Kim, Y. Lee, and G. Kim, “Excitation Functions of the Proton Induced Nuclear Reactions on $^{\text{nat}}\text{Zn}$ up to 40 MeV,” *Nuclear Instruments and Methods in Physics Research Section B: Beam Interactions With Materials and Atoms*, vol. 258, no. 2, pp. 313–320, 2007.
- [59] A. H. Asad, S. Chan, L. Morandeau, D. Cryer, S. V. Smith, and R. I. Price, “Excitation Functions of $^{\text{nat}}\text{Zn}(p, x)$ Nuclear Reactions With Proton Beam Energy Below 18 MeV,” *Applied Radiation and Isotopes*, vol. 94, pp. 67–71, 2014.

Appendix

For further inquiries or to acquire data not presented in this paper please contact the author, Adrian Sidhu, at adriansidhu1@gmail.com.

I Theory Appendices

Six Properties of Ideal Scintillation Material

This list has been taken near verbatim and can be found on page 219 in Knoll[18]. The ideal scintillation material should possess the following properties:

1. The material should convert the kinetic energy of charged particles into detectable light with a high scintillation efficiency;
2. The conversion of kinetic energy into detectable light should be linear in as wide a range as possible;
3. The medium should be transparent to the wavelength of its own emission light to ensure optimal light collection;
4. The decay time of the induced luminescence should be short so that fast signal pulses can be generated;
5. The material should be of good optical quality and be able to be manufactured in sizes appropriate for use in a practical detector;
6. The index of refraction of the material should be similar to that of glass (~ 1.5) to permit efficient coupling of the scintillation light to a PMT or other light sensor.

II Method Appendices

In total, there were around forty different Python scripts which were written and used in this research. However, only the scripts the author found most relevant have been given here. These are the polynomial regression script used for the excitation function of ^{66}Ga (Script 1) and the script which produced the isotope activities and γ -spectra as seen in Table 4.4 and Figs. 4.23 and 4.24 (Script 2). All the other scripts were either adaptations of the these two scripts, or scripts used for simply plotting Excel data. For example, the scripts for all the other excitation functions were adapted from Script 1, while the scripts which produced Figs. 4.9 - 4.16 were just plotting processed Excel data.

Script 1: Polynomial Regression Script for the ^{66}Ga Excitation Function

Given below is the Python script for the polynomial regression plot in Fig. 4.1. The same code was used for all the other excitation function fits, with the only changes being the data sources used and the degree of the polynomial utilised in the fit. There are two important things to mention here. First, the data sources (i.e. the Excel workbooks containing the relevant data) referenced using the Pandas package were local file systems, meaning that this code cannot be replicated without them. In this specific case, all this data is available online (see Table 4.1) but the author can also be contacted for this data. Secondly, the script presented here, while fully functional, is not an exact copy of the script used in this paper. A few additional notes (written in either quotation marks or with a preceding #), that are now irrelevant, have been removed. An example of one of these irrelevant notes was a link to a grid spacing information resource for the matplotlib.pyplot module. Furthermore, additional line breaks (\) have been added to prevent the overflow of text into the margins.

```

1  # -*- coding: utf-8 -*-
2  """
3  Created on Thu Apr 30 20:11:42 2020
4
5  @author: Adrian Sidhu
6  """
7  import matplotlib.pyplot as plt
8  import numpy as np
9  import pandas as pd
10 import xlswriter
11 from sklearn.metrics import r2_score, mean_squared_error
12
13 """NOTE FERENC IS SZELECSENYI"""
14 plt.rcParams["font.family"] = "serif"
15
16 combined = pd.read_excel(r"C:\Users\Adrian Sidhu\Documents\
17 \Bachelor's Thesis\RESEARCH\Ga-66 Production Data\
18 \Ga Production Sheet 2.xlsx", \
19 sheet_name = "Combined")
20 ferenc = pd.read_excel(r"C:\Users\Adrian Sidhu\Documents\
21 \Bachelor's Thesis\RESEARCH\Ga-66 Production Data\
22 \Ga Production Sheet 2.xlsx", \
23 sheet_name = "Ferenc S. et al. 1998 Hermanne")
24 kopecky = pd.read_excel(r"C:\Users\Adrian Sidhu\Documents\
25 \Bachelor's Thesis\RESEARCH\Ga-66 Production Data\

```

```
26 \Ga Production Sheet 2.xlsx", \
27 sheet_name = "Kopecky 1989")
28 nortier = pd.read_excel(r"C:\Users\Adrian Sidhu\Documents\
29 \Bachelor's Thesis\RESEARCH\Ga-66 Production Data\
30 \Ga Production Sheet 2.xlsx", \
31 sheet_name = "Nortier 1991")
32 little = pd.read_excel(r"C:\Users\Adrian Sidhu\Documents\
33 \Bachelor's Thesis\RESEARCH\Ga-66 Production Data\
34 \Ga Production Sheet 2.xlsx", \
35 sheet_name = "Little and Lagunas-Solar 1983")
36 bonardi = pd.read_excel(r"C:\Users\Adrian Sidhu\Documents\
37 \Bachelor's Thesis\RESEARCH\Ga-66 Production Data\
38 \Ga Production Sheet 2.xlsx", \
39 sheet_name = "Bonardi and Birattari 1983")
40 alsaleh = pd.read_excel(r"C:\Users\Adrian Sidhu\Documents\
41 \Bachelor's Thesis\RESEARCH\Ga-66 Production Data\
42 \Ga Production Sheet 2.xlsx", \
43 sheet_name = "Al-Saleh 2007")
44 asad = pd.read_excel(r"C:\Users\Adrian Sidhu\Documents\
45 \Bachelor's Thesis\RESEARCH\Ga-66 Production Data\
46 \Ga Production Sheet 2.xlsx", \
47 sheet_name = "Asad 2014")
48 hermanne99 = pd.read_excel(r"C:\Users\Adrian Sidhu\Documents\
49 \Bachelor's Thesis\RESEARCH\Ga-66 Production Data\
50 \Ga Production Sheet 2.xlsx", \
51 sheet_name = "Hermanne 1999")
52 szelecsenyi03 = pd.read_excel(r"C:\Users\Adrian Sidhu\Documents\
53 \Bachelor's Thesis\RESEARCH\Ga-66 Production Data\
54 \Ga Production Sheet 2.xlsx", \
55 sheet_name = "Szelecsenyi 2003")
56 szelecsenyi05 = pd.read_excel(r"C:\Users\Adrian Sidhu\Documents\
57 \Bachelor's Thesis\RESEARCH\Ga-66 Production Data\
58 \Ga Production Sheet 2.xlsx", \
59 sheet_name = "Szelecsenyi 2005")
60 tarkanyi = pd.read_excel(r"C:\Users\Adrian Sidhu\Documents\
61 \Bachelor's Thesis\RESEARCH\Ga-66 Production Data\
62 \Ga Production Sheet 2.xlsx", \
63 sheet_name = "Tarkanyi 2005")
64 uddin = pd.read_excel(r"C:\Users\Adrian Sidhu\Documents\
65 \Bachelor's Thesis\RESEARCH\Ga-66 Production Data\
66 \Ga Production Sheet 2.xlsx", \
67 sheet_name = "Uddin 2007")
```

```
68 """Note that below, x is energy and y is the cross section!"""
69 x_combined_list = combined['Proton Energy (MeV)'].tolist()
70 y_combined_list = combined['Cross Section (mb)'].tolist()
71
72 x_ferenc_list = ferenc['Proton Energy (MeV)'].tolist()
73 y_ferenc_list = ferenc['Cross Section (mb)'].tolist()
74
75 x_kopecky_list = kopecky['Proton Energy (MeV)'].tolist()
76 y_kopecky_list = kopecky['Cross Section (mb)'].tolist()
77
78 x_nortier_list = nortier['Proton Energy (MeV)'].tolist()
79 y_nortier_list = nortier['Cross Section (mb)'].tolist()
80
81 x_little_list = little['Proton Energy (MeV)'].tolist()
82 y_little_list = little['Cross Section (mb)'].tolist()
83
84 x_bonardi_list = bonardi['Proton Energy (MeV)'].tolist()
85 y_bonardi_list = bonardi['Cross Section (mb)'].tolist()
86
87 x_alsaleh_list = alsaleh['Proton Energy (MeV)'].tolist()
88 y_alsaleh_list = alsaleh['Cross Section (mb)'].tolist()
89
90 x_asad_list = asad['Proton Energy (MeV)'].tolist()
91 y_asad_list = asad['Cross Section (mb)'].tolist()
92
93 x_hermanne99_list = hermanne99['Proton Energy (MeV)'].tolist()
94 y_hermanne99_list = hermanne99['Cross Section (mb)'].tolist()
95
96 x_szelecsenyi03_list = szelecsenyi03\
97 ['Proton Energy (MeV)'].tolist()
98 y_szelecsenyi03_list = szelecsenyi03\
99 ['Cross Section (mb)'].tolist()
100
101 x_szelecsenyi05_list = szelecsenyi05\
102 ['Proton Energy (MeV)'].tolist()
103 y_szelecsenyi05_list = szelecsenyi05\
104 ['Cross Section (mb)'].tolist()
105
106 x_tarkanyi_list = tarkanyi['Proton Energy (MeV)'].tolist()
107 y_tarkanyi_list = tarkanyi['Cross Section (mb)'].tolist()
108
109 x_uddin_list = uddin['Proton Energy (MeV)'].tolist()
```

```
110 y_uddin_list = uddin['Cross Section (mb)'].tolist()
111
112 x_combined_array = np.array(x_combined_list)
113 y_combined_array = np.array(y_combined_list)
114 x_new = np.arange(1.05, 99.95, 0.1)
115
116 degree = 19
117 combined_poly = np.polyfit(x_combined_array, y_combined_array, \
118 degree)
119
120 combined_poly_2 = np.poly1d(combined_poly)
121 #print(combined_poly)
122 #x_new = np.linspace(x_combined_list[0], x_combined_list[-1], 100)
123 #x_new = np.linspace(0, 90, 1800)
124
125 plt.figure(1)
126 plt.plot(x_little_list, y_little_list, 'k.', label = \
127 'Little & Lagunas-Solar (1983)')
128 plt.plot(x_bonardi_list, y_bonardi_list, 'bo', label = \
129 'Bonardi & Birattari (1983)')
130 plt.plot(x_kopecky_list, y_kopecky_list, 'gv', label = \
131 'Kopecky (1990)')
132 plt.plot(x_nortier_list, y_nortier_list, 'c^', label = \
133 'Nortier et al. (1991)')
134 plt.plot(x_ferenc_list, y_ferenc_list, 'm<', label = \
135 'Hermanne (1994)')
136 plt.plot(x_hermanne99_list, y_hermanne99_list, 'y>', label = \
137 'Hermanne et al. (1999)')
138 plt.plot(x_szelecsenyi03_list, y_szelecsenyi03_list, \
139 's', label = 'Szelecsenyi et al. (2003)')
140 plt.plot(x_szelecsenyi05_list, y_szelecsenyi05_list, \
141 'd', label = 'Szelecsenyi et al. (2005)(1)')
142 plt.plot(x_tarkanyi_list, y_tarkanyi_list, 'D', label = \
143 'Tarkanyi et al. (2005)')
144 plt.plot(x_uddin_list, y_uddin_list, 'X', label = \
145 'Uddin et al. (2007)')
146 plt.plot(x_alsaleh_list, y_alsaleh_list, 'P', label = \
147 'Al-Saleh et al. (2007)')
148 plt.plot(x_asad_list, y_asad_list, 'x', label = \
149 'Asad et al. (2014)')
150 #plt.plot(x_combined_array, np.polyval(combined_poly, \
151 x_combined_array), 'b-', label = 'This Work')
```

```

152 plt.plot(x_new, np.polyval(combined_poly, x_new), 'r-',\
153 linewidth = 2, label = 'Average Fit (This Work)')
154 plt.legend(fontsize = 18, loc = 'best')
155 #plt.grid(True)
156 #plt.title('Excitation Function for  $^{nat}Zn(p, x)^{66}Ga$ ')
157 #plt.yscale('log')
158 plt.ylim(bottom = 0.01, top = 190)
159 plt.xlabel('Proton Energy (MeV)', fontsize = 25)
160 plt.ylabel('Cross Section (mb)', fontsize = 25)
161 plt.xticks(fontsize = 25)
162 plt.yticks(fontsize = 25)
163 ax = plt.gca()
164 #ax.set_xticks(np.arange(0, 106.05, 10))
165 ax.set_xticks(np.arange(0, 106.05, 10), minor=True)
166 ax.grid(which='major')
167 ax.grid(which='minor', alpha=0.5)
168
169 print("For degree " + str(degree) + " the coefficient of \
170 determination is " + str(r2_score(y_combined_list,\
171 combined_poly_2(x_combined_list))))
172 print("The RMSE is " + str(np.sqrt(mean_squared_error\
173 (y_combined_list,
174 combined_poly_2(x_combined_list)))) + \
175 '\n\n\n')
176
177 workbook = xlswriter.Workbook('Ga-66 Average Cross \
178 Section Data.xlsx')
179 worksheet = workbook.add_worksheet()
180
181 new_array = [x_new, np.polyval(combined_poly, x_new)]
182 row = 0
183
184 for col, data in enumerate(new_array):
185     worksheet.write_column(row, col, data)
186
187 workbook.close()
188
189 """SECTION FOR UNCERTAINTY"""
190 def uncertainty_calculator_r2(degree_list):
191     total_r2 = []
192     total_rmse = []
193     for i in degree_list:

```

```
194         combined_poly = np.polyfit(x_combined_array, \
195         y_combined_array, i)
196         combined_poly_2 = np.poly1d(combined_poly)
197         total_r2.append(r2_score(y_combined_list, \
198         combined_poly_2(x_combined_list)))
199         total_rmse.append(np.sqrt(mean_squared_error\
200         (y_combined_list, combined_poly_2(x_combined_list))))
201     return total_r2
202
203 def uncertainty_calculator_rmse(degree_list):
204     total_rmse = []
205     for i in degree_list:
206         combined_poly = np.polyfit(x_combined_array, \
207         y_combined_array, i)
208         combined_poly_2 = np.poly1d(combined_poly)
209         total_rmse.append(np.sqrt(mean_squared_error\
210         (y_combined_list, combined_poly_2(x_combined_list))))
211     return total_rmse
212
213 degrees = list(range(1, 90, 1))
214
215 """SECTION FOR EXCEL WORKBOOK EXPORTATION"""
216 workbook = xlswriter.Workbook('Uncertainty_In_Polyfit.xlsx')
217 worksheet = workbook.add_worksheet()
218
219 error_array = [degrees, uncertainty_calculator_r2(degrees), \
220 uncertainty_calculator_rmse(degrees)]
221 row = 0
222
223 for col, data in enumerate(error_array):
224     worksheet.write_column(row, col, data)
225
226 workbook.close()
```


Activity and γ -ray Spectrum Script

Below is the Python script used to produce the data in Table 4.4 and Figs. 4.23 and 4.24. The script presented here, like before, has been modified to fit the page (using line breaks) but is still fully functional if one has access to the relevant data. This is where the theoretical treatment as given by (2.3)-(2.14) has been implemented.

```

1  # -*- coding: utf-8 -*-
2  """
3  Created on Sat May 30 12:34:13 2020
4
5  @author: Adrian Sidhu
6  """
7  """DICTIONARY GOES - Energy (MeV) : Intensity (%)"""
8  import matplotlib.pyplot as plt
9  import numpy as np
10 import pandas as pd
11
12 plt.rcParams["font.family"] = "serif"
13 plt.rc('font', size=25)
14 plt.rcParams["mathtext.fontset"] = "dejavuserif"
15
16 """THIS SECTION IS FOR THE ACTIVITIES"""
17 """IMPORT SECTION"""
18 ga66wd = pd.read_excel(r"C:\Users\Adrian Sidhu\Documents\
19 \Bachelor's Thesis\RESEARCH\Ga-66 Production Data\50cm Spectra\
20 \50cm Spectra Data.xlsx", sheet_name = 'Water Depth v. R')
21 ga67wd = pd.read_excel(r"C:\Users\Adrian Sidhu\Documents\
22 \Bachelor's Thesis\RESEARCH\Gamma Spectra Comparison Data\
23 \FINAL Ga-67 Spectra.xlsx", sheet_name = 'Water Depth v. R')
24 ga68wd = pd.read_excel(r"C:\Users\Adrian Sidhu\Documents\
25 \Bachelor's Thesis\RESEARCH\Gamma Spectra Comparison Data\
26 \FINAL Ga-68 Spectra.xlsx", sheet_name = 'Water Depth v. R')
27
28 cu61wd = pd.read_excel(r"C:\Users\Adrian Sidhu\Documents\
29 \Bachelor's Thesis\RESEARCH\Gamma Spectra Comparison Data\
30 \FINAL Cu-61 Spectra.xlsx", sheet_name = 'Water Depth v. R')
31 cu64wd = pd.read_excel(r"C:\Users\Adrian Sidhu\Documents\
32 \Bachelor's Thesis\RESEARCH\Gamma Spectra Comparison Data\
33 \FINAL Cu-64 Spectra.xlsx", sheet_name = 'Water Depth v. R')
34 cu67wd = pd.read_excel(r"C:\Users\Adrian Sidhu\Documents\
35 \Bachelor's Thesis\RESEARCH\Gamma Spectra Comparison Data\

```

```

36 \FINAL Cu-67 Spectra.xlsx", sheet_name = 'Water Depth v. R')
37
38 zn62wd = pd.read_excel(r"C:\Users\Adrian Sidhu\Documents\
39 \Bachelor's Thesis\RESEARCH\Gamma Spectra Comparison Data\
40 \FINAL Zn-62 Spectra.xlsx", sheet_name = 'Water Depth v. R')
41 zn65wd = pd.read_excel(r"C:\Users\Adrian Sidhu\Documents\
42 \Bachelor's Thesis\RESEARCH\Gamma Spectra Comparison Data\
43 \FINAL Zn-65 Spectra.xlsx", sheet_name = 'Water Depth v. R')
44
45 """"DATA SECTION""""
46 ga66_rsp = list(ga66wd['R (/sp)'])[4:7])
47 ga67_rsp = list(ga67wd['R (/sp)'])[4:7])
48 ga68_rsp = list(ga68wd['R (/sp)'])[4:7])
49
50 cu61_rsp = list(cu61wd['R (/sp)'])[4:7])
51 cu64_rsp = list(cu64wd['R (/sp)'])[4:7])
52 cu67_rsp = list(cu67wd['R (/sp)'])[4:7])
53
54 zn62_rsp = list(zn62wd['R (/sp)'])[4:7])
55 zn65_rsp = list(zn65wd['R (/sp)'])[4:7])
56
57
58 ga66_rnah = []
59 ga67_rnah = []
60 ga68_rnah = []
61
62 cu61_rnah = []
63 cu64_rnah = []
64 cu67_rnah = []
65
66 zn62_rnah = []
67 zn65_rnah = []
68
69 for i in ga66_rsp:
70     ga66_rnah.append(i * ((2.246943267 * (10 ** 13)))) \
71     #The value of 2.24E13 is in units of sp/nA h - thus \
72     #converting sp-1 to (nAh)-1
73 for i in ga67_rsp:
74     ga67_rnah.append(i * ((2.246943267 * (10 ** 13))))
75 for i in ga68_rsp:
76     ga68_rnah.append(i * ((2.246943267 * (10 ** 13))))
77

```

```

78 for i in cu61_rsp:
79     cu61_rnah.append(i * ((2.246943267 * (10 ** 13))))
80 for i in cu64_rsp:
81     cu64_rnah.append(i * ((2.246943267 * (10 ** 13))))
82 for i in cu67_rsp:
83     cu67_rnah.append(i * ((2.246943267 * (10 ** 13))))
84
85 for i in zn62_rsp:
86     zn62_rnah.append(i * ((2.246943267 * (10 ** 13))))
87 for i in zn65_rsp:
88     zn65_rnah.append(i * ((2.246943267 * (10 ** 13))))
89
90 """THIS SECTION IS TO CALCULATE THE
91 ACTIVITY OF EACH SOURCE"""
92 def activity(dep, cur, irr_t_hours, t_hours):
93
94     print('Proton Beam Energy: 90 MeV')
95     print('Zinc Depth: ' + str(dep) + ' mm')
96     print('Beam Current: ' + str(cur) + ' nA')
97     print('Irradiation Time: ' + str(round(irr_t_hours, 6))\
98           + ' hours')
99     print('Time elapsed (from irradiation start) at activity\
100 measurement: ' + str(t_hours) + ' hours')
101
102     """dc stands for the decay constant for each isotope.
103     The decay constants have been calculated using
104     half lives found on the IAEA isotope browser."""
105     irr_t = irr_t_hours * 3600
106     t = t_hours * 3600
107
108
109     ga66_dc = np.log(2) / (9.49 * 3600) #9.49 hours
110     ga67_dc = np.log(2) / (3.2617 * 24 * 3600) #3.2617 days
111     ga68_dc = np.log(2) / (67.71 * 60) #67.71 minutes
112
113     cu61_dc = np.log(2) / (3.339 * 3600) #3.339 hours
114     cu64_dc = np.log(2) / (12.701 * 3600) #12.701 hours
115     cu67_dc = np.log(2) / (61.83 * 3600) #61.83 hours
116
117     zn62_dc = np.log(2) / (9.193 * 3600) #9.193 hours
118     zn65_dc = np.log(2) / (243.93 * 24 * 3600) #243.93 days
119

```

```

120     if dep == 50:
121         P_ga66 = ga66_rnah[0] * cur * (1 / 3600) \
122             #1 / 3600 hours in a second. P is the production\
123             #of an isotope per second.
124         P_ga67 = ga67_rnah[0] * cur * (1 / 3600)
125         P_ga68 = ga68_rnah[0] * cur * (1 / 3600)
126
127         P_cu61 = cu61_rnah[0] * cur * (1 / 3600)
128         P_cu64 = cu64_rnah[0] * cur * (1 / 3600)
129         P_cu67 = cu67_rnah[0] * cur * (1 / 3600)
130
131         P_zn62 = zn62_rnah[0] * cur * (1 / 3600)
132         P_zn65 = zn65_rnah[0] * cur * (1 / 3600)
133
134     if t < irr_t:
135         A_ga66 = P_ga66 * (1 - np.exp(-ga66_dc * t))
136         A_ga67 = P_ga67 * (1 - np.exp(-ga67_dc * t))
137         A_ga68 = P_ga68 * (1 - np.exp(-ga68_dc * t))
138
139         A_cu61 = P_cu61 * (1 - np.exp(-cu61_dc * t))
140         A_cu64 = P_cu64 * (1 - np.exp(-cu64_dc * t))
141         A_cu67 = P_cu67 * (1 - np.exp(-cu67_dc * t))
142
143         A_zn62 = P_zn62 * (1 - np.exp(-zn62_dc * t))
144         A_zn65 = P_zn65 * (1 - np.exp(-zn65_dc * t))
145
146     elif t >= irr_t:
147         T = t - irr_t
148
149         N0_ga66 = P_ga66 * (1 - np.exp(-ga66_dc * irr_t)) \
150             / ga66_dc
151         N0_ga67 = P_ga67 * (1 - np.exp(-ga67_dc * irr_t)) \
152             / ga67_dc
153         N0_ga68 = P_ga68 * (1 - np.exp(-ga68_dc * irr_t)) \
154             / ga68_dc
155
156         N0_cu61 = P_cu61 * (1 - np.exp(-cu61_dc * irr_t)) \
157             / cu61_dc
158         N0_cu64 = P_cu64 * (1 - np.exp(-cu64_dc * irr_t)) \
159             / cu64_dc
160         N0_cu67 = P_cu67 * (1 - np.exp(-cu67_dc * irr_t)) \
161             / cu67_dc

```

```

162
163     NO_zn62 = P_zn62 * (1 - np.exp(-zn62_dc * irr_t))\
164     / zn62_dc
165     NO_zn65 = P_zn65 * (1 - np.exp(-zn65_dc * irr_t))\
166     / zn65_dc
167
168     A_ga66 = ga66_dc * NO_ga66 * np.exp(-ga66_dc * T)
169     A_ga67 = ga67_dc * NO_ga67 * np.exp(-ga67_dc * T)
170     A_ga68 = ga68_dc * NO_ga68 * np.exp(-ga68_dc * T)
171
172     A_cu61 = cu61_dc * NO_cu61 * np.exp(-cu61_dc * T)
173     A_cu64 = cu64_dc * NO_cu64 * np.exp(-cu64_dc * T)
174     A_cu67 = cu67_dc * NO_cu67 * np.exp(-cu67_dc * T)
175
176     A_zn62 = zn62_dc * NO_zn62 * np.exp(-zn62_dc * T)
177     A_zn65 = zn65_dc * NO_zn65 * np.exp(-zn65_dc * T)
178
179
180 elif dep == 55:
181     P_ga66 = ga66_rnah[1] * cur * (1 / 3600)
182     P_ga67 = ga67_rnah[1] * cur * (1 / 3600)
183     P_ga68 = ga68_rnah[1] * cur * (1 / 3600)
184
185     P_cu61 = cu61_rnah[1] * cur * (1 / 3600)
186     P_cu64 = cu64_rnah[1] * cur * (1 / 3600)
187     P_cu67 = cu67_rnah[1] * cur * (1 / 3600)
188
189     P_zn62 = zn62_rnah[1] * cur * (1 / 3600)
190     P_zn65 = zn65_rnah[1] * cur * (1 / 3600)
191
192 if t < irr_t:
193     A_ga66 = P_ga66 * (1 - np.exp(-ga66_dc * t))
194     A_ga67 = P_ga67 * (1 - np.exp(-ga67_dc * t))
195     A_ga68 = P_ga68 * (1 - np.exp(-ga68_dc * t))
196
197     A_cu61 = P_cu61 * (1 - np.exp(-cu61_dc * t))
198     A_cu64 = P_cu64 * (1 - np.exp(-cu64_dc * t))
199     A_cu67 = P_cu67 * (1 - np.exp(-cu67_dc * t))
200
201     A_zn62 = P_zn62 * (1 - np.exp(-zn62_dc * t))
202     A_zn65 = P_zn65 * (1 - np.exp(-zn65_dc * t))
203

```

```

204     elif t >= irr_t:
205         T = t - irr_t
206
207         NO_ga66 = P_ga66 * (1 - np.exp(-ga66_dc * irr_t))\
208         / ga66_dc
209         NO_ga67 = P_ga67 * (1 - np.exp(-ga67_dc * irr_t))\
210         / ga67_dc
211         NO_ga68 = P_ga68 * (1 - np.exp(-ga68_dc * irr_t))\
212         / ga68_dc
213
214         NO_cu61 = P_cu61 * (1 - np.exp(-cu61_dc * irr_t))\
215         / cu61_dc
216         NO_cu64 = P_cu64 * (1 - np.exp(-cu64_dc * irr_t))\
217         / cu64_dc
218         NO_cu67 = P_cu67 * (1 - np.exp(-cu67_dc * irr_t))\
219         / cu67_dc
220
221         NO_zn62 = P_zn62 * (1 - np.exp(-zn62_dc * irr_t))\
222         / zn62_dc
223         NO_zn65 = P_zn65 * (1 - np.exp(-zn65_dc * irr_t))\
224         / zn65_dc
225
226         A_ga66 = ga66_dc * NO_ga66 * np.exp(-ga66_dc * T)
227         A_ga67 = ga67_dc * NO_ga67 * np.exp(-ga67_dc * T)
228         A_ga68 = ga68_dc * NO_ga68 * np.exp(-ga68_dc * T)
229
230         A_cu61 = cu61_dc * NO_cu61 * np.exp(-cu61_dc * T)
231         A_cu64 = cu64_dc * NO_cu64 * np.exp(-cu64_dc * T)
232         A_cu67 = cu67_dc * NO_cu67 * np.exp(-cu67_dc * T)
233
234         A_zn62 = zn62_dc * NO_zn62 * np.exp(-zn62_dc * T)
235         A_zn65 = zn65_dc * NO_zn65 * np.exp(-zn65_dc * T)
236
237
238     elif dep == 60:
239         P_ga66 = ga66_rnah[2] * cur * (1 / 3600)
240         P_ga67 = ga67_rnah[2] * cur * (1 / 3600)
241         P_ga68 = ga68_rnah[2] * cur * (1 / 3600)
242
243         P_cu61 = cu61_rnah[2] * cur * (1 / 3600)
244         P_cu64 = cu64_rnah[2] * cur * (1 / 3600)
245         P_cu67 = cu67_rnah[2] * cur * (1 / 3600)

```

```

246
247     P_zn62 = zn62_rnah[2] * cur * (1 / 3600)
248     P_zn65 = zn65_rnah[2] * cur * (1 / 3600)
249
250     if t < irr_t:
251         A_ga66 = P_ga66 * (1 - np.exp(-ga66_dc * t))
252         A_ga67 = P_ga67 * (1 - np.exp(-ga67_dc * t))
253         A_ga68 = P_ga68 * (1 - np.exp(-ga68_dc * t))
254
255         A_cu61 = P_cu61 * (1 - np.exp(-cu61_dc * t))
256         A_cu64 = P_cu64 * (1 - np.exp(-cu64_dc * t))
257         A_cu67 = P_cu67 * (1 - np.exp(-cu67_dc * t))
258
259         A_zn62 = P_zn62 * (1 - np.exp(-zn62_dc * t))
260         A_zn65 = P_zn65 * (1 - np.exp(-zn65_dc * t))
261
262     elif t >= irr_t:
263         T = t - irr_t
264
265         N0_ga66 = P_ga66 * (1 - np.exp(-ga66_dc * irr_t))\
266             / ga66_dc
267         N0_ga67 = P_ga67 * (1 - np.exp(-ga67_dc * irr_t))\
268             / ga67_dc
269         N0_ga68 = P_ga68 * (1 - np.exp(-ga68_dc * irr_t))\
270             / ga68_dc
271
272         N0_cu61 = P_cu61 * (1 - np.exp(-cu61_dc * irr_t))\
273             / cu61_dc
274         N0_cu64 = P_cu64 * (1 - np.exp(-cu64_dc * irr_t))\
275             / cu64_dc
276         N0_cu67 = P_cu67 * (1 - np.exp(-cu67_dc * irr_t))\
277             / cu67_dc
278
279         N0_zn62 = P_zn62 * (1 - np.exp(-zn62_dc * irr_t))\
280             / zn62_dc
281         N0_zn65 = P_zn65 * (1 - np.exp(-zn65_dc * irr_t))\
282             / zn65_dc
283
284         A_ga66 = ga66_dc * N0_ga66 * np.exp(-ga66_dc * T)
285         A_ga67 = ga67_dc * N0_ga67 * np.exp(-ga67_dc * T)
286         A_ga68 = ga68_dc * N0_ga68 * np.exp(-ga68_dc * T)
287

```

```

288         A_cu61 = cu61_dc * NO_cu61 * np.exp(-cu61_dc * T)
289         A_cu64 = cu64_dc * NO_cu64 * np.exp(-cu64_dc * T)
290         A_cu67 = cu67_dc * NO_cu67 * np.exp(-cu67_dc * T)
291
292         A_zn62 = zn62_dc * NO_zn62 * np.exp(-zn62_dc * T)
293         A_zn65 = zn65_dc * NO_zn65 * np.exp(-zn65_dc * T)
294
295         raw_activities = [A_ga66, A_ga67, A_ga68, A_cu61, A_cu64,\
296         A_cu67, A_zn62, A_zn65] #These are the actual activities of\
297         #each isotope in Bq
298         tot_activity = sum(raw_activities)
299         ratioed_activities = [] #This is the ratio of each\
300         #activity to the total activity, to be used as a\
301         #multiplication factor in the gamma spectrum
302         for i in raw_activities:
303             ratioed_activities.append(i / tot_activity)
304
305         return raw_activities
306         #return ratioed_activities
307
308
309     """VALUES"""
310     depth = 60 #mm, can be either 50mm, 55mm, or 60mm. \
311     #Nothing else. Type = Integer
312     current = 30 #nA. Any positive value, Type = Float
313     irradiation_time = 2 #hours. Type = Float
314     activity_time = 12 #Time for activity measurement! \
315     #In hours. Note this includes the irradiation time!
316
317
318     activity_table = {'Isotope' : ['Ga-66', 'Ga-67', 'Ga-68',\
319     'Cu-61', 'Cu-64', 'Cu-67', 'Zn-62', 'Zn-65'],\
320     'Activity (Bq)' : activity(depth, current,\
321     irradiation_time, activity_time)}
322
323     print("Table of activities for:")
324     print("Depth: " + str(depth) + " mm;")
325     print("Beam current: " + str(current) + " nA;")
326     print("Irradiation time: " + str(irradiation_time) + " hour(s)")
327     print("Time of measurement after irradiation begins: "\
328     + str(activity_time) + " hours")
329     print(pd.DataFrame(activity_table))

```



```
330  """
331
332  """THIS IS THE GAMMA SPECTRA SECTION"""
333
334  """
335  ga66_yspectra = pd.read_excel(r"C:\Users\Adrian Sidhu\
336  \Documents\Bachelor's Thesis\RESEARCH\
337  \Gamma Spectra Comparison Data\Gamma Spectra\
338  \Ga-66 Gamma Spectra.xlsx", sheet_name = 'Sheet1')
339  ga67_yspectra = pd.read_excel(r"C:\Users\Adrian Sidhu\
340  \Documents\Bachelor's Thesis\RESEARCH\
341  \Gamma Spectra Comparison Data\Gamma Spectra\
342  \Ga-67 Gamma Spectra.xlsx", sheet_name = 'Sheet1')
343  ga68_yspectra = pd.read_excel(r"C:\Users\Adrian Sidhu\
344  \Documents\Bachelor's Thesis\RESEARCH\
345  \Gamma Spectra Comparison Data\Gamma Spectra\
346  \Ga-68 Gamma Spectra.xlsx", sheet_name = 'Sheet1')
347
348  cu61_yspectra = pd.read_excel(r"C:\Users\Adrian Sidhu\
349  \Documents\Bachelor's Thesis\RESEARCH\
350  \Gamma Spectra Comparison Data\Gamma Spectra\
351  \Cu-61 Gamma Spectra.xlsx", sheet_name = 'Sheet1')
352  cu64_yspectra = pd.read_excel(r"C:\Users\Adrian Sidhu\
353  \Documents\Bachelor's Thesis\RESEARCH\
354  \Gamma Spectra Comparison Data\Gamma Spectra\
355  \Cu-64 Gamma Spectra.xlsx", sheet_name = 'Sheet1')
356  cu67_yspectra = pd.read_excel(r"C:\Users\Adrian Sidhu\
357  \Documents\Bachelor's Thesis\RESEARCH\
358  \Gamma Spectra Comparison Data\Gamma Spectra\
359  \Cu-67 Gamma Spectra.xlsx", sheet_name = 'Sheet1')
360
361  zn62_yspectra = pd.read_excel(r"C:\Users\Adrian Sidhu\
362  \Documents\Bachelor's Thesis\RESEARCH\
363  \Gamma Spectra Comparison Data\Gamma Spectra\
364  \Zn-62 Gamma Spectra.xlsx", sheet_name = 'Sheet1')
365  zn65_yspectra = pd.read_excel(r"C:\Users\Adrian Sidhu\
366  \Documents\Bachelor's Thesis\RESEARCH\
367  \Gamma Spectra Comparison Data\Gamma Spectra\
368  \Zn-65 Gamma Spectra.xlsx", sheet_name = 'Sheet1')
369
370  """Ga-66 SECTION"""
371  ga66_y_energy = list(ga66_yspectra['y Energy (keV)'])
```

```
372 ga66_y_intensity = list(ga66_yspectra['Intensity (%)'])
373 ga66_yei = list(zip(ga66_y_energy, ga66_y_intensity))
374
375 """Ga-67 SECTION"""
376 ga67_y_energy = list(ga67_yspectra['y Energy (keV)'])
377 ga67_y_intensity = list(ga67_yspectra['Intensity (%)'])
378 ga67_yei = list(zip(ga67_y_energy, ga67_y_intensity))
379
380 """Ga-68 SECTION"""
381 ga68_y_energy = list(ga68_yspectra['y Energy (keV)'])
382 ga68_y_intensity = list(ga68_yspectra['Intensity (%)'])
383 ga68_yei = list(zip(ga68_y_energy, ga68_y_intensity))
384
385 """Cu-61 SECTION"""
386 cu61_y_energy = list(cu61_yspectra['y Energy (keV)'])
387 cu61_y_intensity = list(cu61_yspectra['Intensity (%)'])
388 cu61_yei = list(zip(cu61_y_energy, cu61_y_intensity))
389
390 """Cu-64 SECTION"""
391 cu64_y_energy = list(cu64_yspectra['y Energy (keV)'])
392 cu64_y_intensity = list(cu64_yspectra['Intensity (%)'])
393 cu64_yei = list(zip(cu64_y_energy, cu64_y_intensity))
394
395 """Cu-67 SECTION"""
396 cu67_y_energy = list(cu67_yspectra['y Energy (keV)'])
397 cu67_y_intensity = list(cu67_yspectra['Intensity (%)'])
398 cu67_yei = list(zip(cu67_y_energy, cu67_y_intensity))
399
400 """Zn-62 SECTION"""
401 zn62_y_energy = list(zn62_yspectra['y Energy (keV)'])
402 zn62_y_intensity = list(zn62_yspectra['Intensity (%)'])
403 zn62_yei = list(zip(zn62_y_energy, zn62_y_intensity))
404
405 """Zn-65 SECTION"""
406 zn65_y_energy = list(zn65_yspectra['y Energy (keV)'])
407 zn65_y_intensity = list(zn65_yspectra['Intensity (%)'])
408 zn65_yei = list(zip(zn65_y_energy, zn65_y_intensity))
409
410
411
412
413
```

```

414 """HERE BOTH LINE THICKNESS AND HEIGHT IS PROPORTIONAL TO
415 ACTIVITY OF THE SOURCE - VISUAL AID ONLY, NOT USED IN PAPER"""
416 plt.figure(1)
417 pltwidth = 0.00001
418 for i in range(len(ga66_yei)):
419     if i != 0 and ga66_yei[i][1] > 1:
420         plt.bar(ga66_yei[i][0], ((ga66_yei[i][1] / 100) * \
421             activity(depth, current, irradiation_time, \
422                 activity_time)[0]), width = pltwidth * \
423             ((ga66_yei[i][1] / 100) * \
424                 activity(depth, current, irradiation_time, \
425                     activity_time)[0]), color = 'r')
426     elif i == 0:
427         plt.bar(ga66_yei[i][0], ((ga66_yei[i][1] / 100) * \
428             activity(depth, current, irradiation_time, \
429                 activity_time)[0]), width = pltwidth * \
430             ((ga66_yei[i][1] / 100) * \
431                 activity(depth, current, irradiation_time, \
432                     activity_time)[0]), color = 'r', \
433             label = "$^{66}$Ga")
434 for i in range(len(ga67_yei)):
435     if i != 0:
436         plt.bar(ga67_yei[i][0], ((ga67_yei[i][1] / 100) * \
437             activity(depth, current, irradiation_time, \
438                 activity_time)[1]), width = pltwidth * \
439             ((ga67_yei[i][1] / 100) * \
440                 activity(depth, current, irradiation_time, \
441                     activity_time)[1]), color = 'k')
442     elif i == 0:
443         plt.bar(ga67_yei[i][0], ((ga67_yei[i][1] / 100) * \
444             activity(depth, current, irradiation_time, \
445                 activity_time)[1]), width = pltwidth * \
446             ((ga67_yei[i][1] / 100) * \
447                 activity(depth, current, irradiation_time, \
448                     activity_time)[1]), color = 'k', \
449             label = "$^{67}$Ga")
450 for i in range(len(ga68_yei)):
451     if i != 0:
452         plt.bar(ga68_yei[i][0], ((ga68_yei[i][1] / 100) * \
453             activity(depth, current, irradiation_time, \
454                 activity_time)[2]), width = pltwidth * \
455             ((ga68_yei[i][1] / 100) * \

```

```

456         activity(depth, current, irradiation_time, \
457         activity_time)[2]), color = 'b')
458     elif i == 0:
459         plt.bar(ga68_yei[i][0], ((ga68_yei[i][1] / 100) * \
460         activity(depth, current, irradiation_time, \
461         activity_time)[2]), width = pltwidth * \
462         ((ga68_yei[i][1] / 100) * \
463         activity(depth, current, irradiation_time, \
464         activity_time)[2]), color = 'b', \
465         label = "$~{68}$Ga")
466 for i in range(len(cu61_yei)):
467     if i != 0:
468         plt.bar(cu61_yei[i][0], ((cu61_yei[i][1] / 100) * \
469         activity(depth, current, irradiation_time, \
470         activity_time)[3]), width = pltwidth * \
471         ((cu61_yei[i][1] / 100) * \
472         activity(depth, current, irradiation_time, \
473         activity_time)[3]), color = 'g')
474     elif i == 0:
475         plt.bar(cu61_yei[i][0], ((cu61_yei[i][1] / 100) * \
476         activity(depth, current, irradiation_time, \
477         activity_time)[3]), width = pltwidth * \
478         ((cu61_yei[i][1] / 100) * \
479         activity(depth, current, irradiation_time, \
480         activity_time)[3]), color = 'g', \
481         label = "$~{61}$Cu")
482 for i in range(len(cu64_yei)):
483     if i != 0:
484         plt.bar(cu64_yei[i][0], ((cu64_yei[i][1] / 100) * \
485         activity(depth, current, irradiation_time, \
486         activity_time)[4]), width = pltwidth * \
487         ((cu64_yei[i][1] / 100) * \
488         activity(depth, current, irradiation_time, \
489         activity_time)[4]), color = 'darkorange')
490     elif i == 0:
491         plt.bar(cu64_yei[i][0], ((cu64_yei[i][1] / 100) * \
492         activity(depth, current, irradiation_time, \
493         activity_time)[4]), width = pltwidth * \
494         ((cu64_yei[i][1] / 100) * \
495         activity(depth, current, irradiation_time, \
496         activity_time)[4]), color = 'darkorange', \
497         label = "$~{64}$Cu")

```

```

498 for i in range(len(cu67_yei)):
499     if i != 0:
500         plt.bar(cu67_yei[i][0], ((cu67_yei[i][1] / 100) * \
501             activity(depth, current, irradiation_time, \
502             activity_time)[5]), width = pltwidth * \
503             ((cu67_yei[i][1] / 100) * \
504             activity(depth, current, irradiation_time, \
505             activity_time)[5]), color = 'olive')
506     elif i == 0:
507         plt.bar(cu67_yei[i][0], ((cu67_yei[i][1] / 100) * \
508             activity(depth, current, irradiation_time, \
509             activity_time)[5]), width = pltwidth * \
510             ((cu67_yei[i][1] / 100) * \
511             activity(depth, current, irradiation_time, \
512             activity_time)[5]), color = 'olive', \
513             label = "$^{67}$Cu")
514 for i in range(len(zn62_yei)):
515     if i != 0:
516         plt.bar(zn62_yei[i][0], ((zn62_yei[i][1] / 100) * \
517             activity(depth, current, irradiation_time, \
518             activity_time)[6]), width = pltwidth * \
519             ((zn62_yei[i][1] / 100) * \
520             activity(depth, current, irradiation_time, \
521             activity_time)[6]), color = 'deepskyblue')
522     elif i == 0:
523         plt.bar(zn62_yei[i][0], ((zn62_yei[i][1] / 100) * \
524             activity(depth, current, irradiation_time, \
525             activity_time)[6]), width = pltwidth * \
526             ((zn62_yei[i][1] / 100) * \
527             activity(depth, current, irradiation_time, \
528             activity_time)[6]), color = 'deepskyblue', \
529             label = "$^{62}$Zn")
530 for i in range(len(zn65_yei)):
531     if i != 0:
532         plt.bar(zn65_yei[i][0], ((zn65_yei[i][1] / 100) * \
533             activity(depth, current, irradiation_time, \
534             activity_time)[7]), width = pltwidth * \
535             ((zn65_yei[i][1] / 100) * \
536             activity(depth, current, irradiation_time, \
537             activity_time)[7]), color = 'hotpink')
538     elif i == 0:
539         plt.bar(zn65_yei[i][0], ((zn65_yei[i][1] / 100) * \

```

```

540         activity(depth, current, irradiation_time, \
541         activity_time)[7]), width = pltwidth * \
542         ((zn65_yei[i][1] / 100) * \
543         activity(depth, current, irradiation_time, \
544         activity_time)[7]), color = 'hotpink', \
545         label = "$^{65}$Zn")
546 plt.grid(True)
547 plt.xlabel('Energy (keV)')
548 plt.ylabel('No. of $\gamma$-rays per second (s$^{-1}$)')
549 plt.yscale('log')
550 plt.legend(fontsize = 25)
551 plt.title('Depth: ' + str(depth) + ' mm || Beam current: ' \
552 + str(current) + ' nA || Irradiation Time: ' + \
553 str(irradiation_time) + \
554 ' hours || Time Elapsed Since Irradiation Started: ' + \
555 str(activity_time) + ' hours.', fontsize = 'large')
556
557 """
558 """
559 """HERE BAR HEIGHT PROPORTIONAL TO ACTIVITY,
560 BAR WIDTH CONSTANT,
561 USED TO MAKE GRAPHS IN PAPER"""
562 plt.figure(2)
563 pltwidth = 14
564 for i in range(len(ga66_yei)):
565     if i != 0 and ga66_yei[i][1] > 1:
566         plt.bar(ga66_yei[i][0], ((ga66_yei[i][1] / 100) * \
567         activity(depth, current, irradiation_time, \
568         activity_time)[0]), width = pltwidth, \
569         color = 'r')
570     elif i == 0:
571         plt.bar(ga66_yei[i][0], ((ga66_yei[i][1] / 100) * \
572         activity(depth, current, irradiation_time, \
573         activity_time)[0]), width = pltwidth, \
574         color = 'r', label = "$^{66}$Ga")
575 for i in range(len(ga67_yei)):
576     if i != 0:
577         plt.bar(ga67_yei[i][0], ((ga67_yei[i][1] / 100) * \
578         activity(depth, current, irradiation_time, \
579         activity_time)[1]), width = pltwidth, \
580         color = 'k')
581     elif i == 0:

```

```

582         plt.bar(ga67_yei[i][0], ((ga67_yei[i][1] / 100) * \
583             activity(depth, current, irradiation_time, \
584                 activity_time)[1]), width = pltwidth, \
585                 color = 'k', label = "$^{67}$Ga")
586     for i in range(len(ga68_yei)):
587         if i != 0:
588             plt.bar(ga68_yei[i][0], ((ga68_yei[i][1] / 100) * \
589                 activity(depth, current, irradiation_time, \
590                     activity_time)[2]), width = pltwidth, \
591                     color = 'b')
592         elif i == 0:
593             plt.bar(ga68_yei[i][0], ((ga68_yei[i][1] / 100) * \
594                 activity(depth, current, irradiation_time, \
595                     activity_time)[2]), width = pltwidth, \
596                     color = 'b', label = "$^{68}$Ga")
597     for i in range(len(cu61_yei)):
598         if i != 0:
599             plt.bar(cu61_yei[i][0], ((cu61_yei[i][1] / 100) * \
600                 activity(depth, current, irradiation_time, \
601                     activity_time)[3]), width = pltwidth, \
602                     color = 'g')
603         elif i == 0:
604             plt.bar(cu61_yei[i][0], ((cu61_yei[i][1] / 100) * \
605                 activity(depth, current, irradiation_time, \
606                     activity_time)[3]), width = pltwidth, \
607                     color = 'g', label = "$^{61}$Cu")
608     for i in range(len(cu64_yei)):
609         if i != 0:
610             plt.bar(cu64_yei[i][0], ((cu64_yei[i][1] / 100) * \
611                 activity(depth, current, irradiation_time, \
612                     activity_time)[4]), width = pltwidth, \
613                     color = 'darkorange')
614         elif i == 0:
615             plt.bar(cu64_yei[i][0], ((cu64_yei[i][1] / 100) * \
616                 activity(depth, current, irradiation_time, \
617                     activity_time)[4]), width = pltwidth, \
618                     color = 'darkorange', label = "$^{64}$Cu")
619     for i in range(len(cu67_yei)):
620         if i != 0:
621             plt.bar(cu67_yei[i][0], ((cu67_yei[i][1] / 100) * \
622                 activity(depth, current, irradiation_time, \
623                     activity_time)[5]), width = pltwidth, \

```

```

624         color = 'olive')
625     elif i == 0:
626         plt.bar(cu67_yei[i][0], ((cu67_yei[i][1] / 100) * \
627             activity(depth, current, irradiation_time, \
628                 activity_time)[5]), width = pltwidth, \
629                 color = 'olive', label = "$^{67}$Cu")
630 for i in range(len(zn62_yei)):
631     if i != 0:
632         plt.bar(zn62_yei[i][0], ((zn62_yei[i][1] / 100) * \
633             activity(depth, current, irradiation_time, \
634                 activity_time)[6]), width = pltwidth, \
635                 color = 'deepskyblue')
636     elif i == 0:
637         plt.bar(zn62_yei[i][0], ((zn62_yei[i][1] / 100) * \
638             activity(depth, current, irradiation_time, \
639                 activity_time)[6]), width = pltwidth, \
640                 color = 'deepskyblue', label = "$^{62}$Zn")
641 for i in range(len(zn65_yei)):
642     if i != 0:
643         plt.bar(zn65_yei[i][0], ((zn65_yei[i][1] / 100) * \
644             activity(depth, current, irradiation_time, \
645                 activity_time)[7]), width = pltwidth, \
646                 color = 'hotpink')
647     elif i == 0:
648         plt.bar(zn65_yei[i][0], ((zn65_yei[i][1] / 100) * \
649             activity(depth, current, irradiation_time, \
650                 activity_time)[7]), width = pltwidth, \
651                 color = 'hotpink', label = "$^{65}$Zn")
652
653
654 plt.grid(True)
655 plt.xlabel('Energy (keV)', fontsize = 25)
656 plt.ylabel('$\gamma$-ray Activity (Bq)', fontsize = 25)
657 plt.ticklabel_format(axis="y", style="sci", scilimits=(0,0))
658 plt.xticks(fontsize = 25)
659 plt.yticks(fontsize = 25)
660 #plt.yscale('log')
661 plt.legend(fontsize = 25, loc = 'best')
662 """plt.title('Depth: ' + str(depth) + ' mm || Beam current: ' +
663 str(current) + ' nA || Irradiation Time: ' + str(irradiation_time)
664 + ' hours || Time Elapsed Since Irradiation Started: ' +
665 str(activity_time) + ' hours.', fontsize = 'large')"""

```



```
666 """THIS IS JUST THE GAMMA SPECTRA,  
667 NEITHER HEIGHT NOR WIDTH IS  
668 PROPORTIONAL TO ACTIVITY:  
669 ONLY USED TO EXAMINE  
670 ABSOLUTE SPECTRUM"""  
671 plt.figure(3)  
672 pltwidth = 10  
673 for i in range(len(ga66_yei)):  
674     if i != 0 and ga66_yei[i][1] > 1:  
675         plt.bar(ga66_yei[i][0], 100, width = pltwidth, \  
676                 color = 'r')  
677     elif i == 0:  
678         plt.bar(ga66_yei[i][0], 100, width = pltwidth, \  
679                 color = 'r', label = "$^{66}$Ga")  
680 for i in range(len(ga67_yei)):  
681     if i != 0:  
682         plt.bar(ga67_yei[i][0], 100, width = pltwidth, \  
683                 color = 'k')  
684     elif i == 0:  
685         plt.bar(ga67_yei[i][0], 100, width = pltwidth, \  
686                 color = 'k', label = "$^{67}$Ga")  
687 for i in range(len(ga68_yei)):  
688     if i != 0:  
689         plt.bar(ga68_yei[i][0], 100, width = pltwidth, \  
690                 color = 'b')  
691     elif i == 0:  
692         plt.bar(ga68_yei[i][0], 100, width = pltwidth, \  
693                 color = 'b', label = "$^{68}$Ga")  
694 for i in range(len(cu61_yei)):  
695     if i != 0:  
696         plt.bar(cu61_yei[i][0], 100, width = pltwidth, \  
697                 color = 'g')  
698     elif i == 0:  
699         plt.bar(cu61_yei[i][0], 100, width = pltwidth, \  
700                 color = 'g', label = "$^{61}$Cu")  
701 for i in range(len(cu64_yei)):  
702     if i != 0:  
703         plt.bar(cu64_yei[i][0], 100, width = pltwidth, \  
704                 color = 'g')  
705     elif i == 0:  
706         plt.bar(cu64_yei[i][0], 100, width = pltwidth, \  
707                 color = 'g', label = "$^{64}$Cu")
```

```
708 for i in range(len(cu67_yei)):
709     if i != 0:
710         plt.bar(cu67_yei[i][0], 100, width = pltwidth, \
711             color = 'olive')
712     elif i == 0:
713         plt.bar(cu67_yei[i][0], 100, width = pltwidth, \
714             color = 'olive', label = "$^{67}$Cu")
715 for i in range(len(zn62_yei)):
716     if i != 0:
717         plt.bar(zn62_yei[i][0], 100, width = pltwidth, \
718             color = 'deepskyblue')
719     elif i == 0:
720         plt.bar(zn62_yei[i][0], 100, width = pltwidth, \
721             color = 'deepskyblue', label = "$^{62}$Zn")
722 for i in range(len(zn65_yei)):
723     if i != 0:
724         plt.bar(zn65_yei[i][0], 100, width = pltwidth, \
725             color = 'hotpink')
726     elif i == 0:
727         plt.bar(zn65_yei[i][0], 100, width = pltwidth, \
728             color = 'hotpink', label = "$^{65}$Zn")
729 plt.grid(True)
730 plt.xlabel('Energy (keV)')
731 plt.yticks([])
732 plt.legend(fontsize = 25)
```